THE CRITICAL ROLE OF MRGPRS IN NON-HISTAMINERGIC PRURITUS OF CHOLESTASIS AND ALLERGIC CONTACT DERMATITIS

by
James Meixiong

A dissertation submitted to Johns Hopkins University
in conformity with the requirements for the degree of Doctor of Philosophy

Baltimore, MD
June 2019

Abstract

Clinically relevant chronic itch conditions commonly result from kidney failure, cholestasis, and skin disorders like allergic contact dermatitis (ACD). Recently, numerous members of the Mas-related G-protein coupled receptor (*Mrgpr*) family of GPCRs have been identified as receptors for non-histaminergic pruritogens. In this thesis, I utilized Ca^{2+} imaging, mouse genetics, and mouse models of disease to determine the role of Mrgprs in two non-histaminergic pruritus conditions: cholestasis and ACD. In chapter one, I demonstrate that pathophysiologic levels of bilirubin observed in cholestasis, bound two *Mrgprs*, mouse MRGPRA1 and human MRGPRX4, activated sensory neurons via Mrgprs, and elicited Mrgpr-dependent pruritus. Genetic deletion of either *Mrgpra1* or *Bvlra*, the bilirubin-producing enzyme, attenuated mouse models of cholestatic itch. In chapter two, I present evidence that human MRGPRX4 is a bile acid receptor. To assess the *in vivo* relevance of bile acid activation of MRGPRX4, I generated a humanized mouse with targeted expression of MRGPRX4 to itch-encoding sensory neurons. Bile acids activated MRGPRX4-positive sensory neurons at higher levels compared to wild-type (WT) neurons. Compared to WT animals, MRGPRX4-mice scratched more upon acute injection of bile acids and in a model of cholestatic itch. In the final chapter, I examine the role of recently identified mast-cell expressed Mrgprs, murine Mrgprb2 and human MRGPRX2, in pruritus. Here I report that, in contrast to the IgE /FcεRI- histamine axis, Mrgprb2 activation of murine mast cells resulted in differential release of pruritogenic mediators, excited different subsets of itch-sensory neurons, and evoked non-histaminergic itch. In preclinical models of ACD, an inflammatory skin disorder, the Mrgprb2-mast cell axis critically regulated itch, and both mast cells and Mrgpr agonists were upregulated in human ACD skin. Overall, data from

this thesis suggests that targeting MRGPRs (MRGPRX4 for cholestatic itch and MRGPRX2 for ACD itch) is a promising strategy for alleviating non-histaminergic itch conditions.

READERS: Dr. Xinzhong Dong and Dr. Michael Caterina

Preface:
Statement of Research

The work presented in this thesis was performed under the direction of Dr. Xinzhong Dong and the author's thesis committee: Dr. Michael Caterina, Dr. Alex Kolodkin, and Dr. Solomon H. Snyder. With the exception of Dr. Michael Caterina who is of the Department of Biological Chemistry at the Johns Hopkins School of Medicine, the aforementioned are all of the Solomon H. Snyder Department of Neuroscience, Johns Hopkins School of Medicine. The portion of this work related to the identification of Mrgprs as receptors of bilirubin was performed under the direction of both Dr. Xinzhong Dong, and Dr. Solomon H. Snyder and was done with assistance from Chirag Vasavda, a graduate student in the Snyder lab. The presented data was obtained between August, 2015 and May, 2019, and all experiments were performed by the author except where otherwise noted.

Acknowledgements

I would like to thank my PI, Dr. Xinzhong Dong, and my thesis advisory mentors Drs. Solomon Snyder, Michael Caterina, and Alex Kolodkin for their invaluable time and assistance. Thanks to both the Johns Hopkins Transgenics Core and the Howard Hughes Mouse Genetics team for their work in generating numerous mouse lines. Much appreciation to many other valuable colleagues who have contributed to this thesis: Chirag Vasavda, Michael Anderson, Dr. Dustin Green, Dr. Qin Zheng, Lijun Qi, Dr. Nathachit Limjunyawong, Dr. Priyanka Pundir, Yixun Geng, Mark F. Sabbagh, Eric Hu, Dr. Brian S. Kim, Dr. Shawn G. Kwatra, and Dr. James P. Hamilton. Thank you to my parents, Dr. Wen-Cheng Xiong and Dr. Lin Mei for inspiring me to pursue research. Special thanks to my wife, Dr. Sze Yan Janelle Ho for supporting me both spiritually and professionally through this journey. Without you, none of this would have been possible.

Table of Contents

Page

Figures

Commonly Used Abbreviations:

MRGPR- mas-related G-protein coupled receptor; DRG- dorsal root ganglia; ACD- allergic contact dermatitis; MC- mast cell; ($^{-/-}$) or KO – Knockout

1. Introduction

1.1 An introduction to itch

Itch sensation is transmitted by small-diameter, unmyelinated C-fibers of the dorsal root ganglia (DRG) and trigeminal ganglia (TG). Itch fibers exclusively innervate skin and terminate in the dorsal horn of the spinal cord where they synapse with secondary neurons that transmit signal to brain. Anatomically, itch-sensing neurons are indistinguishable from pain-sensing neurons. As such, itch neurons were originally hypothesized to be a subpopulation of nociceptive, pain-sensing neurons. However, in recent years, this model has been upturned, and itch neurons are now recognized as being both molecularly and functionally distinct from pain-sensing counterparts.

1.1.1 Channels and receptors involved in itch sensation

A large variety of environmental stimuli ranging from single molecule chemicals to physical properties like temperature and force can elicit pain and itch. To detect this wide range of nociceptive inputs, sensory neurons utilize a host of channels and receptors. For example, many small-diameter pain- and itch-sensing neurons express transient receptor potential channel (TRP) V1 and/or TRPA1(Caterina et al., 2000; Caterina et al., 1999). At 42°C, the threshold for noxious heat, TRPV1 fluxes cations and depolarizes neurons (Caterina et al., 1999). Similarly, numerous pain-producing chemicals, such as cinnamaldehyde and mustard oil, activate sensory neurons via TRPA1(Jordt et al., 2004; Macpherson et al., 2007).

Both TRPV1 and TRPA1 are critical for itch transmission. Pruritogen-responsive dorsal horn neurons in mouse, rat, and monkey, are also activated by TRP agonists like capsaicin and mustard oil as assessed by *in vivo* electrophysiological recording (Davidson

et al., 2012; Klein et al., 2011; Simone et al., 2004). TRPV1 knockout ($^{-/-}$) mice, animals with well-characterized deficits in pain sensation, have drastically decreased histaminergic itch, and TRPA1$^{-/-}$ mice scratch less when injected with chloroquine, a non-histaminergic pruritogen (Imamachi et al., 2009; Wilson et al., 2011).

In addition to channels, itch neurons express receptors capable of detecting noxious substances. G-protein coupled receptors (GPCRs) are one major class of itch-associated receptors. GPCRs are a superfamily of proteins expressed in almost every cell in the body that detect stimuli as varied as lipids, ions, and proteins (Fredriksson et al., 2003; Kroeze et al., 2003; Lagerstrom and Schioth, 2008). GPCRs, 5-hydroxytryptamine (serotonin) receptor 1F (*Htr1f*), mas-related G-protein coupled receptor (*Mrgpr*) *a3*, and *Mrgprd,* have been identified by single cell transcriptomics as prominent markers for three distinct classes of itch-sensitive afferent neurons (Usoskin et al., 2015). Importantly, receptor expression is not completely specific to each class. For example, there is some Htr1f expression (9%) detected in the Mrgpra3^{+} class and vice versa (8%) (Usoskin et al., 2015). *Htr1f* is also expressed in additional classes of sensory neurons involved in pain (Ernberg et al., 2000; Sommer, 2004). In contrast, *Mrgpra3* and *Mrgprd* are specific to itch neurons, with undetectable expression in non-itch sensory neuron classes.

1.1.2 Itch circuits and itch specificity in spinal cord

In 2001, the first itch-sensing neurons were identified in the cat spinothalamic tract (STT). As determined by electrophysiology, these neurons were histamine-sensitive, mechano-insensitive, and thermo-insensitive (Andrew and Craig, 2001). Since this initial identification, populations of STT neurons sensitive to cowhage, a non-histaminergic

pruritogen, were also identified (Davidson et al., 2007). Itch-sensing STT neurons were activated by pain-associated stimuli such as capsaicin and noxious heat. At the time, these results were viewed as evidence for itch and pain sensation being transmitted by the same neurons and as evidence against the existence of itch-specific neurons (Davidson et al., 2007; Schmelz et al., 2003).

With the advent of mouse genetics, spinal sensory circuits became susceptible to more detailed investigation. Since then, genetic analyses have overturned old paradigms by providing evidence for two populations of itch-specific neurons in spinal cord, Gastrin-related peptide receptor^{+} (GRPR^{+}) neurons and Natriuretic peptide receptor A^{+} (NPRA^{+}) (Mishra and Hoon, 2013; Sun et al., 2009). Ablation of either GRPR^{+} or NPRA^{+} neurons in lamina I decreased peripheral itch without alterations in pain behavior (Sun et al., 2009). Concordantly, activation of both GRPR with GRP homologs bombesin and neuromedin B and NPRA with natriuretic polypeptide elicited pruritus and not pain, suggesting labeled-line specificity (Gmerek and Cowan, 1983). Intriguingly, both the receptors themselves, GRPR and NPRA, and their respective ligands, GRP and natriuretic polypeptide B (NPPB), are believed to be critical for itch signaling. Both receptor knockout mice, *GRPR*$^{-/-}$, and ligand knockout mice, GRP$^{-/-}$ and NPPB$^{-/-}$, have deficits in acute itch with intact thermal and mechanical pain response (Sun et al., 2009). GRP and NPPB have been detected in primary sensory neurons of the DRG (Barry et al., 2016; Liu et al., 2014; Zhao et al., 2013). However, GRP expression in DRG is controversial as numerous groups have been unable to detect GRP transcript and protein in DRG. Instead, these labs report GRP expression in spinal cord (Fleming et al., 2012; Mishra and Hoon, 2013; Solorzano et al., 2015).

In the spinal cord, itch neurons are regulated by interneurons engaged in various circuits. One prominent example is a circuit whereby scratch, a painful stimulus, inhibits itch sensation. Similar to the circuit model of Gate Control Theory where touch afferents activate interneurons that inhibit secondary pain neurons (Melzack and Wall, 1965), pain afferents activate basic helix-loop-helix b5 (Bhlhb5)-dependent interneurons which inhibit secondary itch neurons (Ross et al., 2010). In mice, silencing $TRPV1^+$ primary pain-sensing neurons decreases pain afferent signaling and results in chronic, pathologic itch (Lagerstrom et al., 2010). Concordantly, loss of Bhlhb5-dependent interneurons results in severe chronic itch and heightened acute itch behavior (Ross et al., 2010).

Bhlhb5-dependent interneurons gate chemical itch. A different class of interneurons, neuropeptide Y $(NPY)^+$ neurons, regulates mechanical itch associated with stimulation of hairy skin. Ablation of NPY^+ neurons in mice results in pathologic chronic itch. In NPY^+ neuron-ablated animals, low-threshold (0.02g - 0.4g) mechanical itch is upregulated while high-threshold mechanical itch and chemical itch are not (Bourane et al., 2015). $BhlhB5^{-/-}$ mice have normal NPY expression (Ross et al., 2010). Similarly, NPY^+ interneuron ablation spares Bhlhb5-dependent interneurons (Bourane et al., 2015). Based on this and corroboratory behavior, NPY^+ and BhlhB5-dependent neurons are hypothesized to be non-overlapping populations with unique functions of gating mechanical and chemical itch respectively.

1.2 *Mas-related G-Protein Coupled Receptors* (Mrgprs) in itch biology

1.2.1 As markers of peripheral itch neurons

In 2013, itch-specific peripheral neurons were first identified. These neurons express Mrgpra3, exclusively innervate epidermis, and are responsive to mechanical

stimuli, heat, and numerous pruritogens (Han et al., 2013). Ablation of Mrgpra3^{+} neurons decreases acute pruritus associated with chloroquine, SLIGRL, BAM8-22, histamine, endothelin-1, α-Me-HT, and two models of chronic itch: allergic and dry skin. Importantly, ablation of Mrgpra3^{+} neurons does not affect pain, and activation of these neurons results in exclusive itch. Based on these data, Mrgpra3^{+} neurons, despite expression of pain-associated channels, are hypothesized to be itch specific neurons in the peripheral nervous system.

While Mrgpra3^{+} neurons are itch-specific, not all Mrgpr-expressing neurons are exclusively involved in itch. For example, Mrgprd^{+} neurons are believed to be a population of non-peptidergic mechanical pain-sensing afferents. Genetic ablation of Mrgprd^{+} neurons reduces sensitivity to noxious mechanical injury and not heat or cold (Cavanaugh et al., 2009; Rau et al., 2009; Wang and Zylka, 2009). *In vivo* calcium imaging of Mrgprd^{+} neurons reveals that they are activated by painful pinch (Vrontou et al., 2013).

1.2.2 Initial identification of Mrgprs

Mrgpra3 is a member of the Mrgpr family of GPCRs. This family was first identified in a subtractive cDNA screen between WT and neurogenin1 (Ngn1)$^{-/-}$ mice, animals lacking TrkA^{+}, small-diameter nociceptive neurons (Dong et al., 2001). This screening strategy biased discovery for nociceptor-specific sequences. Indeed, Mrgpra1, the first Mrgpr sequence cloned, was found to be enriched in a subset of nociceptors in mouse DRG and TG. Using this sequence as a template, a bioinformatic search identified over 50 sequence similar Mrgprs in mice (27 with intact open reading frames). In humans, eight intact MRGPR open reading frames were cloned (Dong et al., 2001). Of the human

genes, four of them, MRGPRX1-X4, appeared to be most similar to the murine MrgA subfamily. However, one-to-one homology between mouse and human sequences could not be confidently assigned. In contrast, human MRGPRs: D, E, F, and G all had single-gene mouse orthologs.

After initial identification of the Mrgpr family, two subsequent studies used degenerate-oligonucleotide PCR to clone a sequence-similar receptor, termed sensory-neuron specific receptor (SNSR) from rat DRG, brain, and spinal cord tissue (Bender et al., 2002; Lembo et al., 2002). Due to sequence similarity, the International Union of Basic and Clinical Pharmacology (IUPHAR) has since reclassified SNSRs as Mrgprs (Bader et al., 2014). Today, IUPHAR recognizes the existence of several Mrgpr subfamilies: A, B, C, D, E, F, G, H, and a primate-specific X.

1.2.3 Expression and genetic expansion in mice

Mrgprs are expressed in sensory neurons of the DRG and trigeminal ganglia (TG), numerous brain regions, the enteric nervous system, and, more recently, in immune cells like dendritic and mast cells. Some Mrgprs, such as Mrgpra1 in mice and MRGPRX1 in primates, are specifically expressed in sensory neurons of the DRG and TG (Dong et al., 2001; Lembo et al., 2002). Others, like Mrgpre, Mrgprf, and Mrgprb2, are expressed in different regions and cell types. Mrgpre (MRGPRE in humans) is expressed in numerous brain regions of the central nervous system and the enteric nervous system (Avula et al., 2011; Zhang et al., 2005). Mrgprf is also expressed in the enteric nervous system and in smooth muscle cells (Avula et al., 2011). Mrgprb2, a murine receptor, and MRGPRX2, a human receptor, are expressed in mast cells (Kashem et al., 2011; McNeil et al., 2015; Subramanian et al., 2011a; Subramanian et al., 2011b).

Study of Mrgpr function has been complicated by a murine-specific expansion of the Mrgpr locus which resulted from an L1 retrotransposon insertion and multiple rounds of unequal crossover (Dong et al., 2001; Zylka et al., 2003). Mice express dozens of sequence-similar Mrgpr coding sequences, making compensation a likely experimental hurdle. With this consideration in mind, our lab has employed a cluster deletion strategy (Cluster$^{-/-}$) to study Mrgpr function in mice. Cluster$^{-/-}$ mice are missing 12 intact Mrgpr coding regions. These mice are viable and produce healthy progeny. Compared to WT, Cluster$^{-/-}$ animals have similar numbers of nociceptive neurons and no appreciable changes in proportions of sensory neuron type, indicating that Mrgpr expression is not important for itch neuron survival or targeting of neuronal fibers to skin. In recent years, behavioral studies in Cluster$^{-/-}$ animals and cellular ligand-activity assays have identified functional, but not sequence-based, pairings between mouse and human receptors. For example, Mrgpra3/c11 are considered the mouse orthologs of MRGPRX1 and Mrgprb2 the ortholog of MRGPRX2, based on shared response to ligands.

1.2.4 As itch receptors

As GPCRs, Mrgprs can engage second messenger pathways in order to change cellular function. Mrgprs have been demonstrated to be coupled to numerous G-protein subunits and thereby capable of affecting intracellular signaling through a variety of pathways (Bader et al., 2014; Han et al., 2002; Solinski et al., 2014). For example, in sensory neurons, Mrgpra3 signaling is blocked by both gallein, a Gβγ inhibitor, and ruthenium red, a nonspecific inhibitor of numerous TRP channels. These data indicate that activation of Mrgpra3 signals through both Gβγ and TRP channels in order to excite neurons (Liu et al., 2009). In a divergent signaling pathway, Mrgprc11-associated

calcium flux is blocked by inhibitors of phospholipase C (PLC) signaling and not by gallein.

In 2009, Mrgpra3/MRGPRX1 were shown to be receptors for chloroquine, an antimalarial drug associated with non-histaminergic itch (Liu et al., 2009). Chloroquine elicits intense pruritus in mice in an Mrgpra3-dependent manner. Cluster$^{-/-}$ mice (lacking Mrgpra3) are protected from chloroquine itch while having intact serotonin itch, mast cell-mediated itch, and pain response (Liu et al., 2009).

Chloroquine-associated itch was the first linking of Mrgprs as a receptor for a non-histaminergic pruritogen. Since that study, several Mrgprs have been identified as receptors for additional non-histaminergic pruritogens including bovine adrenal medulla peptide 8-22 (BAM8-22) (Mrgprc11), protease-produced peptides like SLIGRL (Mrgprc11), and β-alanine (Mrgprd) (Liu et al., 2011). BAM8-22, proteases, and β-alanine all elicit itch in humans without wheal and flare, which provides physiological evidence of mast cell involvement (Sikand et al., 2011).

Both BAM8-22, a ligand for Mrgprc11, and chloroquine, an activator of murine Mrgpra3, activate human MRGPRX1(Liu et al., 2009). In this case, ligand-receptor pairs highlight a possible functional link between mouse Mrgpra3 and Mrgprc11 receptors. Alternatively, SLIGRL, another ligand of Mrgprc11, activates both MRGPRX1 and MRGPRX2, linking a single murine Mrgpr to two different human MRGPRs.

1.2.5 As mast cell - expressed receptors

Murine Mrgprb2 and human MRGPRX2 are two Mrgprs with specific expression in non-neuronal cells. Both receptors are exclusively expressed in mast cells, resident sentinel cells of skin, lung, and intestine (McNeil et al., 2015; Subramanian et al., 2011a;

Tatemoto et al., 2006). Mast cell granules contain a range of bioactive molecules including histamine, serotonin, proteases, prostaglandins, and cytokines (Theoharides et al., 2012). Classical studies of mast cell activation have focused on antigen binding IgE and cross-linking of IgE receptor. However, numerous basic secretagogue peptides including various toxins, neuropeptides, and hormones can activate mast cells through non-IgE mechanisms (McNeil et al., 2015; Solinski et al., 2014; Subramanian et al., 2011a; Subramanian et al., 2011b; Tatemoto et al., 2006). Recently, Mrgprb2/X2 have been identified as the long sought after basic secretagogue receptors that are activated by THIQ motif-containing small molecules and positively charged compounds.

1.3 Non-histaminergic itch conditions of interest

As sensory neuron-expressed receptors for pruritic agents, Mrgprs have been previously linked to acute itch. However, Mrg receptor involvement in chronic itch conditions has not been addressed. Chronic pruritus is a complex and often debilitating symptom that accompanies a range of cutaneous and non-cutaneous diseases (Ständer et al., 2007; Yosipovitch and Bernhard, 2013a). The most widely known pruritogen is histamine, which is secreted by mast cells in the skin and activates histamine receptors on nearby sensory neurons (Bautista et al., 2014; Ikoma et al., 2006; LaMotte et al., 2014; Yosipovitch and Bernhard, 2013b). While viable treatments exist for histamine-mediated itch, most non-histaminergic conditions are more difficult to treat because the mediators are often unknown (Kremer et al., 2011). Major causes of clinically relevant non-histaminergic itch include primary skin disorders, like allergic contact dermatitis, chronic kidney disease, and liver and gallbladder disease. In this thesis, I focus primarily on two itch conditions: cholestatic pruritus and allergic contact dermatitis.

1.3.1 Cholestatic pruritus

In the United States, hundreds of thousands of patients with cholestasis report experiencing a severe, generalized pruritus (itch). Cholestasis, or the slowing or stoppage of bile flow, can result from numerous liver and gallbladder diseases. Cholestatic patients do not exhibit classic signs of histamine release such as erythema or swelling (Bergasa, 2014), and cholestatic itch does not respond to histamine receptor antagonists (Bergasa, 2014; Beuers et al., 2014; Hegade et al., 2016). Instead, the most effective treatments for cholestatic itch are physical removal of the causative obstruction when applicable (such as in the case of gallstones), draining bile, or a liver transplant (Appleby et al., 2015; Hegade et al., 2016; Hofmann and Huet, 2006). Because on the success rate of these procedures, the causative pruritogens of cholestatic pruritus are hypothesized to originate from bile. Leading candidates include opioids, lysophosphatidic acid, bilirubin, and bile acids.

Endogenous opioids, bile acids, and autotaxin, the enzyme that produces lysophosphatidic acid, are upregulated in both cholestatic animal and patient serum (Swain et al., 1992; Thornton and Losowsky, 1988, 1989a, b). Opiod and bile acid serum levels do not correlate with itch while autotaxin levels have high positive prediction value for cholestatic pruritus (Kremer et al., 2012). In small clinical trials, both opioid antagonists and bile acid binding resins have been demonstrated to be effective in controlling cholestatic itch (Bergasa, 1998; Bergasa et al., 1998; Bergasa et al., 1992; Swain et al., 1992). However, the effectiveness of bile acid binding resins has been challenged (Kremer et al., 2010; Kuiper et al., 2010).

Cholestasis will often result in jaundice, a yellowing of the skin and eyes that occurs due to elevated levels of bilirubin depositing in skin. Bilirubin is a downstream metabolite of heme. In cells, heme is broken down by heme oxygenase 1 (HMOX1) to biliverdin, which is reduced by biliverdin reductase (BVR) to bilirubin. Bilirubin is extremely lipophilic can cross cell membranes. In serum, bilirubin is typically bound to albumin. In the liver, bilirubin is conjugated to glucuronic acid by UGT1A*28 to form a water-soluble compound. Both conjugated and unconjugated bilirubin are excreted in bile. Bilirubin is not thought to play a role in cholestatic pruritus because serum levels of bilirubin do not correlate with severity of pruritus in human patients (Bergasa, 2014). Furthermore, there are numerous examples of non-pruritic jaundice conditions such as Dubin-Johnson and Crigler-Najjar disease (Strassburg, 2010). At physiologic and mildly elevated concentrations (0.2-2.7 mg/dL, 3.4 - 46.2 μM), bilirubin is benign and thought to have a cardioprotective effect (Bulmer et al., 2013; Vitek et al., 2002).

1.3.2 Allergic contact dermatitis

Allergic contact dermatitis (ACD) is a type IV hypersensitivity reaction that typically presents as an intensely pruritic, eczematous skin rash that is not amenable to antihistamine treatment (Kostner et al., 2017). Disease develops when an organism comes in contact with a hapten that combines with skin antigens to promote a dendritic-cytotoxic T-cell response against skin cells (Kostner et al., 2017). After initial sensitization to an exogenous hapten, further contact will elicit a severe dermatologic reaction.

Mast cells have been demonstrated to modulate ACD disease severity via release of both pro- and anti-inflammatory cytokines (Askenase et al., 1983; Dudeck et al., 2011;

Gimenez-Rivera et al., 2016; Grimbaldeston et al., 2007). In ACD skin, multiple potential Mrgprb2 and MRGPRX2, mast cell receptor, agonists, such as neuropeptides, are upregulated. Release of cytokines from both mast cells and other immune cells have been demonstrated to be involved in ACD-itch, including IL-33 activation of neuronal ST2 and T-cell release of IL-31 (Liu et al., 2016; Takamori et al., 2018).

1.4 Thesis goals

Mrgprs have been identified as receptors for numerous non-histaminergic pruritogens. However, at the time of this thesis's inception, all previously published Mrgpr ligands were non-physiologic molecules, and Mrgpr involvement in clinically relevant pathological itch had not been addressed. Based on acute itch studies and expression data, I hypothesized that Mrgprs could play a role in mediating chronic itch conditions. The goals of my thesis were to test this hypothesis. I was specifically interested in cholestasis and ACD due to widespread prevalence and a lack of effective treatment. As secondary goals, I was interested in probing the potential interactions between mast cells and sensory nerves and also functionally characterizing the recently identified mast-cell Mrgprs, b2 and X2.

2. Methods

Group data were expressed as mean ± SEM unless otherwise noted. Two-tailed unpaired Student's t-tests, Two-way ANOVA, Fisher's exact test, and Chi-squared tests were used to determine significance in statistical comparisons, and differences were considered significant at $P < 0.05$. Statistical power analysis was used to justify sample size, and variance was determined to be similar among all treatment groups as determined by F test unless otherwise noted. No samples or animals subjected to successful procedures and/or treatments were excluded from analysis. All behavior experiments were designed in a blocked manner with consideration for both genotype and treatment.

2.1 Experimental animal models

Mice were housed 2-5 per cage with a 12-hour light/dark cycle and *ad libitum* access to rodent chow and water. Behavior assessments were performed during the light phase. All experimental protocols were approved by the Animal Care and Use Committee at the Johns Hopkins University School of Medicine (Protocol Number: MO16M40). All mice used for this study were born and bred within Hopkins Miller Research Building Animal facility and weaned at 3-3.5 weeks of age. Mice used for experiments were 1.5-3 months old males and females (20 - 30g) on the C57BL/6 background unless otherwise noted.

Mrgpr-clusterΔ$^{-/-}$, *Mrgpra1*^{GFP}, *Mrgprd*^{PLAP}, Tg(*Mrgpra3-Cre*), Tg(*Pirt-Cre*), Mrgprb2$^{-/-}$, and Tg(*Mrgprb2*-Cre) were generated as previously described (Dong et al., 2001; Liu et al., 2009; 2007; Han et al., 2012; Kim et al., 2014; McNeil et al., 2015). Rosa26^{lslGCaMP6s}, Rosa26^{lsltdTomato}, and cKit$^{W\text{-}sh}$ (SASH) mice were purchased from Jackson Labs. (Kim et al., 2016)*Mrgpra1*$^{-/-}$ mice were generated using CRISPR-Cas9 on

the C57BL/6 background using the following guide RNA sequence: TTCCCAGCAGCACCTGTGCA GGG. *Blvra*$^{-/-}$ mice were generated at Ozgene (Australia) on a C57BL/6J background. +X4 humanized mice were generated by crossing Tg(*Mrgpra3-Cre*) mice with newly generated ROSA26^{lslMRGPRX4} mice (129svJ/Bl6 mixed background). ROSA26^{lslMRGPRX4} mice were generated by homologous recombination of an MRGPRX4 cDNA construct under loxp-STOP-loxp control to the ROSA26 locus.

2.1.1 Behavior

All applicable behavioral tests were performed and analyzed with the experimenter blind to genotype and with littermates if possible. All mice used were 8-12 week males and females (20 to 30 g). There were no significant differences in itch between male and female mice. All itch behavior experiments were performed between 8 a.m. and 12 p.m. On the day before the experiment, animals were placed in the test chamber for 30 minutes before being subjected to a series of three mock injections with 5-minute break periods in between. On the day of the experiment, animals were first allowed to acclimatize to the test chamber for 10 minutes before injection. Pruritic compounds were subcutaneously injected into the nape of the neck (50μL volume) or cheek (10μL volume), and scratching behavior was observed for 30 minutes. A bout of scratching was defined as a continuous scratching movement with either hindpaw directed to the injection site. In the cheek injection model, a wipe was defined as a single forepaw stroking the site of the injection. Use of both forepaws on the face or cheek was considered as grooming behavior. Scratching behavior was quantified by counting the number of scratching bouts at 5 min intervals over the 30-min observation period. Wiping was quantified at 2 min intervals over a ten-minute observation period. All

pharmacological antagonists were given intraperitoneally thirty minutes prior to injection of pruritogen.

Bilirubin is highly susceptible to oxidation and photolysis. Accordingly, bilirubin was freshly prepared just prior to each experiment in either DMSO or 0.1 M NaOH and then maintained in the dark. For calcium imaging analyses, bilirubin was diluted into calcium imaging buffer a few seconds before use. Final concentration of DMSO in all applicable tested solutions was < 0.5%. To maintain the integrity of bilirubin in human plasma samples, samples were stored at -80°C until use. Plasma stocks were maintained in the dark to minimize photolysis during injection or experimental manipulation. Plasma bilirubin was evaluated by HPLC as described above. All other drugs were prepared as 100 µl – 1,000 µl aliquots and stored at -20°C before thawing at 4°C. Freeze/thaw cycles were avoided whenever possible. To remove microprecipitates, we centrifuged our bilirubin solutions at 21,000g for 20 min to ensure that bilirubin was in solution. Whenever physiologically and experimentally reasonable, we excluded divalent cations in our in vitro biophysical experiments.

2.1.2 Models of Cholestatic Itch

1-naphthyl isothiocyanate (ANIT; Sigma) was solubilized in olive oil (Sigma). Animals were dosed with 25 mg/kg ANIT *per os* daily for five days. On day five, animals were acclimatized for itch behavior. On day six, animals were placed in test chambers and videotaped for one hour. The number of scratching bouts, defined as a continuous scratching movement with either hindpaw, was counted and binned in five minute intervals during the one hour period. After itch behavior was assessed, animals were administered pentobarbital (50 mg/kg, *i.p.)*. Blood was collected by cardiac puncture and

placed into heparinized tubes (BD Biosciences). After centrifugation, plasma was collected, aliquoted, and stored at -20°C until analysis. Bile acid levels were assessed by a fluorometric kit from Cell Biolabs. When applicable, mice were then proceeded for histology. For QWF antagonism of cholestatic itch, Day 5 ANIT-treated animals were dosed with either 1mg/kg QWF dissolved in PBS or PBS vehicle *i.v.* via tail vein injection approximately 10 minutes before behavioral assessment of spontaneous itch. The dose was chosen based on previous studies (Azimi et al., 2017) as well as published pK data indicating stability in plasma ($t_{1/2}$ = 70 min).

2.1.3 Models of allergic contact dermatitis

For ovalbumin associated itch, we first sensitized animals by injecting 50 μg of ovalbumin in phosphate-buffered saline (PBS) with 2 mg of aluminum hydroxide i.p. 10 days later, animals were re-injected i.p. with 20 μg of ovalbumin in PBS containing 2 mg of aluminum hydroxide. After one week, 50 μg of ovalbumin in saline was administer and scratching behavior was quantified. Contact dermatitis model was performed by first shaving the abdomens of animals the day prior to experimentation. Shaved abdomens were treated with 40μl of either 3% DNCB, SADBE, or Oxazolone dissolved in acetone: olive oil (4:1 v/v) QD for three days. After four days, the nape of the neck of animals were shaved. The next day, 1% DNCB, SADBE, or Oxazolone dissolved in acetone: olive oil (4:1 v/v) was applied to shaved skin QD for three days. The next day, animals were habituated by being placed in the test chamber for 1 hour. The following day, behavior was assessed, and skin samples were collected. For skin thickness measurements, animals were sensitized with 100μl of either 3% DNCB, SADBE, or Oxazolone dissolved in acetone: olive oil (4:1 v/v) on shaved abdomen. Five days later,

10µl of respective agent was applied to each side of the right ear. At the same time, 10µl of vehicle was applied to each side of the left ear. 24 hours later, ear thickness of both right and left ears was assessed with Mitutoyo digimatic calibrator.

2.2 Human sample collection

Plasma from patients suffering from hyperbilirubinemia, specifically cholestasis, was isolated under a protocol approved by the Institutional Review Board at the Johns Hopkins University School of Medicine (Study number: IRB00154650). Control plasma was isolated from donors who did not exhibit kidney or liver disease, had no complaints of itch, and were free from any detectable viral infection (HCV, HBV, HIV). Both cholestatic and control plasma were isolated under protocols approved by the Institutional Review Board at the Johns Hopkins University School of Medicine (Cholestasis Study number: IRB00154650; Control study number: NA_00013177, the Johns Hopkins Department of Dermatology Patient Database and Tissue Bank). Whole blood was collected into PAXgene tubes (PreAnalytiX 761115) and centrifuged for 5 minutes at 300g. Plasma was then collected, aliquoted, and stored at -20°C until experimentation. At time of plasma collection, a 5D itch questionnaire was administered.

De-identified human skin tissues were obtained under IRB-exempt protocols through the Division of Dermatology at Washington University School of Medicine and the Skin Biology and Diseases Resource-based Center at the Perelman School of Medicine at the University of Pennsylvania. Allergic contact dermatitis lesional skin was obtained from eleven patients aged 17 - 89. Eight patients were female, and three patients were male. Healthy control skin was taken from eight patients aged 29 – 47. All healthy skin was collected from female patients. Besides allergic contact dermatitis where

indicated, all patients were otherwise healthy. Skin tissue sections from were obtained from biopsy specimens that were fixed in 10% neutral buffered formalin and embedded in paraffin.

2.3 *In vitro* Ca^{2+} imaging and analysis

All cultured cells were maintained in DMEM supplemented with 10% FBS and 1% Penicillin/Streptomycin at 37°C, 5% CO_2. All data included were generated from cells tested for mycoplasma and found to be negative. Cells were imaged in calcium imaging buffer (CIB; 10 mM HEPES, 1.2 mM $NaHCO_3$, 130 mM NaCl, 3 mM KCl, 2.5 mM $CaCl_2$, 0.6 mM $MgCl_2$, 20 mM glucose, and 20 mM sucrose at pH 7.4 and 290-300 mOsm). To monitor changes in intracellular [Ca^{2+}] ([Ca^{2+}]$_i$), cells were loaded with either Fura 2-AM (HEK293 cells) or Fluo 4-AM (DRG neurons and mast cells) for 30 min in the dark at 37°C in CIB just prior to imaging. With Fura 2-AM, emission at 510 nm was monitored from excitation at both 340 nm and 380 nm. With Fluo 4-AM, emission at 520 nm was monitored from excitation at 488 nm. Cells were identified as responding if the intracellular [Ca^{2+}] rose by either 50% compared to baseline or 50% compared to the [Ca^{2+}]$_i$ change assayed during addition of 50 mM KCl (neurons only). Damaged, detached, high-baseline, and motion-activated cells were excluded from analysis.

HEK293 cells

In initial screens, HEK293 cells stably expressing the murine G-protein alpha-subunit $G_{\alpha 15}$, a unique G_α protein that non-selectively couples a large variety of GPCRs to phospholipase C [30], were plated on poly-D-lysine-coated coverslips and transiently transfected with constructs encoding the MRGRPR of interest. 12-24 h later, cells were loaded with the Fura 2-AM. Unless otherwise specified, compounds were perfused into

the imaging chamber for approximately thirty seconds after a baseline period was established. Response was then monitored at 5 s intervals for an additional 60 s.

DRG neurons

DRGs were incubated with Fluo-4 AM 24 hour after dissociation (native genotype) or 48 hour after dissociation (virally transduced). Unless otherwise noted, cells were imaged for 20 sseconds to establish a baseline before compounds were added. After 30 s, a 2 min wash was applied before addition of another substances. At the end of every imaging trial, 50 mM KCl was added as a positive control. Cells included in calculating percentages all displayed at least a 50% increase in $[Ca^{2+}]_i$ compared to baseline upon addition of KCl. For ruthenium red inhibitor experiments, neurons were incubated with 10 μM ruthenium red for 5 minutes prior to imaging. Percentage activated was determined as earlier described.

Mast cells

Mast cells were purified as described and plated onto glass coverslips coated with 30 mg/mL fibronectin and allowed to recover for 2 h at 37°C. Cells were then loaded with Fluo-4 AM.

EC_{50} and IC_{50} determinations

HEK293 cells stably expressing either MRGPRA1, MRGPRX4, and MRGRPC11 were seeded in poly-D-lysine-coated 96-well plates at 10,000 cells/well. Cells were loaded with Fura 2–AM, washed twice, and maintained in CIB. Haem metabolites were freshly dissolved in DMSO in dim light and then diluted into a buffer comprised of 20 mM Tris and 150 mM NaCl at pH 8.8. Potential changes in pH were evaluated prior to each experiment. EC_{50} values were determined from dose-responses performed in

triplicate, repeated 2-4 times. To determine potential antagonism by QWF against bilirubin, cells were treated with varying doses of QWF for 1 min in CIB prior to application of agonist.

2.4 *In vivo* DRG Ca^{2+} imaging

DRG exposure surgery was performed as previously described (Kim et al., 2014). Throughout the surgery, mice were kept on a heating pad (DC temperature controller, FHC) to maintain body temperature at 37°C ± 0.5°C as monitored by rectal probe. Mice were anesthetized by i.p. injection of sodium pentobarbital (40 mg/kg) and their backs were shaved and disinfected. Ophthalmic ointment (Lacrilube; Allergen Pharmaceuticals) was then applied. An approximately 2-cm midline incision was made at the lower part of the lumbar enlargement and 0.1 mL of 1% lidocaine was injected into the paravertebral muscles before they were dissected away to expose L3–L5 vertebrae. Using rongeurs, the surface aspect of the L4 DRG transverse process was removed and the underlying DRG was exposed. Bleeding was stopped using styptic cotton.

In vivo imaging of whole L4 DRG was performed for 1–3 hours immediately following surgery. Images were acquired using a laser-scanning confocal microscope (Leica LSI microscope) equipped with a 53 0.5 NA macro dry objective and fast EM-CCD camera. Live images were acquired at 8 to 10 frames in frame-scan mode per 7–8 seconds, at depths of 0 to 70 mm below the dura with the DRG in the focal plane. Throughout imaging, body temperature was maintained at 37°C ± 0.5°C with a heating pad and rectal temperature monitoring. Anesthesia was maintained with 2% isofluorane and pure oxygen delivered through nosecone. Mice were laid abdomen-down on a custom-designed microscope stage. The spinal column was secured at two sites using

clamps. Imaging was monitored during the activation of DRG neuron cell bodies by peripheral stimuli (5µl of the stated concentration of either mast cell or neuronal activators) delivered via Hamilton syringe.

For imaging data analysis, raw image stacks were collected, deconvoluted, and imported into ImageJ (NIH). Optical planes from sequential time points were re-aligned and motion corrected using the stackreg rigid-body cross-correlation-based image alignment plugin. The number of counted activated neurons between different mice and different DRG imaging periods was normalized to the total number of neurons present in the DRG. The total number was counted using the thresholding function in ImageJ software from a high-quality, Z-stack image of DRG at baseline. The size of activated neurons was calculated using the area function in ImageJ.

Calcium signaling amplitudes were normalized F_t/F_0 as a function of time. F_0 was defined as the average pixel intensity during the first two to six frames of each imaging experiment. Changes in fluorescence were measured from all neurons that displayed a change from baseline and selected for further analysis. In subsequent analysis, neurons that displayed $< 0.2\ F_0$ change in baseline, were only active during the injection period, and displayed a $> 0.2\ F_0$ change during either the baseline or the saline imaging periods were excluded from analysis. The peak area was measured using the area under the curve (AUC) functionality in GraphPad PRISM. Signal peaks were defined as a $>0.2F_0$ increase over baseline followed by either a return to baseline ± 10% or normalization of signal by $>0.2F_0$. Shoulder peaks were defined as those peaks that occur before both a return from peak to baseline ± 10% F_0 and before normalization of signal by $>0.2F_0$ and were excluded from analysis. There is significant activation associated with injection into

the paw. In determining whether a neuron was activated within an imaging window, the neuron, represented by its designated region of interest (ROI) needed to exhibit multiple peaks of $> 0.2F_0$ from baseline outside of the first minute after injection. All putative responding cells and counted peaks included in analysis were verified visually using the raw imaging data and individual neuron calcium traces. The average F_t/F_0 values for specific ROIs were tested for statistical significance by repeated measures ANOVA, followed by Mann-Whitney statistics. Fiji (NIH), LIF (Leica), and PRISM software were used to analyze and plot Ca2+ imaging data.

3. Results

3.1 Identification of a bilirubin receptor that may mediate a component of cholestatic itch (text adapted from Meixiong, Vasavda et al., *eLife* 2019)

Despite the long-standing association between jaundice and pruritus (Talwalkar et al., 2003), bilirubin itself has not been tested as a pruritogen. To determine whether bilirubin elicits pruritus, I subcutaneously injected bilirubin into the napes of mice. Pathophysiologic concentrations of bilirubin stimulated scratching in a dose-dependent manner at the site of injection (**Figure 1A**). Pre-incubating bilirubin with excess human serum albumin, which binds bilirubin with high affinity (Breaven et al., 1973; Griffiths et al., 1975; Jacobsen and Broderson, 1983), elicited fewer scratches (**Figure 1A**). The behavioral profile of bilirubin-induced scratching mirrored that of two well-characterized pruritogens, histamine and chloroquine (**Figure 1B**). Notably, histamine and chloroquine only elicit itch when injected into mice at millimolar concentrations despite having nanomolar affinity towards their receptors. In comparison, bilirubin elicited a similar degree of itch even when injected at lower concentrations than histamine or chloroquine (**Figure 1B**). Since mice indiscriminately scratch if injected at the nape with substances that trigger either itch or pain, we also injected mice at the cheek. Unlike at the nape, painful sensations at the cheek evoke a distinct wiping behavior instead of scratching, whereas itchy sensations still elicit scratching (Shimada and LaMotte, 2008). Injecting bilirubin in the cheek prompted dose-

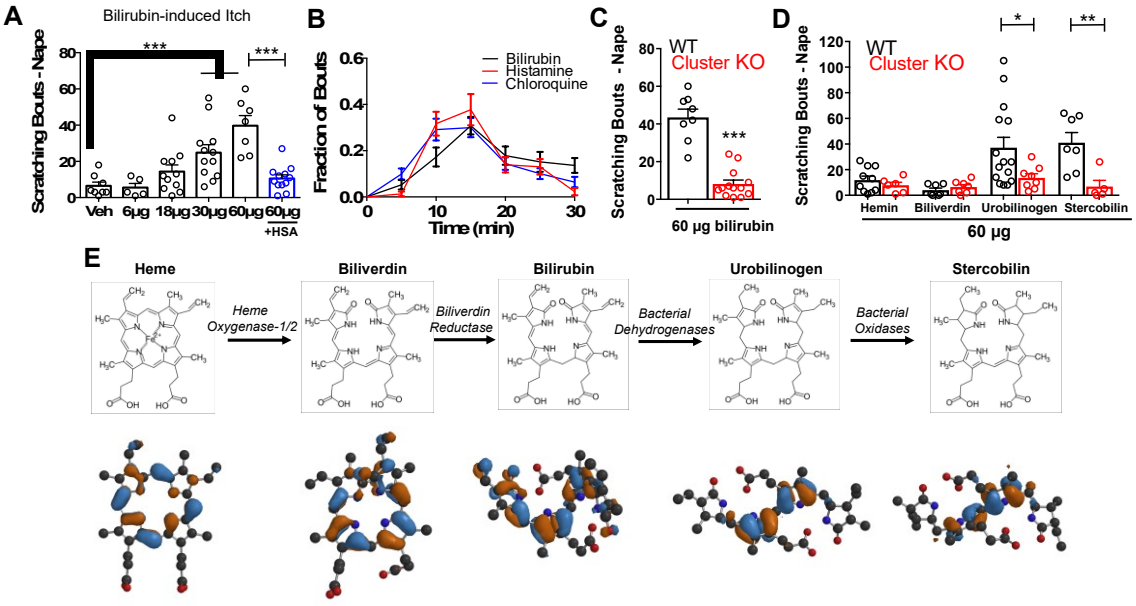

Figure 1. Bilirubin elicits non-histaminergic, *Mrgpr*-dependent pruritus. (**A**) Scratching bouts associated with injection of bilirubin. The indicated amount of bilirubin was injected into the nape of mice. The blue bar (+HSA) represents animals injected with 60 µg bilirubin pre-incubated with 1% human serum albumin. Veh n=8; 6 µg n=5, 18 µg n=11, 30 µg n=12, 60 µg n= 7, +HSA n=12. (**B**) Time course of itch behavior associated with bilirubin, histamine, or chloroquine. Scratching bouts were binned according to 5-minute intervals. Bilirubin n=16, Histamine n= 13, Chloroquine n=11. (**C**) 60 µg bilirubin was injected into the nape of WT and Mrgpr-cluster KO littermates. WT n=8, Mrgpr-cluster KO n= 13. (**D**) 60 µg of the indicated metabolite was injected into WT and Mrgpr-cluster KO littermates. Hemin (WT n=10, Mrgpr-cluster KO n=6), Biliverdin (WT n= 7, Mrgpr-cluster KO n= 7), Urobilinogen (WT n=15, Mrgpr-cluster KO n=8), Stercobilin (WT n=7, Mrgpr-cluster KO n=5). (**E**) The pathway of heme degradation. The skeletal formula of each metabolite is depicted above its optimal 3D geometry, as calculated by a B3LYP functional and 6-31G(d) basis set. Blue and orange represent orbital parity of each metabolite's HOMO obtained from DFT calculations. (**A, C, D**) Mean ± s.e.m. depicted. Each open circle represents an individual mouse. *, $P < 0.05$; **, $P < 0.01$; ***, $P < 0.001$; two-tailed unpaired Student's *t*-test.

dependent scratching just as it did at the nape (**Figure 2A**). Bilirubin elicited neither wiping nor licking, indicating that it selectively triggers itch and not pain (**Figure 2B-C**).

We injected mice with similarly structured metabolites to determine the specificity of bilirubin's pruritic activity (**Figure 1E**). The two metabolites directly epistatic to bilirubin, hemin and biliverdin, did not induce scratching despite also being tetrapyrroles (**Figure 1D**). While hemin, biliverdin, and bilirubin display only minor atomic and electronic differences between them, they vary substantially in their

physiochemical properties and structures (**Figure 1E**). To better understand these differences, we performed density functional theory (DFT) calculations (Becke, 1993; Hohenberg and Kohn, 1964; Kohn and Sham, 1965; Stephens et al., 1994) followed by

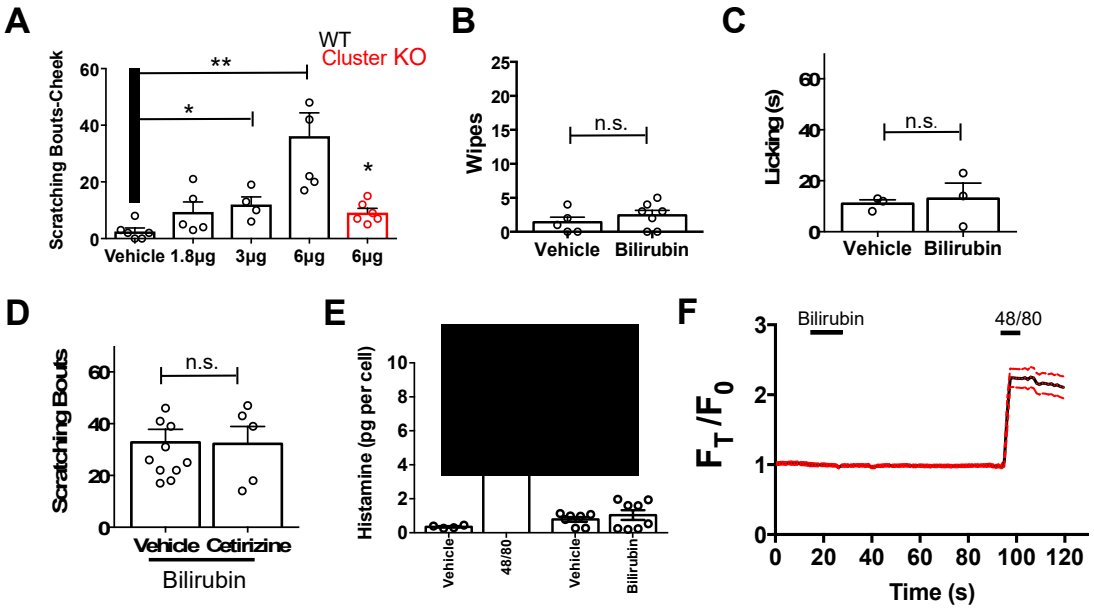

Figure 2. Bilirubin elicits non-histaminergic pruritus and not pain. (**A**) Scratching bouts associated with cheek injection of bilirubin. The indicated amount of bilirubin was injected in a 10 µl volume and the number of scratching bouts was assessed for 30 min. Vehicle n=6, 1.8 µg n=5, 3 µg n=4, 6 µg n=5, 6 µg (Mrgpr-cluster$\Delta^{-/-}$) n= 6. (**B**) Wiping associated with injection of 6 µg bilirubin into the cheek. Wipes were assessed for 10 min post-injection, vehicle n= 5, bilirubin n=7. (**C**) Lick time associated with injection of 6µg bilirubin into the paw. Licking was assessed for 10 min post-injection. n=3 per condition. (**D**) H1 blocker does not inhibit bilirubin-induced pruritus. Either vehicle or 30 mg/kg Cetirizine was given *i.p.* 30 min prior to injection of bilirubin at the nape of the neck. Scratching bouts were assessed for 30 min post-injection. Vehicle n= 10, Cetirizine n = 5. (**E**) Mast cell histamine release in response to 100 µM bilirubin. Vehicle for Compound 48/80 n=4, Compound 48/80 (10 µg/mL) n=4, Vehicle n=6, Bilirubin n=8. (**F**) Ca^{2+} imaging of murine peritoneal mast cells. After a 10s baseline, 100 µM bilirubin was added. 15s later, a 1min wash was applied before addition of 10µg/mL compound 48/80. Drugs were applied when indicated by the black bars. Mean ± 95% CI depicted. n=26. (**A-E**) Mean plus s.e.m. depicted. Open circles represent independent data points. *, $P < 0.05$; **, $P < 0.01$; ***, $P < 0.001$; two-tailed unpaired Student's *t*-test. n.s., not significant.

single point energy calculations to determine the optimal geometry of each metabolite. Unlike in heme and biliverdin, bilirubin's four pyrroles are extended and do not lie in the same plane (**Figure 1E**). DFT calculations revealed that urobilinogen and stercobilin, two bacterial metabolites derived from bilirubin, adopt a similar extended conformation. Both

urobilinogen and stercobilin were able to stimulate scratching behavior (**Figure 1D**), indicating that bilirubin's non-polar pyrroles may be important for its pruritic activity.

Patients with jaundice-associated pruritus receive little benefit from antihistamines (Carstens et al., 2014). Consistent with these clinical findings, the histamine receptor 1 blocker cetirizine (30 mg/kg, *i.p.)* failed to alleviate scratching behavior in mice injected with bilirubin (**Figure 2D**). Furthermore, bilirubin did not elicit a calcium response or induce appreciable histamine release from peritoneal mast cells (**Figure 2E-F**).

The Mas-related G-protein coupled receptor (*Mrgpr*) family of receptors is a major mediator of non-histaminergic pruritus (Han et al., 2012; Liu et al., 2012; 2009; Sikand et al., 2011). To test whether *Mrgpr*s mediate bilirubin-induced pruritus, we injected mice lacking a cluster of 12 *Mrgpr* genes (Mrgpr-cluster$\Delta^{-/-}$ or Mrgpr-cluster KO) with bilirubin (Liu et al., 2009). Mrgpr-cluster KO animals scratched approximately 75% less than wild type (WT) mice, indicating that one or more of the 12 *Mrgpr*s within the cluster mediates bilirubin-induced pruritus (**Figure 1C**).

To identify which *Mrgpr* is sensitive to bilirubin, we individually expressed each of the 12 *Mrgpr*s deleted in the Mrgpr-cluster KO mouse in human embryonic kidney (HEK) 293 cells and monitored changes in intracellular calcium upon applying bilirubin. To ensure we would observe a calcium response following a true ligand-receptor interaction, we expressed the receptors in HEK293 cells stably expressing the G-protein alpha-subunit $G_{\alpha 15}$, a G_{α} protein that couples GPCRs to intracellular calcium stores via phospholipase C (PLC).

Among the twelve cell lines expressing an *Mrgpr*, only MRGPRA1-expressing cells exhibited a calcium response to bilirubin (EC_{50} of 145.9 μM [96, 220]) (**Figure 3A, D**). The same cells that responded to bilirubin also responded to FMRF, an MRGPRA1

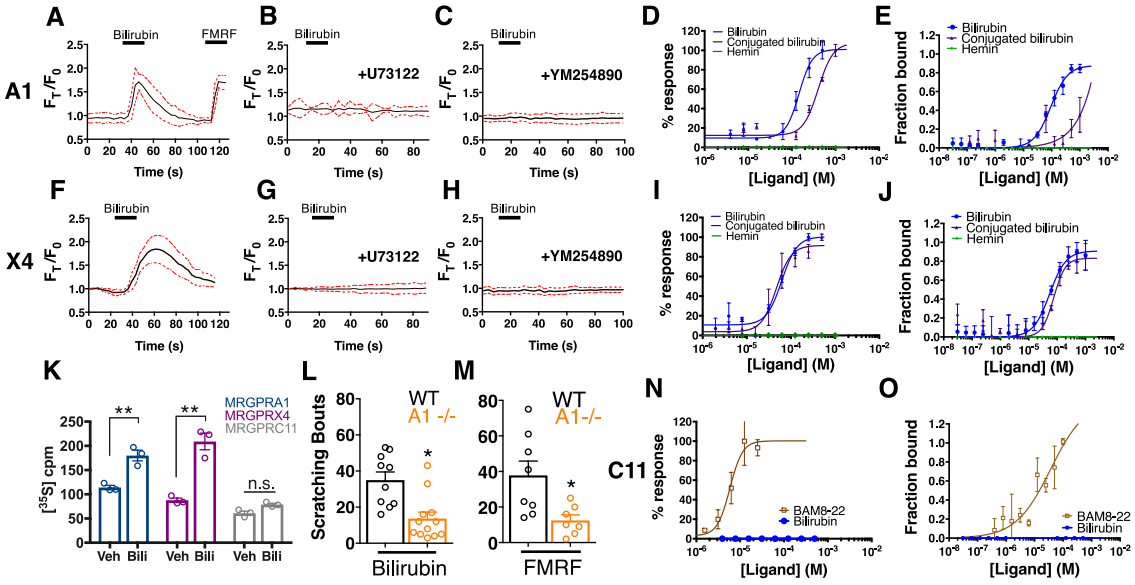

Figure 3. Bilirubin activates murine MRGPRA1 and human MRGPRX4. Ca^{2+} imaging and transformed binding isotherms of HEK293 cells stably expressing MRGPRA1 (**A-E**) or MRGPRX4 (**F-J**). (**A-C**, **F-H**) 50 μM bilirubin was added where indicated by black bars. After 15 s, a 1 min wash was applied. Mean ± 95% confidence interval (CI) depicted. n=10. In (**A**) 30 μM FMRF was added after washing as indicated by the black bar. In (**B-C**) and (**G-H**), cells were pre-incubated with either 10 μM of the PLC inhibitor U73122 or 10 μM of the $G_{\alpha q}$ inhibitor YM254890 for 30 min prior to imaging. Concentration–Ca^{2+} response curves of bilirubin, conjugated bilirubin, and hemin towards (**D**) MRGPRA1, (**I**) MRGPRX4, and (**N**) MRGPRC11 and BAM8-22 towards MRGPRC11, an established peptide ligand. Data are a representative experiment of 3 independent replicates performed in triplicate, depicted as mean ± s.e.m. Transformed binding isotherms for bilirubin, conjugated bilirubin, and hemin to (**E**) MRGPRA1, (**J**) MRGPRX4, and (**O**) MRGPRC11 and BAM8-22 to MRGPRC11. Data are an average of 3 independent experiments, depicted as mean ± s.e.m. (**K**) Bilirubin-stimulated G-protein activity of partially-purified MRGPRA1, MRGPRX4, and MRGPRC11 membrane complexes. [^{35}S]GTPγS binding was measured in the presence of 0.5% DMSO or 50 μM bilirubin. Mean ± s.e.m. depicted. **, $P < 0.01$; two-tailed unpaired Student's *t*-test. (**L**) Scratching bouts from injection of 60 μg of bilirubin in WT and A1 KO animals. WT n=10, A1 KO n=12. (**M**) Scratching bouts from injection of 60 μg of FMRF in WT and A1 KO animals. WT n=8, A1 KO n=7. (**L-M**) Mean ± s.e.m. depicted. Open circles represent individual mice. *, $P < 0.05$ by two-tailed unpaired Student's t-test.

agonist (Dong et al., 2001). To ensure that bilirubin initiated signaling at MRGPRA1 and not downstream, we pre-treated MRGPRA1-expressing cells with inhibitors of GPCR

signaling: the PLC inhibitor U73122 or the $G_{\alpha q}$ inhibitor YM-254890. Both compounds abolished bilirubin-induced calcium responses (**Figure 3B-C**).

In addition to bilirubin, glucuronidated bilirubin is often upregulated in jaundice-associated itch. We assessed whether ditaurate bilirubin, a distinct but similar bilirubin derivative, could activate MRGPRA1. Indeed, ditaurate bilirubin activated MRGPRA1-expressing cells (**Figure 3D)**. Hemin failed to activate MRGPRA1 (**Figure 3D),** consistent with our earlier behavioral findings in which hemin did not evoke scratching. No other *Mrgpr* among the 12 that we screened responded to bilirubin (**Figure 4**).

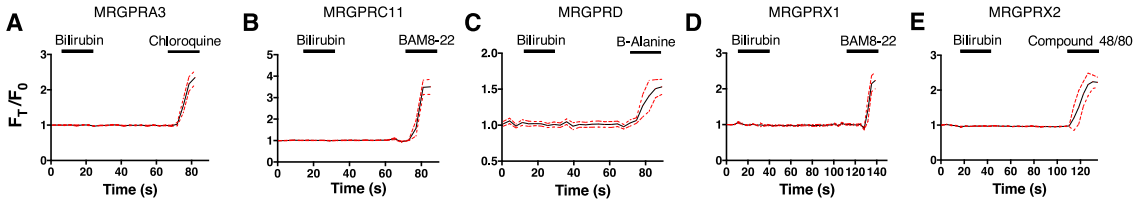

Figure 4. Bilirubin does not activate other itch-associated Mrgprs. (**A-E**) Ca^{2+} imaging of HEK293 cells transiently expressing (**A**) MRGPRA3, (**B**) MRGPRC11, (**C**) MRGPRD, (**D**) MRGPRX1, or (**E**) MRGPRX2. 50 μM bilirubin was added where indicated by black bars. After fifteen seconds, a one minute wash was applied. After washing, either (**A**) 1 mM chloroquine, (**B**) 3 μM BAM8-22, (**C**) 1 mM β-alanine, (**D**) 3 μM BAM8-22, or (**E**) 10 μg/mL compound 48/80 was added as indicated by black bars. Mean ± 95% CI depicted. n=10.

The human *MRGPRX* family of receptors has functional similarities between species but have no obvious structural homologs in rodents (Solinski et al., 2014; Zylka et al., 2003). The mouse *Mrgpra* family is closest in sequence homology to the human *MRGPRX* family (Dong et al., 2001; Lembo et al., 2002; Zhang et al., 2005). Of the four human MRGPRX receptors, only MRGPRX4-expressing cells responded to bilirubin (EC_{50} of 61.9 μM [44, 87]) (**Figure 3F, I**). U73122 and YM-254890 inhibited bilirubin-induced calcium responses in MRGPRX4-expressing cells just as with MRGPRA1

(**Figure 3G-H**). Conjugated bilirubin also activated MRGPRX4, whereas hemin had no effect (**Figure 3I)**.

To confirm that bilirubin directly binds the identified receptors, we assayed thermophoresis of each receptor in the presence and absence of bilirubin. Thermophoresis of a molecule is affected by physical parameters such as size, charge, and solvation. By extension, the thermophoresis of one molecule is altered when it interacts with another, and can therefore be used to measure interactions between molecules (Duhr and Braun, 2006). Using this approach, we determined that bilirubin bound MRGPRA1 with a K_D of 92.9 ± 15 μM and MRGPRX4 with a K_D of 54.4 ± 13 μM (**Figure 3E, J**). Bilirubin exhibited little to no affinity for the closely related BAM8-22 receptor MRGPRC11 (**Figure 3O**). Hemin, which did not activate MRGPRA1 or MRGPRX4 by calcium imaging (**Figure 3D, I**), also did not bind MRGPRA1 or MRGPRX4 (**Figure 3E, J**). Conjugated bilirubin bound both MRGPRA1 and MRGPRX4, although with a lower affinity than unconjugated bilirubin (**Figure 3E, J**). To make certain that bilirubin activates MRGPRA1 and MRGPRX4 upon binding, we measured exchange of guanosine diphosphate (GDP) for guanosine triphosphate (GTP), one of the first events in GPCR signaling. Bilirubin increased GTP binding to MRGPRA1 and MRGPRX4 membrane complexes, but not to MRGPRC11 (**Figure 3K**). To confirm that bilirubin activates MRGPRA1 *in vivo* to trigger itch, we generated an *Mrgpra1* (A1 KO) knockout mouse line using CRISPR-Cas9 (Jinek et al., 2012) (**Figure 5**). A1 KO animals scratched significantly less than WT mice after exposure to either bilirubin or the established agonist FMRF, demonstrating that Mrgpra1 is functional in adult mice (**Figure 3L-M**)**.** The K_D of bilirubin towards MRGPRA1 and MRGPRX4 suggests that bilirubin likely

does not interact with these receptors in healthy individuals. Additional ligands with nanomolar affinities towards MRGPRA1 or MRGPRX4 may exist that modulate the receptors in normal physiology.

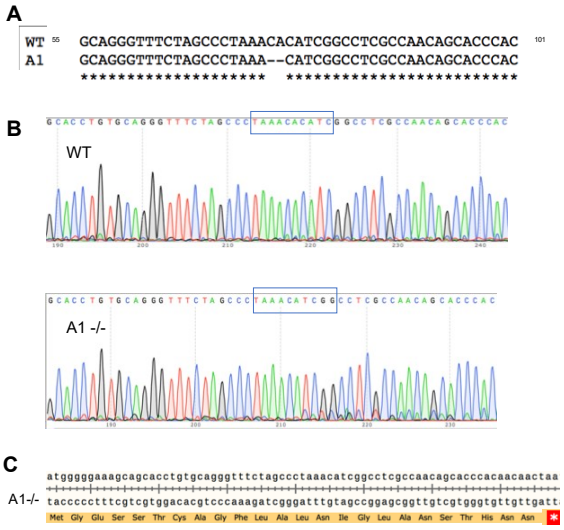

Figure 5. CRISPR deletion of MRGPRA1. (A) Comparison of WT and A1 KO genomic sequences. Location of 2 base pair (bp) deletion shown by dashes. Numbers correspond to MRGPRA1 open reading frame. **(B)** Sequencing data depicting the 2 bp deletion. **(C)** A translation of the open reading frame of MRGPRA1 KO beginning with the start codon. The 2 bp deletion creates a frameshift which results in early termination, marked by a red asterisk.

We reasoned that if bilirubin triggers itch through MRGPRA1 and MRGPRX4, bilirubin should activate these receptors in sensory itch neurons. Previous studies have demonstrated that both Mrgpra1 and MRGPRX4 are expressed in sensory neurons within the dorsal root ganglia (DRG) (Dong et al., 2001; Flegel et al., 2015; Lembo et al., 2002). Mrgpra1 is expressed in a subset of adult DRG and trigeminal ganglia (TG) sensory neurons that innervate the skin and ramify in lamina I and II of the spinal cord (**Figure 6A-D**). Bilirubin elicited robust action potentials in small-diameter (< 30 µm) WT DRG sensory neurons at a proportion consistent with the percentage of sensory neurons that encode itch (5 of 50). Bilirubin failed to elicit action potentials in A1 KO neurons (0 of 60), suggesting bilirubin activates sensory neurons through MRGPRA1 (**Figure 6E**).

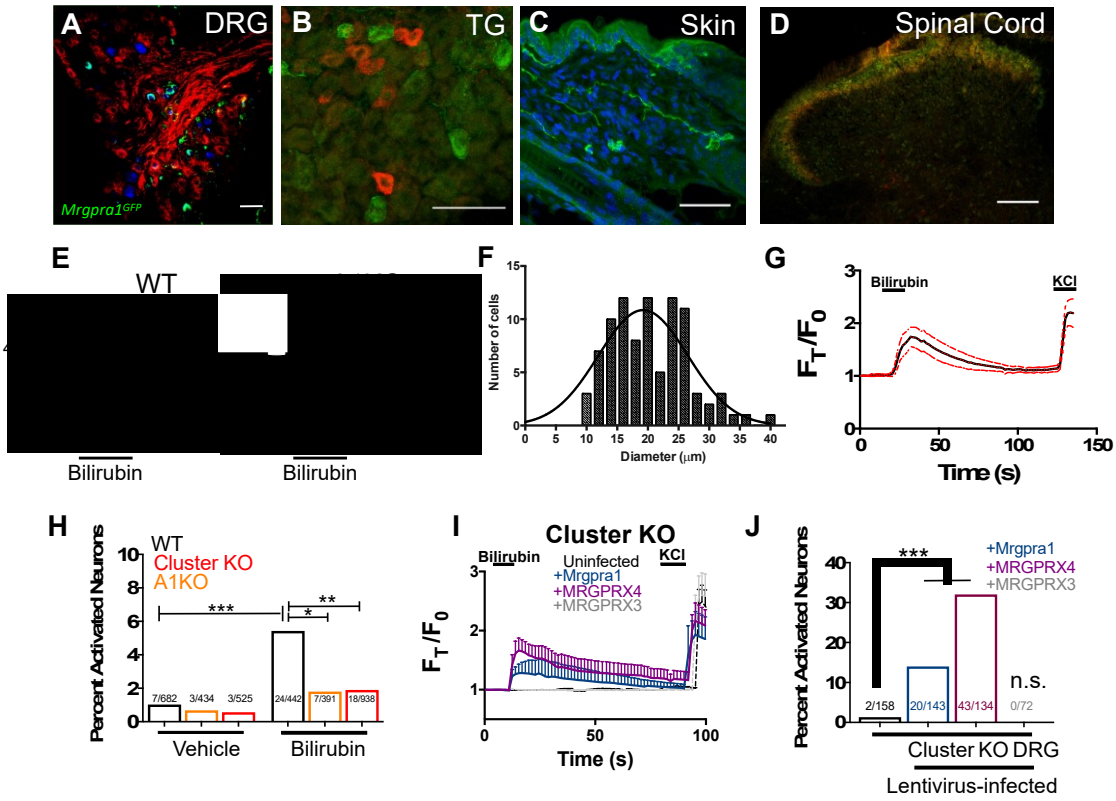

Figure 6. Bilirubin activates sensory neurons in an MRGPR-dependent manner. (**A-D**) Confocal microscopy immunofluorescence images of adult mouse tissue sections from Mrgpra1^{GFP} animals with GFP expression under the control of the endogenous *Mrgpra1* locus. (**A**) Mrgpra1 expression in dorsal root ganglia. Green depicts Mrgpra1^{GFP}. Red depicts anti-PLAP antibody staining where PLAP expression is controlled by the endogenous *Mrgprd* locus (*Mrgprd*^{PLAP}). Blue depicts antibody staining against calcitonin gene-related peptide (CGRP). Scale bar is 50 μM. (**B**) Trigeminal ganglia (TG) stained with Mrgpra1^{GFP} (green) and anti-Substance P antibody (red). Scale bar is 50 μm. (**C**) Back skin stained with anti-GFP antibody (green) to visualize Mrgpra1^{GFP} nerve fibers in the dermis. Blue represents DAPI counterstain. Scale bar is 50 μm. (**D**) Spinal cord (SC) (lamina 1 and 2) stained with anti-GFP and IB4-564. Mrgpra1^{GFP} (green) staining was found in lamina 2 along with IB4 (red) positive terminals. Scale bar is 100 μm. (**E**) Representative whole-cell current-clamp recording of either WT or A1 KO DRG neurons. In WT DRG, bilirubin elicited action potentials in 5 out of 50 small-diameter neurons. In A1 KO DRG, bilirubin elicited action potentials in 0 out of 60 small-diameter neurons. Fisher's exact test $P < 0.05$. (**F**) Histogram of bilirubin-activated neuronal soma diameter. (**G**) Ca^{2+} imaging of WT DRG neurons. Mean ± 95% CI depicted. Compounds applied where indicated by black bars. After a 10 s baseline, 50 μM bilirubin was added. 50 mM KCl was added at the end of each trial. n=20 neurons. **(H)** Percent activation of WT, A1 KO, and Mrgpr-cluster KO DRG by vehicle and 50 μM bilirubin. *, $P < 0.05$; **, $P < 0.01$; ***, $P < 0.001$; Chi-squared test. A neuron was considered to be activated if $\Delta F > 0.2$ for at a least 30 s. **(I)** Ca^{2+} imaging of Mrgpr-cluster KO DRG neurons 48 hrs after either mock infection with lentivirus (n=10) or infected with lentivirus encoding *Mrgpra1* (n=6), *MRGPRX4* (n=10), or *MRGPRX3* (n=20). 50 μM bilirubin was added when indicated by the black bar. After 20 s, a 1 min wash was applied before addition of 50 mM KCl. Compounds applied where indicated by black bars. Mean ± 95% CI depicted. n=10 neurons. **(J)** Percent activation of uninfected, *Mrgpra1*-infected, *MRGPRX4*-infected, and *MRGPRX3*-infected Cluster -/- neurons by bilirubin. ***, $P < 0.001$. Chi-squared test.

Bilirubin-sensitive neurons had an average somal diameter of 20.4 ± 1.3 μm, a diameter characteristic of itch sensory neurons (**Figure 6F**). Applying bilirubin to neurons elicited calcium transients in approximately 5% of WT DRG neurons (**Figure 6G**), whereas significantly fewer sensory neurons from either Mrgpr-cluster KO or A1 KO mice responded (**Figure 6H**). We sought to determine whether expression of either MRGPRA1 or MRGPRX4 was sufficient to render neurons sensitive to bilirubin. To address this question, we infected Mrgpr-cluster KO DRGs with lentivirus carrying either *Mrgpra1*, *MRGPRX4*, or *MRGPRX3*. Bilirubin activated 14% of *Mrgpra1*-and 32% of *MRGPRX4*-transduced Mrgpr-cluster KO DRGs (**Figure 6I-J**). Mrgpr-cluster KO DRGs infected with the control gene *MRGPRX3* did not respond to bilirubin.

Bilirubin-responsive neurons partially overlapped with neurons that responded to 1mM chloroquine, a ligand for MRGPRA3 that typifies itch sensory neurons (Han et al., 2012) (**Figure 7A-C**). To validate that bilirubin activates MRGPRA3-positive itch neurons, we performed calcium imaging on DRG neurons isolated from Tg(*Mrgpra3-Cre)*;*lsl-tdTomato* mice, which express the fluorescent protein tdTomato in *Mrgpra3*-expressing neurons. Bilirubin activated a substantial percentage of *tdTomato*-positive neurons (**Figure 7D**). To confirm that bilirubin activates sensory neurons *in vivo*, we injected 5μL of vehicle or bilirubin into paws of Tg(*Pirt-Cre)*;*lsl-GCaMP6s* mice, which express the fluorescent calcium reporter GCaMP6s in DRG sensory neurons (Kim et al., 2014). Bilirubin, but not vehicle, activated numerous DRG sensory neurons in the paws of GCaMP6s mice (**Figure 7E)**. Inhibiting transient receptor potential (TRP) and other Ca^{2+} channels with ruthenium red prevented bilirubin from activating sensory neurons (**Figure 7F-G**) (Imamachi et al., 2009; Liu et al., 2009; Roberson et al., 2013).

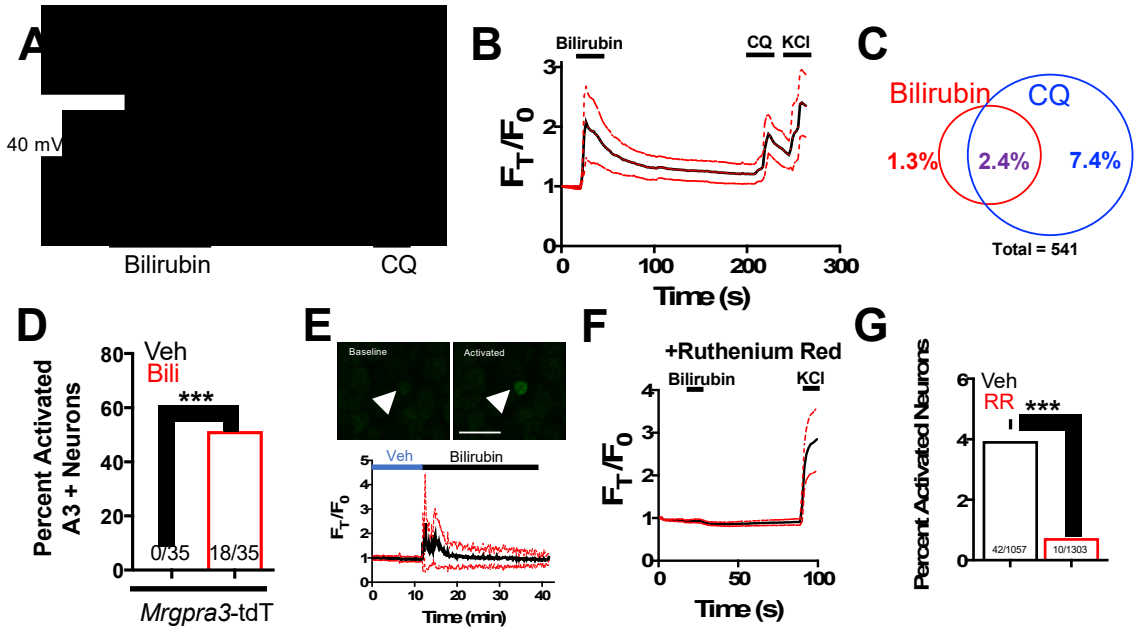

Figure 7. Bilirubin activates a population of small-diameter, chloroquine-sensitive sensory neurons in a TRP channel dependent mechanism. (**A**) A representative whole-cell current-clamp recording of a WT DRG neuron responsive to addition of both 50 μM bilirubin and 1mM chloroquine (CQ). **(B)** Ca^{2+} imaging of WT DRG neurons. Mean ± 95% CI depicted. Compounds applied where indicated by black bars. After a 10 s baseline, 50 μM bilirubin was added. After 20 s, a 3 min wash was applied before 1 mM chloroquine was added. After 15 s, 50 mM KCl was added. n=10 neurons. (**C**) Venn diagram of total neurons activated by either bilirubin and/or chloroquine (Bilirubin alone=7, Chloroquine=40, Overlap=13). (**D**) Percent activation of Tg(*Mrgpra3-Cre)*;lsl-tdTomato neurons as assessed by calcium imaging with vehicle, 1 mM Chloroquine, or 50 μM bilirubin. (**E**) *In vivo* Ca^{2+} imaging of Pirt-Cre; lsl-GCaMP6s animals. Briefly, a surgery was performed to expose L4 DRG. Baseline measurements were taken before a vehicle injection in ipsilateral paw and subsequent injection of 5μL of 100μM bilirubin. Depicted is a representative Ca^{2+} imaging trace of bilirubin-activated neurons, n=20, identified by post hoc imaging analysis. The black trace is the mean F_t/F_0 and red dotted lines represent 95% confidence intervals. (**F**) Neurons were incubated with 10 μM ruthenium red for 10 min before application of 50 μM bilirubin. **(G)** Percent activation of WT neurons, incubated with either vehicle or 10 μM ruthenium red, by 50 μM bilirubin.

We wondered whether chronic elevation of bilirubin *in vivo*, like in cholestasis, stimulates *Mrgpr*-dependent itch. Bile is the primary means by which bilirubin is excreted, and patients with cholestasis exhibit elevated levels of bilirubin and other pruritogenic substances in their blood (Alemi et al., 2013). To induce hyperbilirubinemia and model intrahepatic cholestasis, we administered α-napthyl isothiocyanate (ANIT) to mice (Eliakim et al., 1959). We treated WT, Mrgpr-cluster$\Delta^{-/-}$, and A1 KO animals with

25 mg/kg ANIT for five days before assessing spontaneous itch (**Figure 8A**). WT,

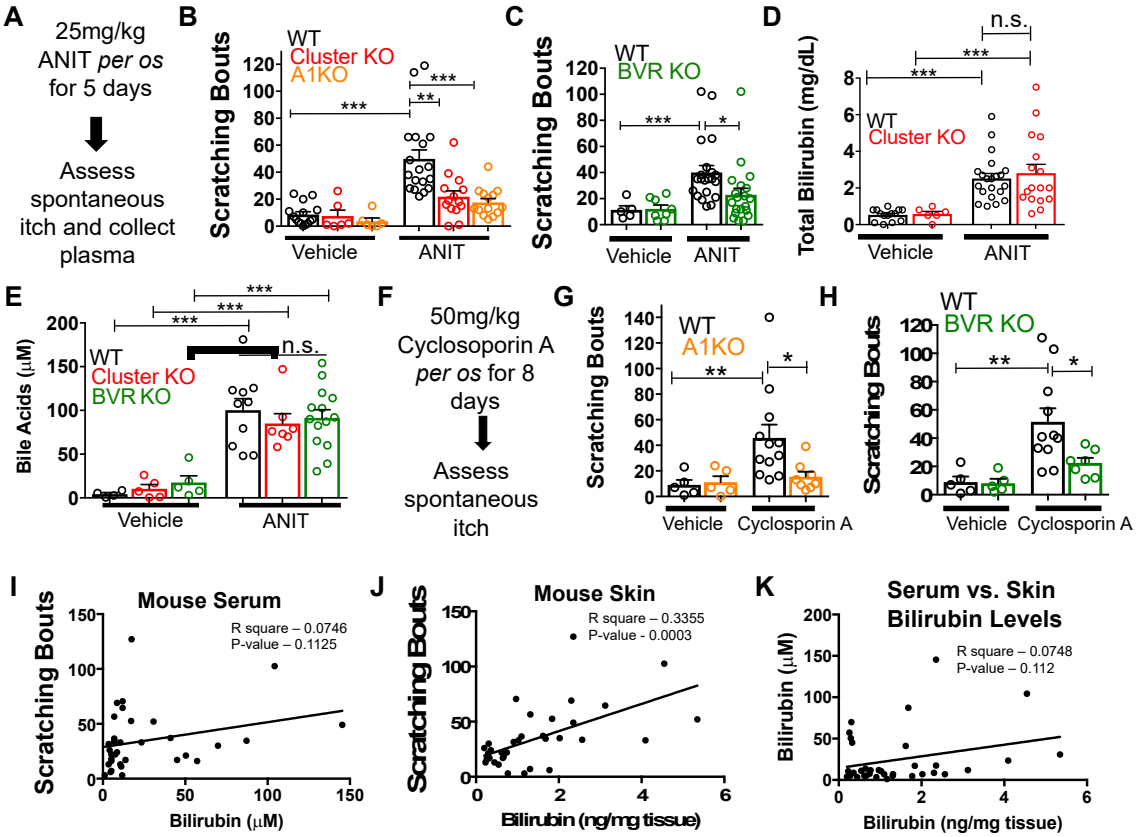

Figure 8. MrgprA1 KO, Mrgpr-clusterΔ$^{-/-}$, and BVR KO animals exhibit decreased cholestatic pruritus. (**A**) Experimental flowchart for ANIT model of cholestasis. (**B**) Scratching bouts for vehicle and ANIT-treated mice among WT, Mrgpr-clusterΔ$^{-/-}$, and A1 KO groups. Bouts were assessed in a 30 min period. For the vehicle cohort: WT n=15, Mrgpr-cluster KO n=6, A1 KO n=6. For ANIT cohort: WT n=20, Mrgpr-cluster KO n=14, A1 KO n=14. (**C**) Scratching bouts for vehicle and ANIT-treated animals among WT and BVR KO groups. Bouts were assessed in a 30 min period. For the vehicle cohort: WT n=5 and BVR KO n=8. For ANIT cohort: WT n=21 and BVR KO n=20. (**D**) Plasma bilirubin levels (mg/dL) from WT and Mrgpr-cluster KO ANIT-treated and vehicle-treated animals. For the vehicle cohort: WT n=14, Mrgpr-cluster KO n=6. For the ANIT cohort: WT n=21, Mrgpr-cluster KO n=17. (**E**) Plasma bile acid levels (μM) from ANIT-treated and vehicle-treated animals. For the vehicle cohort: WT n=4, Mrgpr-cluster KO n=5, BVR KO n=5. For the ANIT cohort: WT n=10, Mrgpr-cluster KO n=7, BVR KO n=14. (**F**) Experimental flowchart for Cyclosporin A model of cholestasis. (**G**) Scratching bouts for vehicle and Cyclosporin A-treated WT and A1 KO animals. For the vehicle cohort: n=5 for all. For Cyclosporin A cohort: WT n=10 and A1 KO n=8. (**H**) Scratching bouts from vehicle and Cyclosporin A treated WT and BVR KO animals. For the vehicle cohort: n=5. For Cyclosporin A cohort: WT n=11 and BVR KO n=7. (**I**) Correlation of serum bilirubin levels from cholestatic animals and scratching bouts. Line of best fit: Y = 0.23 (X) + 28.78. (**J**) Correlation of skin bilirubin levels from cholestatic animals and scratching bouts. Line of best fit: Y = 12.34 (X) + 16.7. (**K**) Correlation of skin and serum bilirubin levels from cholestatic animals. Line of best fit: Y = 7.015(X) – 14.52. **(A-H)** Mean ± s.e.m. depicted. Open circles represent individual data points. *, $P < 0.05$; **, $P < 0.01$; ***, $P < 0.001$ by unpaired two-tailed Student's t-test.

Mrgpr-cluster$\Delta^{-/-}$, and A1 KO animals exhibited equivalently severe hepatocellular injury judged by increases in plasma bilirubin, bile acids, alkaline phosphatase (ALP), aspartate aminotransferase (AST), alanine aminotransferase (ALT), and gamma-glutamyl transferase (GGT) (**Figure 8D-E, Figure 9A-D**).

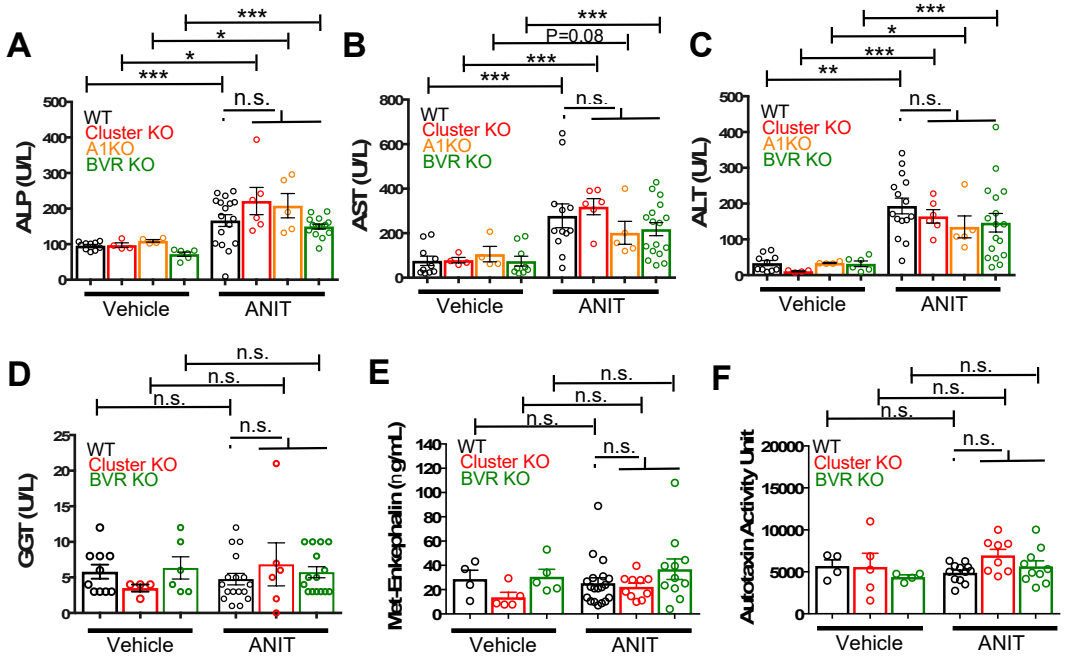

Figure 9. Plasma levels of pathological markers of liver injury are similar between WT, Mrgpr-cluster$\Delta^{-/-}$, A1 KO, and BVR KO animals. (A) Plasma alkaline phosphatase (ALP) levels among vehicle and ANIT-treated animals. For vehicle cohort: WT n=10, Mrgpr-cluster KO n=4, A1 KO n=4, BVR KO n=6. For ANIT cohort: WT n=17, Mrgpr-cluster KO n=6, A1 KO n=5, BVR KO n=15. **(B)** Plasma aspartate aminotransferase (AST) levels among vehicle and ANIT-treated animals. For vehicle cohort: WT n=10, Mrgpr-cluster KO n=4, A1 KO n=4, BVR KO n=9. For ANIT cohort: WT n=12, Mrgpr-cluster KO n=6, A1 KO n=5, BVR KO n=17. **(C)** Alanine aminotransferase (ALT) levels among vehicle and ANIT-treated animals. For vehicle cohort: WT n=10, Mrgpr-cluster KO n=4, A1 KO n=4, BVR KO n=6. For ANIT cohort: WT n=15, Mrgpr-cluster KO n=6, A1 KO n=5, BVR KO n=17. **(D)** Gamma-glutamyl transferase (GGT) levels among vehicle and ANIT-treated animals. For vehicle cohort: WT n=10, Mrgpr-cluster KO n=4, BVR KO n=6. For ANIT cohort: WT n=17, Mrgpr-cluster KO n=6, BVR KO n=15. **(E)** Met-enkephalin levels among plasma from vehicle and ANIT-treated animals. For vehicle cohort: WT n=4, Mrgpr-cluster KO and BVR KO n=5. For ANIT cohort: WT n=19, Mrgpr-cluster KO n=10, BVR KO n=11. **(F)** Autotaxin activity among plasma from vehicle and ANIT-treated animals. For vehicle cohort: WT and BVR KO n=4, Mrgpr-cluster KO n=5. For ANIT cohort: WT n=12, Mrgpr-cluster KO n=8, BVR KO n=10. (**A-F**) Mean ± s.e.m. depicted. Open circles represent independent data points. *, $P < 0.05$; **, $P < 0.01$, ***, $P < 0.001$; two-tailed unpaired Student's *t*-test. n.s., not significant.

As expected, ANIT treatment significantly increased pruritus in all animals (**Figure 8B**). However, Mrgpr-cluster KO and A1 KO mice scratched markedly less than WT mice (**Figure 8B**), suggesting that MRGPRA1 mediates a component of

hepatobiliary pruritus. In humans, bile acids, endogenous opioids, and LPA are often increased in cholestatic sera and have been shown to mediate pruritus (Alemi et al., 2013; Bergasa et al., 1998; 1992; Kremer et al., 2010). The serum of ANIT-treated animals exhibited elevated bilirubin and bile acids (**Figure 8D-E**), whereas neither the endogenous opioid peptide met-enkephalin (Thornton and Losowsky, 1989a; 1989b) nor the LPA-producing enzyme autotaxin were elevated (**Figure 9E-F**). To assess whether other cholestatic pruritogens act at MRGPRs in mice, we injected WT and Mrgpr-cluster KO with deoxycholic acid (a bile acid), opiates, and LPA. These other cholestatic pruritogens elicited equivalent degrees of scratching in WT and Mrgpr-cluster KO animals (**Figure 10A-D)**. Mrgprs are promiscuous receptors. It should be noted that there

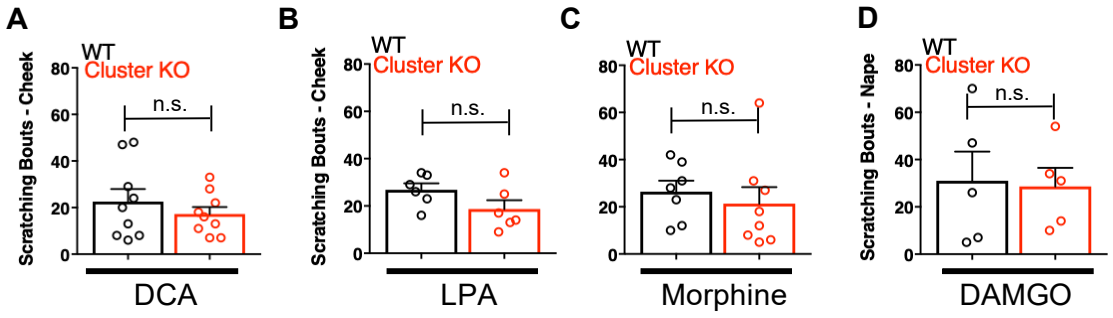

Figure 10. Mrgpr-cluster KO animals have intact itch to other cholestatic pruritogens and bilirubin synergism with chloroquine itch. (A) Scratching bouts to 1.3mM deoxycholic acid (DCA) injected into cheek. WT n = 9, Mrgpr-cluster KO n=9. **(B)** Scratching bouts to 4 mM lysophosphatidic acid (LPA) injected into cheek. WT n = 6, Mrgpr-cluster$\Delta^{-/-}$n=6. **(C)** Scratching bouts to 25µg of morphine injected into back. WT n = 7, Mrgpr-cluster$\Delta^{-/-}$n=8. **(D)** Scratching bouts to 25µg of DAMGO injected into back. WT n = 5, Mrgpr-cluster KO n=5. **(E)** Synergism of bilirubin with chloroquine pruritus. Scratching bouts to 1mM chloroquine plus either vehicle or 500µM bilirubin injected into back. For 1mM chloroquine plus vehicle: WT n = 9, A1 KO n=5. For 1mM chloroquine plus 500µM bilirubin: WT n = 11, A1 KO n=5. **(A-E)** Mean ± s.e.m. depicted. Open circles represent independent data points. **, $P < 0.01$, ***, $P < 0.001$; two-tailed unpaired Student's *t*-test. n.s., not significant.

remain multiple bile acids, LPA molecules, and opiates which remain untested and could be agonists against Mrgprs. Based on this data, we hypothesized that Mrgpr-cluster KO and A1 KO mice scratched less with ANIT because MRGPRA1 mediates bilirubin-induced itch.

To determine whether bilirubin is activating MRGPRA1 to stimulate itch in cholestasis, we induced cholestasis in a mouse that lacks the biosynthetic enzyme for bilirubin, biliverdin reductase (BVR KO) (Kutty and Maines, 1981) (**Figure 1E, Figure 11A**). BVR KO mice lack *Blvra*, which is the gene that encodes for bilirubin reductase.

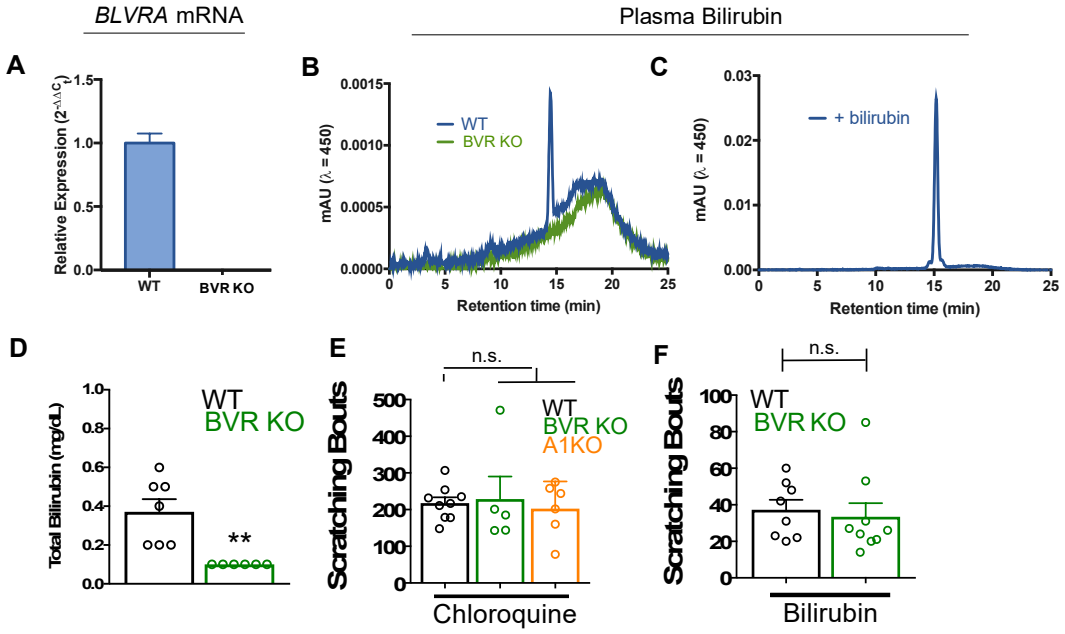

Figure 11. BVR KO and A1 KO animals have intact itch circuits. (A) Quantitative PCR analysis of *BLVRA* transcript from whole brain of WT and BVR KO mice. **(B)** Representative chromatogram of HPLC analysis of plasma from WT and BVR KO mice separated via a C18 column and analysed by absorbance at 450 nm. **C.** HPLC chromatogram of plasma from a WT mouse spiked with excess bilirubin. **(D)** Total bilirubin levels from plasma of WT and BVR KO animals. WT n=7, BVR KO n=6. **(E)** Scratching bouts to 150 µg (50 µL of 10 mM) of chloroquine. After chloroquine injection, scratching bouts were assessed in a 30-minute period. WT n=9, BVR KO n=5, A1 KO n=6. **(F)** Scratching bouts to 60 µg (100 µL of 1 mM) of bilirubin. After bilirubin injection, scratching bouts were assessed in a 30 min period. WT n=8, BVR KO n=9. **(D-F)** Mean plus S.E.M. depicted. Open circles represent independent data points. **, $P < 0.01$ by student's t-test. n.s., not significant.

BVR KO mice do not have detectable levels of bilirubin in plasma (**Figure 11B-D**). When treated with ANIT, BVR KO mice scratched significantly less than WT mice (**Figure 8C**). Plasma levels of bile acids, ALP, AST, ALT, GGT, met-enkephaline, and autotaxin were indistinguishable between treated BVR KO animals and WT controls (**Figure 9A-D**). The diminished response to ANIT is not due to aberrant itch circuits, as

BVR KO mice scratched normally when injected with either chloroquine or exogenous bilirubin (**Figure 11E-F**).

To confirm that the observed differences in cholestatic pruritus were not just specific to ANIT, we administered the hepatotoxin cyclosporin A to WT, A1 KO, and BVR KO mice (Laupacis et al., 1981). We treated mice with either 50 mg/kg cyclosporin A or vehicle for eight days before assessing spontaneous itch (**Figure 8F**). Cyclosporin A induced spontaneous itch in WT animals, whereas A1 KO and BVR KO mice again scratched significantly less than WT mice (**Figure 8G-H**).

Notably, we found that plasma bilirubin correlates poorly with cholestatic itch in patients and in cholestatic animals (**Figure 8I**). We hypothesized that the levels of bilirubin in the skin would correlate better with itch than serum bilirubin largely because bilirubin likely binds and activates the sensory neurons in the skin. Unlike with serum, skin bilirubin appears to be a much stronger predictor of itch severity in mice (**Figure 8J**). This is consistent with how the anatomical distribution of itch sensory neurons and may explain why studies aimed at identifying plasma pruritogens that correlate with itch severity may have missed bilirubin. Secondarily, we find that plasma bilirubin does not correlate well with skin bilirubin, further suggesting that plasma bilirubin may be a poor predictor of itch severity and may not necessarily serve as a proxy for skin bilirubin (**Figure 8K**). The amount of bilirubin in the skin is likely affected by several factors and equilibria, such as serum albumin.

We assessed whether pharmacologically antagonizing MRGPRs could alleviate cholestatic itch. Recently, a 3-amino acid peptide, QWF, was identified as an MRGPRA1 antagonist (Azimi et al., 2016). QWF abolished bilirubin-associated calcium signaling in

MRGPRA1-expressing cells with an IC_{50} of 2.9 μM [1, 5] (**Figure 12A**). Mirroring its pharmacology *in vitro*, co-injecting 0.25 mg/kg QWF with bilirubin significantly alleviated pruritus associated with bilirubin (**Figure 12B**). QWF specifically antagonized

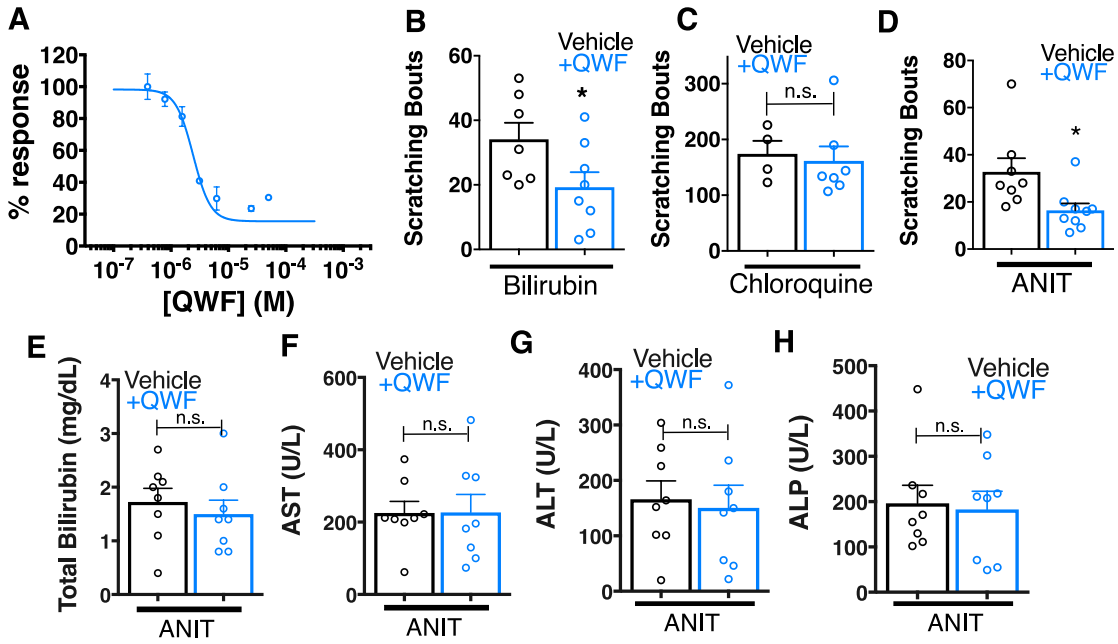

Figure 12. QWF treatment blocks bilirubin activation of Mrgpra1 and cholestatic pruritus. (A) Concentration-response curve for bilirubin induced Ca^{2+} signal in MRGPRA1-expressing HEK cells. 200 μM bilirubin was maintained in competition with indicated doses of QWF. Mean ± s.e.m. depicted. n=3 replicates in duplicate. **(B-C)** Scratching bouts from (**B**) 60 μg (100 mL of 1 mM) bilirubin or (**C**) 150 μg chloroquine co-injected with either vehicle or 1 mg/kg QWF. After injection, the number of scratching bouts in 30 min was assessed. For bilirubin: Vehicle n=7, QWF n=8. For chloroquine: Vehicle n=4, QWF n=7. **(D)** Scratching bouts from WT ANIT-treated animals. Either vehicle or 1 mg/kg QWF was delivered *i.p.* Vehicle n=8, QWF n=9. **(E-H)** Plasma (**E**) bilirubin, (**F**) AST, (**G**) ALT, and (**H**) ALP levels from of vehicle and QWF-dosed WT animals that have undergone ANIT liver injury. **(B-H)** Mean ± s.e.m. depicted. Open circles represent independent data points. n.s., not significant; *, $P < 0.05$ by two-tailed unpaired Student's *t*-test.

bilirubin, as it did not attenuate chloroquine-MRGPRA3 associated itch (**Figure 12C**). Lastly, we evaluated whether the MRGPRA1 antagonist QWF could alleviate cholestatic pruritus. We dosed WT animals with ANIT as previously described, but intraperitoneally injected mice with either vehicle or 1 mg/kg QWF thirty minutes prior to behavioral analysis. Mice treated with QWF scratched significantly less than vehicle-treated animals (**Figure 12D**). QWF treatment did not change plasma levels of total bilirubin, AST, ALT,

or ALP, suggesting that QWF treatment did not alter the underlying liver pathology (**Figure 12E-H**).

Nasobiliary drainage is the most effective treatment for cholestatic pruritus (Hegade et al., 2016). Based on this clinical observation, we predicted that plasma isolated from cholestatic animals would elicit pruritus (**Figure 13A**). Indeed, plasma

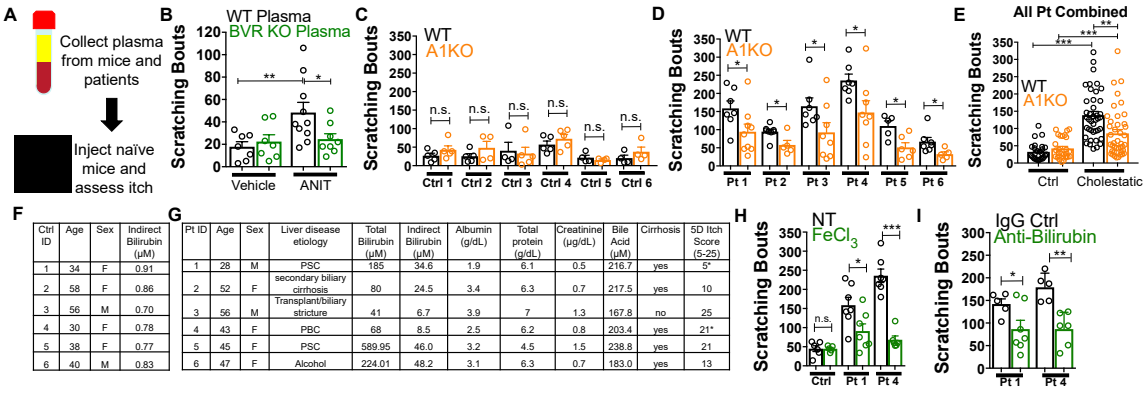

Ctrl ID	Age	Sex	Indirect Bilirubin (μM)
1	34	F	0.91
2	58	F	0.86
3	56	M	0.70
4	30	F	0.78
5	38	F	0.77
6	40	M	0.83

Pt ID	Age	Sex	Liver disease etiology	Total Bilirubin (μM)	Indirect Bilirubin (μM)	Albumin (g/dL)	Total protein (g/dL)	Creatinine (μg/dL)	Bile Acid (μM)	Cirrhosis	5D Itch Score (5-25)
1	28	M	PSC	185	34.6	1.9	6.1	0.5	216.7	yes	5*
2	52	F	secondary biliary cirrhosis	80	24.5	3.4	6.3	0.7	217.5	yes	10
3	56	M	Transplant/biliary stricture	41	6.7	3.9	7	1.3	167.8	no	25
4	43	F	PBC	68	8.5	2.5	6.2	0.8	203.4	yes	21*
5	45	F	PSC	589.95	46.0	3.2	4.5	1.5	238.8	yes	21
6	47	F	Alcohol	224.01	48.2	3.1	6.3	0.7	183.0	yes	13

Figure 13. Bilirubin from mouse and human cholestatic plasma contributes to pruritus in a Mrgpra1-dependent manner. (**A**) Experimental flowchart of plasma injection assay. (**B**) Scratching bouts from WT mice injected with either vehicle- or ANIT-treated plasma from WT and BVR KO animals. For the vehicle plasma cohort: n=7. For cholestatic ANIT-treated plasma: WT n=10 and BVR KO n=8. (**C**) Scratching bouts from either WT or A1 KO mice injected with control donor plasma. Ctrl 1, WT n=5, A1 KO n=5. Ctrl 2, WT n=5, A1 KO n=5. Ctrl 3, WT n=5, A1 KO n=4. Ctrl 4, WT n=4, A1 KO n=5. Ctrl 5, WT n=4, A1 KO n=4. Ctrl 6, WT n=4, A1 KO n=4. (**D**) Scratching bouts from either WT or A1 KO mice injected with either cholestatic patient plasma. Patient 1, WT n=7, A1 KO n=9. Patient 2, WT n=8, A1 KO n=5. Patient 3, WT n=7, A1 KO n=8. Patient 4, WT n=6, A1 KO n=8. Patient 5, WT n=5, A1 KO n=6. Patient 6, WT n=7, A1 KO n=5. (**E**) Scratching bouts from either WT or A1 KO mice injected with plasma collected from all tested control donor samples and all tested cholestatic patient samples. For Control: WT n=27, A1 KO n=27. For cholestatic patient: WT n= 41, A1 KO n=41. (**F-G**) Biochemical characteristics of patient and control plasma. (**F**) Age, sex, and bilirubin levels of control plasma collected. All control plasma donors did not suffer from any chronic itch condition. (**G**) 5D itch questionnaire was administered at time of plasma collection. Asterisk denotes patients taking anti-pruritic medication at time of plasma collection and questionnaire administration. Patient 1 was taking sertraline (100mg QD) and Patient 4 was taking Gabapentin (800 mg TID). A score of 25 represents the maximum level of itchiness. (**H**) Scratching bouts from mice injected with either untreated (NT) control human plasma, $FeCl_3$-treated control human plasma, NT cholestatic patient 1 and 4 plasma (same data from Patient WT data in (**D**), or $FeCl_3$-treated patient plasma. For control plasma, NT n=6 and $FeCl_3$ n=5. For Patient 1 plasma, NT n=7 and $FeCl_3$ n=7. For Patient 4 plasma, NT n=7 and $FeCl_3$ n=6. (**I**) Scratching bouts from mice injected with either normal rabbit IgG –treated patient plasma or anti-bilirubin IgG – treated patient plasma. For Patient 1, Normal IgG n=5, Anti-bilirubin n=7. For Patient 4, Normal IgG n=5, Anti-bilirubin n=6. (**B-I**) Mean ± s.e.m. depicted. Open circles represent independent data points. n.s., not significant; *, $P < 0.05$; **, $P < 0.01$; ***, $P < 0.001$ by unpaired two-tailed Student's t-test.

from WT animals with cholestasis elicited itch when injected into naïve WT animals (**Figure 13B**). Cholestatic plasma isolated from BVR KO mice, which lacks bilirubin (**Figure 11B-D**), elicited significantly fewer scratches than WT cholestatic plasma (**Figure 13B**). The levels of ALP, AST, and ALT were indistinguishable between WT and BVR KO cholestatic plasma (**Figure 9A-D**), presumably because ANIT induced similar hepatotoxicity in WT and BVR KO mice. Instead, BVR KO plasma likely results in less pruritus because it lacks bilirubin.

We also isolated plasma from six patients suffering from various conditions that result in hyperbilirubinemia and six age- and sex-matched control patients (**Figure 13C-G**). All six cholestatic patients' plasma evoked itch in WT animals (**Figure 13D**). When injected into A1 KO animals, each patient's plasma elicited less itch (**Figure 13D**). Compared to plasma from itchy patients, plasma from healthy donors with low levels of bilirubin elicited less itch in WT animals (**Figure 13C**). Plasma from healthy donors injected into A1 KO animals elicited similar scratching behavior (**Figure 13C**). To assess whether removing bilirubin from cholestatic plasma may be therapeutic, we depleted bilirubin both by selective oxidation with $FeCl_3$ or an anti-bilirubin antibody before evaluating its pruritic capacity. We verified depletion of bilirubin by HPLC (**Figure 14A-**

B). Injecting WT mice with plasma (cholestatic patients 1 and 4) treated with $FeCl_3$ or an

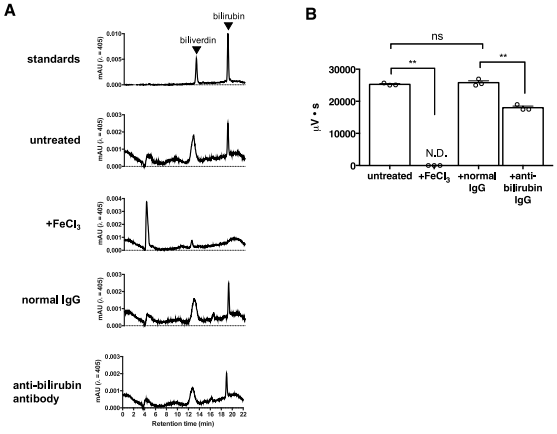

Figure 14. $FeCl_3$ and anti-bilirubin antibody depletion of plasma bilirubin. (**A**) Representative HPLC chromatogram of 100 μM biliverdin + 100 μM bilirubin standards and treated plasma samples. Absorbance was measured at 405 nm. **(B)** Quantification of plasma bilirubin in untreated, $FeCl_3$, normal rabbit IgG, and bilirubin antibody-treated samples. Points represent technical replicates. Mean ± s.e.m. depicted **, $P < 0.01$; n.s., not significant by two-way ANOVA followed by *post-hoc* Tukey test.

anti-bilirubin antibody evoked less pruritus compared to untreated or control IgG-treated patient plasma (**Figure 13H-I**).

3.2 MRGPRX4 is a G-protein coupled receptor activated by bile acids that may contribute to cholestatic pruritus (text adapted from Meixiong et al., *PNAS* 2019)

Once we identified murine receptor Mrgpra1 and human receptor MRGPRX4 as receptors for bilirubin that may mediate a component of cholestatic itch, I screened additional bile constituents against a panel of both mouse and human MRGPRs. From this screen, bile acids were identified as potential Mrgpr ligands. Primary bile acids are formed in liver hepatocytes via cytochrome P450 (CYP) metabolization of cholesterol (**Figure 15A**). Primary bile acids are further metabolized to form additional bile species before being conjugated to either glycine or taurine for more efficient biliary secretion. In the intestine, bacteria metabolize bile acids to form secondary bile acids, which can return to the bloodstream and liver through enterohepatic circulation (**Figure 15A**).

As measured by intracellular Ca^{2+} changes, numerous bile acids, both primary and secondary, activated MRGPRX4. (**Figure 15B-C**). We tested bile acid activity against 12 closely related mouse Mrgprs (**Figure 16A**) as well as sequence-similar human receptors, MRGPRX1-3. No mouse receptors, including the previously identified mouse ortholog Mrgpra1 or sequence-similar human receptors, were activated by bile acids (**Figure 16B-E**). Based on this result, we concluded that bile acids specifically activated MRGPRX4 among the Mrgpr family members.

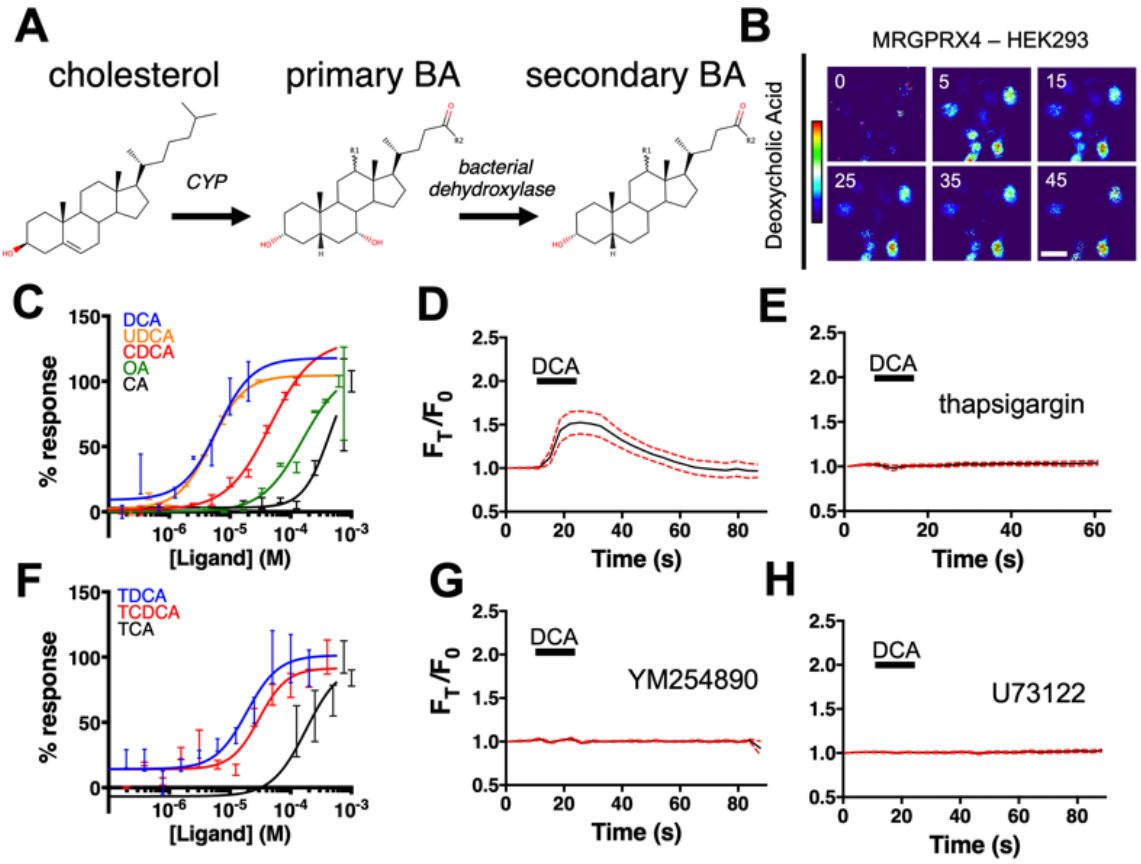

Figure 15. Bile acids activate MRGPRX4, a human sensory neuron expressed GPCR. (*A*) The molecular stereostructures of primary and secondary bile acids and their metabolic precursor, cholesterol. Major structural differences are highlighted in red. *R1* denotes the potential presence of an α hydroxyl substituent in some bile acid derivatives. *R2* denotes additional substituents that vary among bile acids. (*B-H*) Ca^{2+} imaging of HEK293 cells stably expressing MRGPRX4. (*B*) Representative Fura-2 fluorescence heat map images of HEK cells showing changes in intracellular [Ca^{2+}] induced by deoxycholic acid (10 μM). Scale bar, 20 μm. (*C, F)* Concentration–Ca^{2+} response curves of bile acids against MRGPRX4. Data are a representative experiment of 3 independent replicates performed in triplicate, depicted as mean ± s.e.m. (*C)* Concentration–Ca^{2+} response curves of unconjugated bile acids: deoxycholic acid (DCA), chenodeoxycholic acid (CDCA), ursodeoxycholic acid (UDCA), cholic acid (CA), and oleic acid (OA). (*F)* Concentration–Ca^{2+} response curves of tauro-conjugated bile acids: deoxycholic acid (TDCA), chenodeoxycholic acid (TCDCA), and cholic acid (TCA). (*D-E, G-H*) Ca^{2+} imaging traces. 10 μM deoxycholic acid (DCA) was added where indicated by black bars. Mean ± 95% confidence interval (CI) depicted. n= 15. In (*E, G, H*), cells were pre-incubated with either 10 μM SERCA inhibitor thapsigargin (*E*), 10 μM of the $G_{\alpha q}$ inhibitor YM254890 (*G*), or 10 μM PLC inhibitor U73122 (*H*) for 30 min prior to imaging.

Ca^{2+} imaging of MRGPRX4-expressing HEK293 cells displayed robust Ca^{2+} flux in response to 10 μM deoxycholic acid (DCA) (**Figure 15B, D**). Thapsigargin, a non-

competitive inhibitor of the sarco-endoplasmic reticulum Ca^{2+} ATPase, completely inhibited bile acid-associated Ca^{2+} influx (**Figure 15E**), indicating that MRGPRX4-induced Ca^{2+} signal was dependent on intracellular Ca^{2+} stores. Previous studies have identified MRGPRX4 as being $G_{\alpha q}$-linked (Lansu et al., 2017; Meixiong et al., 2019). In line with this, DCA-associated Ca^{2+} flux appears to be similarly $G_{\alpha q}$-linked, since both the $G_{\alpha q}$ inhibitor, YM254890, and the PLC inhibitor, U73122, inhibited Ca^{2+} signal (**Figure 15G-H**).

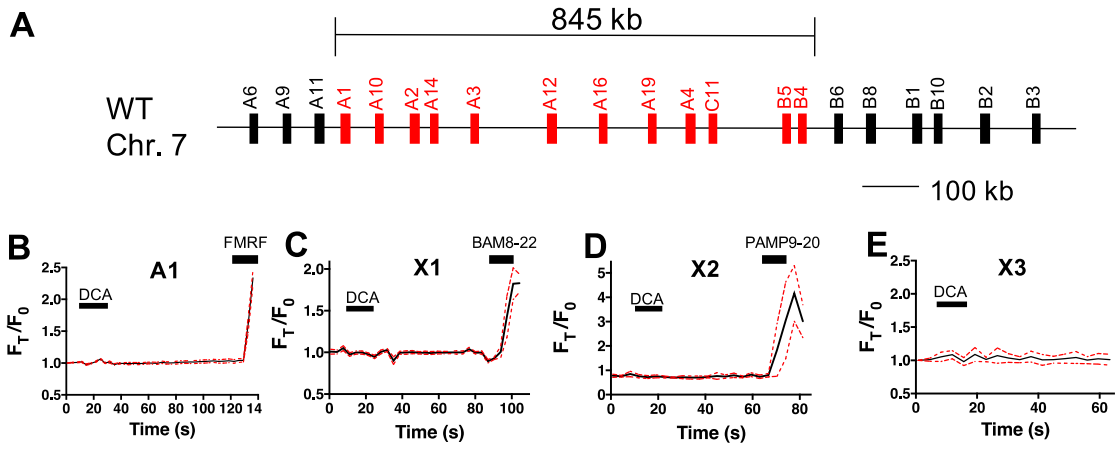

F

Bile acid	EC_{50} (μM) [95% CI]
DCA	**6.19** [1.71, 22.5]
CDCA	**46.2** [28.2, 75.8]
CA	**430.5** [174.6, 1061.0]
OA	**157.0** [75.1, 328.6]
UDCA	**4.93** [4.00, 6.07]

G

Tauro-bile acid	EC_{50} (μM) [95% CI]
T-DCA	**18.9** [10.4, 34.3]
T-CDCA	**30.1** [19.0, 47.7]
T-CA	**178.8** [74.8, 427.2]

Figure 16. DCA does not activate the murine ortholog Mrgpra1 or related human Mrgprs. (*A*) Graphical depiction of DCA-screened murine Mrpgrs. (*B-E*) Ca^{2+} imaging of HEK293 cells stably expressing (*B*) MRGPRA1, (*C*) MRGPRX1, (*D*) MRGPRX2, or (*E*) MRGPRX3. Mean ± 95% CI depicted. n=10. 10 µM DCA was added where indicated by black bars., When applicable, a positive control was added at the end of imaging trial, (*B*) 30µM FMRF, (*C*) 3 µM BAM8-22, or (*D*) 10µM PAMP9-20. (*F*) Table of EC_{50}s with 95% confidence intervals(CI) of unconjugated bile acids against MRGPRX4. (*G*) Table of EC_{50}s with 95% CI of tauro-conjugated bile acids against MRGPRX4.

Of the bile acids tested, DCA and ursodeoxycholic acid (UDCA) displayed the highest potency in terms of MRGPRX4-associated Ca^{2+} signal (**Figure 15C, Figure 16F**).

Both DCA and UDCA had EC_{50}s of approximately 5 μM, similar to their activity towards previously published receptors like TGR5 (Kawamata et al., 2003). Unlike TGR5 however, MRGPRX4 displayed a larger range of potency for various bile acids. For example, cholic acid (CA), displayed much lower potency against MRGPRX4 (EC_{50} ~ 430 μM), well outside physiologic range. In contrast, the EC_{50} of CA towards TGR5 is approximately 10 μM (Kawamata et al., 2003).

Primary bile acids can be conjugated to either glycine or taurine to form water-soluble bile salts. We tested three tauro-conjugated bile acids, tauro-DCA (TDCA), tauro-CDCA (TCDCA), and tauro-cholic acid (TCA) against MRGPRX4. All conjugated bile acids were capable of activating MRGPRX4 at concentrations similar to the respective unconjugated bile acid (**Figure 15F, Figure 16G**).

MRGPRX4 is primarily expressed in sensory neurons of the dorsal root ganglia (DRG). In order to test whether bile acids interact with MRGPRX4 in neurons, we generated humanized mice expressing MRGPRX4. We crossed Tg(*Mrgpra3-GFP-Cre*) (A3-Cre) animals with newly generated $ROSA26^{loxSTOPloxl\text{-}MRGPRX4}$ (lsl-MRGPRX4) animals (**Figure 17A**). A3-Cre animals express Cre recombinase under control of the Mrgpra3 promoter, which labels approximately 5% of the dorsal root ganglia sensory neurons that specifically encode for itch (Han et al., 2013). In lsl-MRGPRX4 animals, expression of MRGPRX4 is under Cre-loxp control. Progeny that inherit both A3-Cre and lsl-MRGPRX4 (+X4) would be expected to express MRGPRX4 in mouse Mrgpra3-containing itch neurons (**Figure 17A**). Cre-null but transgene-positive mice (Cre-, lsl-MRGPRX4) were studied as comparative controls.

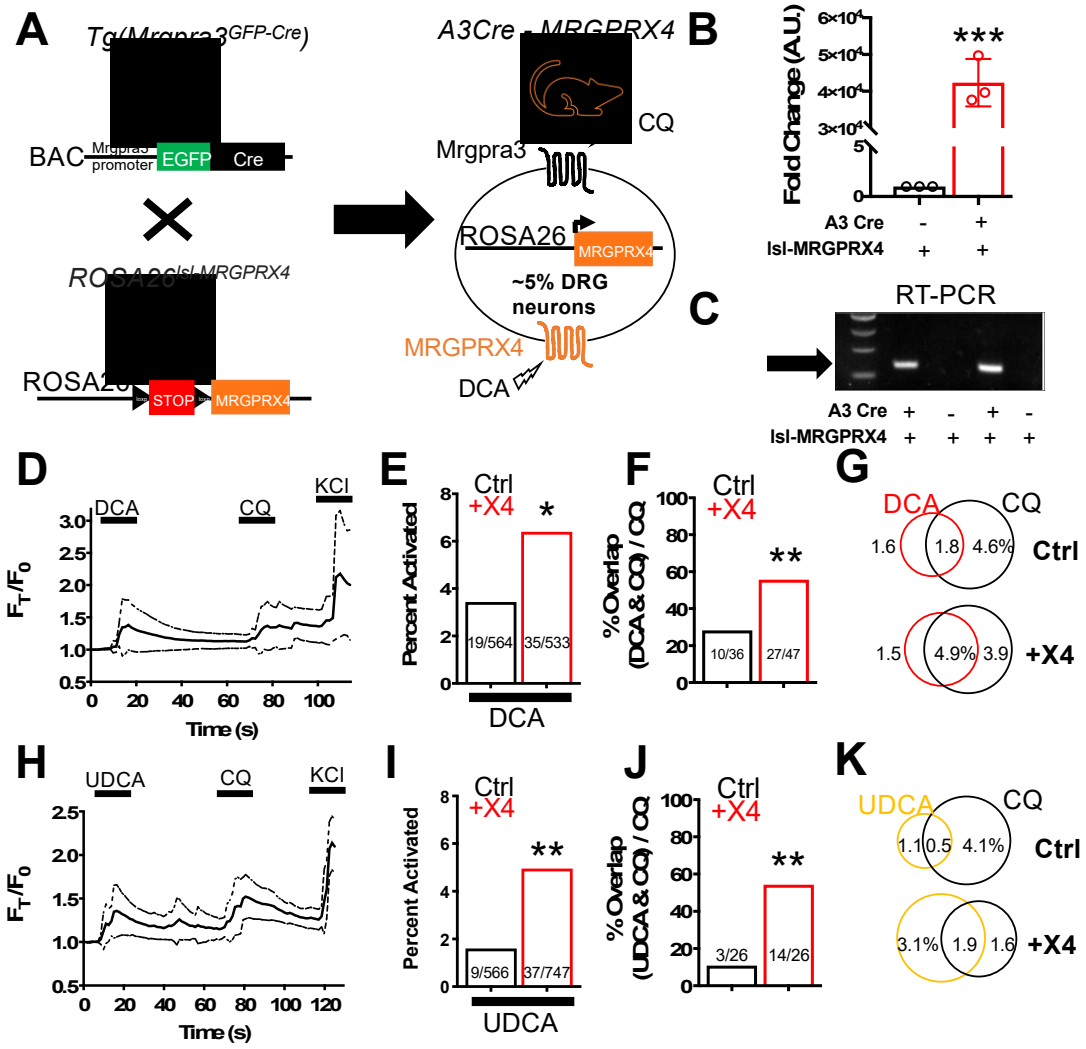

Figure 17. +X4 humanized mouse sensory neurons are more readily activated by bile acids. (*A*) Diagram showing mating strategy to generate humanized (+X4) mice. Mrgpra3-cre expression is restricted to mouse dorsal root ganglia (DRG). Approximately 5% of DRG would be expected to express receptor. qPCR (*B*) and (*C*) RT-PCR of RNA collected from both control (A3-Cre negative) and +X4 (A3-Cre positive) mice expressing Rosa26$^{lsl\text{-}MRGPRX4}$. (*B*) Mean ± 95% CI depicted. n=3 representative samples. ***, $P < 0.001$, student's t test. (*C*) Arrow indicates the expected band based on primer design. 4 independent samples collected from different mice depicted. (*D, H*) Ca^{2+} imaging traces of Ctrl and +X4 DRG neurons. Mean ± 95% CI depicted. n=10 neurons. After a 10 s baseline, either 10 μM DCA (*D*) or 100 μM UDCA (*H*) applied where indicated by black bars. After 1 min, 1 mM chloroquine was added. (*E, I*) Percent activation of Ctrl and +X4 DRG neurons from either 10 μM DCA (*E*) or 100 μM UDCA (*I*). (*F, J*) Percent overlap of CQ activated Ctrl and +X4 DRG neurons (~5% of total) activated by both DCA and CQ (*F*) and both UDCA and CQ (*J*). (*E-F, I-J*) *, $P < 0.05$; **, $P < 0.01$; Chi-squared test. A neuron was considered to be activated if $\Delta F > 0.2$ for at a least 30 s. (*G, K*) Venn diagrams of DCA (*G*), UDCA (*K*), and CQ activated neurons as a percent of total DRG neurons.

+X4 animals expressing A3-Cre and lsl-MRGPRX4 have high levels of MRGPRX4 mRNA in sensory neurons as assayed by both qPCR and RT-PCR (**Figure 17B-C**). Based on previously determined potencies, we selected DCA and UDCA for further experimentation. As assayed by Ca^{2+} imaging, DCA activated a subpopulation of small diameter (approximately 20 μm) +X4 DRG neurons (**Figure 17D; Figure 18A-B**).

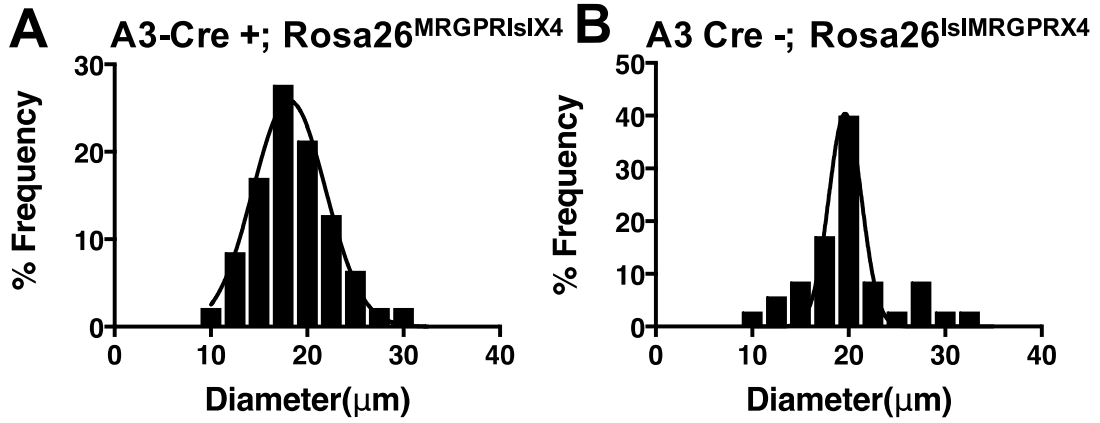

Figure 18. DCA activates small-diameter Ctrl and +X4 sensory neurons. (*A-B*) Histograms of bilirubin-activated neuronal soma diameter. (*A*) +X4 Mean = 18.8μm. n= 47. (*B*) Ctrl Mean = 20.1μm. n= 35.

At the tested concentration, TGR5 receptor present in both control (Ctrl) and +X4 neurons would be activated. Indeed, DCA activated 3.4% of control neurons, likely due to activation of TGR5 (**Figure 17E**). Approximately 25% of control neurons activated by DCA were also activated by chloroquine (CQ), a ligand for Mrgpra3 (**Figure 17F-G**). Based on the genetic strategy employed for +X4 generation, we hypothesized that DCA would activate a higher percentage of Mrgpra3, CQ-sensitive, sensory neurons in +X4 animals. DCA activated 6.4% of +X4 sensory neurons (**Figure 17E**). In addition, DCA activated significantly more CQ-sensitive, Mrgpra3-expressing, neurons in +X4 DRG (**Figure 17F-G**). Based on this data, we concluded that +X4 humanized sensory neurons expressed functional MRGPRX4 receptor that could be activated by DCA.

TGR5 has been previously identified as being expressed in Mrgpra3-positive itch neurons (Alemi et al., 2013). To better disambiguate MRGPRX4 and TGR5 activity, we selected UDCA as a ligand for additional experimentation. All bile acids tested against MRGPRX4 are reported to activate TGR5 (Sato et al., 2008). However, UDCA, the second most potent activator of MRGPRX4, is a significantly less potent TGR5 agonist (Kawamata et al., 2003). Based on these data, we predicted that lower concentrations of UDCA would activate more +X4 neurons than control neurons. Indeed, UDCA activated a similar percentage of +X4 DRG neurons compared to DCA but activated a significantly smaller percentage of control neurons (**Figure 17H-I**). Additionally, UDCA activated only 10% of CQ-sensitive control neurons while activating 54% of +X4 neurons (**Figure 17J-K**).

To test the *in vivo* relevance of bile acid agonism of MRGPRX4, we injected bile acids into control and +X4 animals and assessed acute itch. As before, the genetic strategy of MRGPRX4 humanization results in +X4 animals expressing MRGPRX4 receptor in Mrgpra3^{+} itch neurons. Therefore, we hypothesized that a true, *in vivo* ligand-MRGPRX4 interaction would activate Mrgpra3^{+} neurons and produce itch behavior. Compared to control, +X4 animals scratched significantly more in response to injection of pathophysiologic concentrations of DCA, UDCA, CDCA, and TDCA at the nape (**Figure 19A-D**). This increase was specific to bile acids, as histamine and chloroquine,

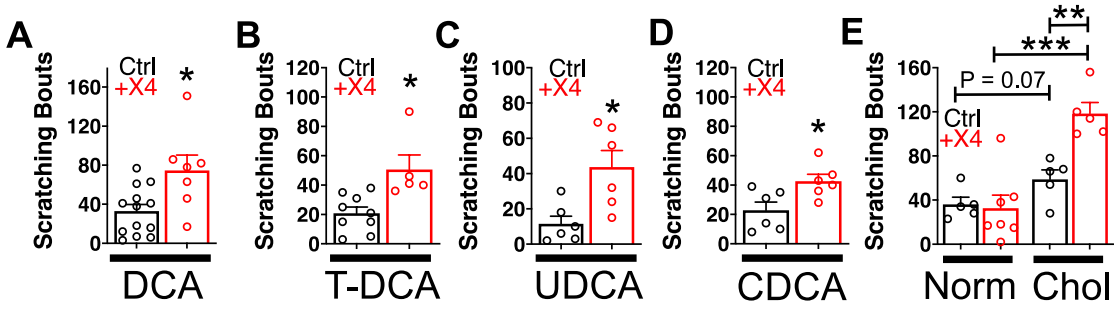

Figure 19. +X4 humanized mice scratch more to unconjugated and conjugated bile acids. (*A*) Scratching bouts associated with injection of DCA. 50 µL of 1 mM DCA was injected into the nape of Ctrl and +X4 mice. Ctrl n=13; +X4 n=6. (*B*) Scratching bouts associated with injection of T-DCA. 50µL of 1mM T-DCA was injected into the nape of Ctrl and +X4 mice. Ctrl n=9; +X4 n=5. (*C*) Scratching bouts associated with injection of UDCA. 50 µL of 2 mM UDCA was injected into the nape of Ctrl and +X4 mice. Ctrl n=6; +X4 n=6. (*D*) Scratching bouts associated with injection of CDCA. 50 µL of 2 mM CDCA was injected into the nape of Ctrl and +X4 mice. Ctrl n=6; +X4 n=6. (*E*) Scratching bouts associated with injection of human plasma from either normal or cholestatic patients (Chol) into Ctrl and +X4 mice. 50 µL of plasma was injected into the nape of mice. For normal plasma: Ctrl n= 5; +X4 n=7. For Chol plasma: Ctrl n= 5; +X4 n=5. (*A-D)* Mean ± s.e.m. depicted. Each open circle represents an individual mouse. (*A-D)* *, $P < 0.05$; **, $P < 0.01$; ***, $P < 0.001$; two-tailed unpaired Student's *t*-test.

two canonical pruritogens, stimulated similar levels of itch in control and +X4 animals (**Figure 20A-B**). Additionally, injection of cholestatic patient plasma, containing bile acids and numerous other pruritogens (**Figure 19C**), elicited greater itch in +X4 animals compared to control animals (**Figure 19D**). This difference between Ctrl and +X4 animals was not observed upon injection of control plasma (**Figure 19D**). Compared to normal plasma, patient plasma elicited greater itch in control animals (**Figure 19D**). This could result from numerous pruritogens acting at established itch receptors in mice, such as bilirubin at Mrgpra1 or bile acids at TGR5.

Having established that unconjugated and conjugated bile acids elicited greater acute itch in +X4 animals, we sought to determine whether this observation remained true in a mouse model of cholestatic itch. To induce cholestasis, we administered α-napthyl isothiocyanate (ANIT) to mice. ANIT is a well-established model that elicits intrahepatic cholestasis in mice (Meixiong et al., 2019; Tanaka et al., 2009). We treated control and

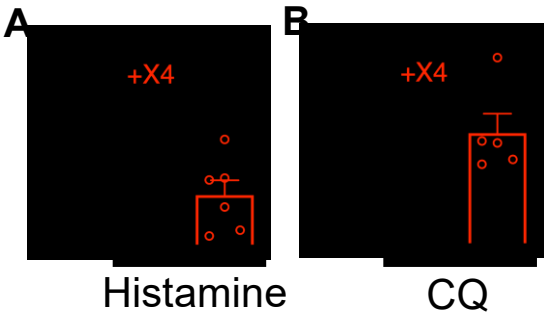

C

Total Bilirubin (μM)	Indirect Bilirubin (μM)	Albumin (g/dL)	Total protein (g/dL)	Creatinine (μg/dL)	Bile Acid (μM)
329	27	2.9	5.3	1.2	221.6

Figure 20. +X4 humanized mice scratch normally in response to non-bile acid pruritogens. (*A*) Scratching bouts associated with injection of histamine. 50μL of 9mM histamine was injected into the nape of Ctrl and +X4 mice. Ctrl n=6; +X4 n=6. (*B*) Scratching bouts associated with injection of Chloroquine (CQ). 50μL of 10 mM CQ was injected into the nape of Ctrl and +X4 mice. Ctrl n=6; +X4 n=5. (*C*) Biochemical characteristics of patient plasma injected.

+X4 animals with 25 mg/kg ANIT daily for five days while assessing spontaneous itch and weight 24 hours after each treatment (**Figure 21A**). Over the course of the experiment, cholestatic itch in +X4 animals was significantly different from control

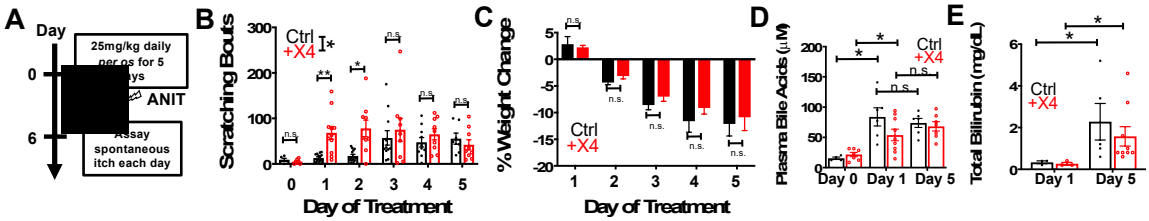

Figure 21. +X4 humanized mice display increased cholestatic itch concordant with serum bile acid elevation. (*A*) Experimental flowchart of cholestatic model. ANIT was given daily *per os* for 5 days. 24 hours subsequent to every treatment, spontaneous itch was assessed for 1 hour. (*B*) Spontaneous scratching bouts from ANIT-treated animals. itch was assessed for 1 hour. Scratching bouts from Ctrl and +X4 were significantly different. P<0.05 by ANOVA. For Day 0: Ctrl n= 5, +X4 n=7. For Day 1: Ctrl n= 14, +X4 n= 11. For Day 2: Ctrl n= 13, +X4 n= 9. For Day 3: Ctrl n= 11, +X4 n= 9, For Day 4: Ctrl n= 10, +X4 n= 9. For Day 5: Ctrl n= 7, +X4 n= 9. (*C*) Percent weight change from baseline of Ctrl and +X4 mice during ANIT treatment. For Day 1: Ctrl n= 5, +X4 n= 7. For all other days: Ctrl n= 4, +X4 n= 6. (*D*) Plasma bile acid levels from Ctrl and +X4 mice at indicated days of ANIT treatment. For Day 0: Ctrl n= 4, +X4 n=4. For Day 1: Ctrl n= 6, +X4 n= 9. For Day 5: Ctrl n= 6, +X4 n= 7. (*E*) Total plasma bilirubin levels at indicated days of treatment. For Day 1: Ctrl n= 3, +X4 n= 3. For Day 5: Ctrl n= 5, +X4 n= 9. (*B-E*) Mean ± SEM depicted. Circles represent individual mice. n.s.= not significant; *, $P < 0.05$; **, $P < 0.01$; student's t test.

animals (**Figure 21B**). The majority of this difference was observed at early timepoints. Specifically, +X4 animals scratched significantly more than baseline just 24 hours after a single dose of ANIT (**Figure 21B**). ANIT does not appear to directly activate MRGPRX4, since acute treatment of ANIT did not elicit itch in either WT or +X4 animals over the

first hour after administering ANIT (**Figure 22A**). Subsequent treatment did not significantly increase pruritus. In control animals, itch was not significantly elevated until the third day of treatment (**Figure 21B**). Like +X4 mice, control mice did not scratch more with subsequent treatments. During days 3-5 of treatment, control and +X4 itch were indistinguishable (**Figure 21B**). Control and +X4 animals displayed no differences in weight change from ANIT treatment. Both groups lost significant weight over the 5-day treatment course (**Figure 21C**). Control and +X4 animals had similar degrees of cholestatic injury after either 1 or 5 days of ANIT treatment, as assessed by plasma levels of bile acids, total bilirubin, albumin, aspartate aminotransferase (AST), alkaline phosphatase (ALP), and alanine aminotransferase (ALT) (**Figure 21D-E; Figure 22B-E**).

Based on observed time course of itch behavior, we hypothesized that humanized +X4 mice scratched more at earlier timepoints due to a ligand of MRGPRX4, such as bile acids, being elevated during those periods. Indeed, at Day 1, ANIT treatment resulted in significant elevation of plasma bile acids, similar to levels observed on Day 5.

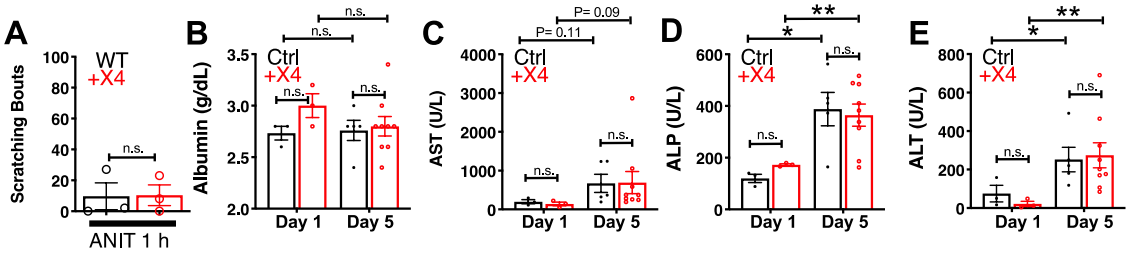

Figure 22. +X4 humanized mice exhibit similar degrees of cholestasis compared to Ctrl mice. (*A*) Scratching bouts from wild-type and +X4 animals 1 hour after a single 25mg/kg dose of ANIT. For both WT and +X4, n=3. (*B*) Plasma albumin levels (g/dL) from indicated days of ANIT treatment. (*C*) Plasma aspartate aminotransferase (AST) levels (U/L) from indicated days of ANIT treatment. (*D*) Plasma alkaline phosphatase (ALP) levels (U/L) from indicated days of ANIT treatment. (*E*) Plasma alanine aminotransferase (AST) levels (U/L) from indicated days of ANIT treatment. (*A-E*) Mean ± SEM depicted. Circles represent plasma from individual mice. For Day 1: Ctrl n= 3, +X4 n= 5. For Day 5: Ctrl n= 5, +X4 n= 9. n.s.= not significant; *, $P < 0.05$; **, $P < 0.01$; student's t test.

Importantly, plasma bilirubin, albumin, and liver enzyme levels were not elevated at Day

1 (**Figure 21E; 22B-E**). This distinction suggested that the increase in itch on Days 1-2 in +X4 animals resulted from an increase in bile acids and not bilirubin, another ligand of MRGPRX4. We hypothesized that +X4 cholestatic itch is similarly elevated compared to control at later timepoints (Days 3-5) due to signaling from intact bilirubin itch receptor Mrgpra1 in Ctrl animals and other potential pruritogen-receptor interactions.

3.3 Activation of mast cell-expressed Mas-related G-protein coupled receptors drives non-histaminergic itch (text adapted from Meixiong et al., *Immunity* 2019)

In addition to exploring the role of sensory-neuron expressed Mrgprs in non-histaminergic itch, I was interested in assessing the contribution of mast cell-expressed Mrgprs in itch. In the context of nociceptive itch (i.e., pruriception), mast cells are key cellular mediators via release of histamine which activates receptors present on itch-sensory neurons of the dorsal root ganglia (DRG) (Shim and Oh, 2008). Canonically, mast cell activation is understood to result from antigen binding to immunoglobulin E (IgE) antibody and crosslinking of the high-affinity IgE receptor, Fc epsilon RI (FcεRI). Activation of either Mrgprb2 or MRGPRX2 results in mast cell degranulation that is both spatially and temporally distinct from FcεRI-mediated degranulation (Gaudenzio et al., 2016; McNeil et al., 2015). These observations provoke the hypothesis that mast cell Mrgpr pathways may promote itch in a unique fashion separate from classical IgE-mediated itch.

Despite their well-described roles in histaminergic itch, how mast cells interact with pruriceptive sensory nerves *in vivo* has not been investigated. Here we report that activation of mast cells via Mrgprb2 induced itch distinct from classical IgE-FcεRI histaminergic itch. Compared to FcεRI activation, Mrgprb2 activation resulted in differential release of pruritogens. Using intravital Ca^{2+} imaging of sensory neurons, we showed that Mrgprb2-stimulation of mast cells, compared to IgE-FcεRI signaling, activated a distinct population of itch-sensory neurons. Histamine H_1 receptor (H_1R) blockade is not effective in treating numerous chronic itch disorders associated with mast cell activation such as allergic contact dermatitis (ACD) (Askenase et al., 1983; Dudeck

et al., 2011; Erickson et al., 2018; Gimenez-Rivera et al., 2016; Grimbaldeston et al., 2007). In contrast, we demonstrated that Mrgprb2 was critical for itch in the setting of ACD and thus a possible target for therapeutic intervention.

Mrgprb2 (murine) and MRGPRX2 (human) are expressed in mast cells and not in other immune or neuronal cells (Flegel et al., 2015; McNeil et al., 2015; Motakis et al., 2014). We confirmed that Mrgprb2 expression was specific to mast cells and not sensory neurons by crossing *Mrgprb2*-Cre mice expressing Cre recombinase under control of the *Mrgprb2* promoter with a tdTomato (tdT) reporter mouse line (*Mrgprb2*-Cre;tdT). *Mrgprb2*-Cre;tdT mice had no detectable tdT fluorescence in either DRG or spinal cord (**Figure 23A-C**). Concordantly, no *Mrgprb2* signal was detected in DRG or spinal cord

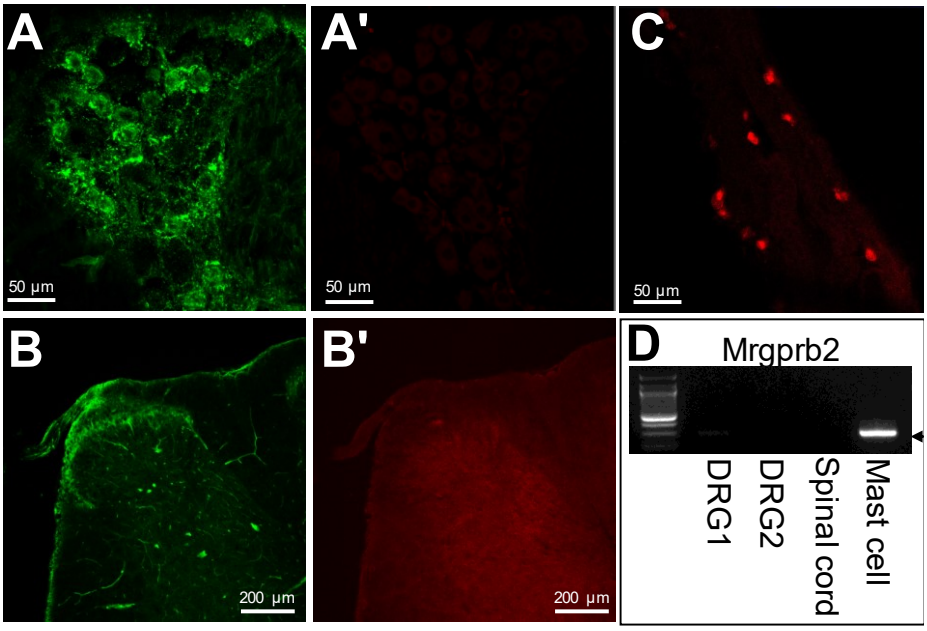

Figure 23. Mrgprb2 is not expressed in dorsal root ganglia sensory neurons and the spinal cord. Dorsal root ganglia (DRG) (**A, A'**) and spinal cord (**B, B'**) sections taken from Mrgprb2-Cre; tdTomato animals, mice expressing both Mrgprb2-Cre and lox-stop-lox tdTomato (tdT) fluorescent reporter. Isolectin B4 conjugated to Alexa Fluor 488 depicted in green in DRG (**A**) and the spinal cord (**B**). tdT fluorescent reporter is undetectable in both DRG (**A'**) and the spinal cord (**B'**). (**C**) Skin section taken from MRgprb2-Cre; tdT mouse. Red depicts positive tdT staining of mast cells. (**D**) Stringent RT-PCR for Mrgprb2 from cDNA collected from two dorsal root ganglia, spinal cord, and mast cell preps. Experiment was repeated at least two times. The arrow indicates the expected band size for Mrgprb2.

using RT-PCR (**Figure 23D**). We employed pro-adrenomedullin peptide 9-20 (PAMP9-

20) and compound 48/80, previously identified ligands of Mrgprb2 and MRGPRX2 (McNeil et al., 2015), to test whether activation of mast cells via Mrgprs was sufficient to induce itch *in vivo*. PAMP9-20 is a potent hypotensive peptide that is produced by a variety of cell types including cells of the adrenal medulla and keratinocytes (Kapas et al., 2001; Kuwasako et al., 1997) and compound 48/80 is a canonical basic secretagogue activator of mast cells (Paton, 1951). Subcutaneous injection of either PAMP9-20 or compound 48/80 elicited itch in wild-type (WT) mice (**Figure 24A, 25A**) that was reduced in Mrgprb2-deficient (*Mrgprb2*$^{-/-}$) mice (**Figure 24A, 25A**). Neither substance elicited pain in the cheek model of behavior (i.e., wiping), indicating the specificity of acute Mrgprb2 activation for itch (**Figure 24B, 25B-C**). To test whether pruritus resulted from mast cell activation, we injected PAMP9-20 into both cromolyn-treated and cKit$^{W\text{-}sh}$ (SASH) mice. Cromolyn is a mast cell stabilizer that inhibits granule release while SASH mice are c-Kit receptor-deficient animals that lack mast cells. Both cromolyn-treated animals and SASH mice displayed reduced PAMP9-20 itch compared to control animals (**Figure 24C-D**). *Mrgprb2*$^{-/-}$ animals had intact mast cell itch responses to non-Mrgpr stimuli such as acute injection of anti-IgE, an antibody against mouse IgE, and repeated ovalbumin (OVA) exposure (**Figure 24E-F**). Anti-IgE directly crosslinks IgE and activates FcεRIα, while OVA sensitization results in a variety of OVA-specific immune responses including the generation of OVA-specific IgE (Reddy et al., 2012). Although the cellular expression of FcεRIα differs between mice and humans (de Andres et al., 1997), in mice, anti-IgE would be expected to specifically activate skin-resident mast cells (**Figure 25D-E**).

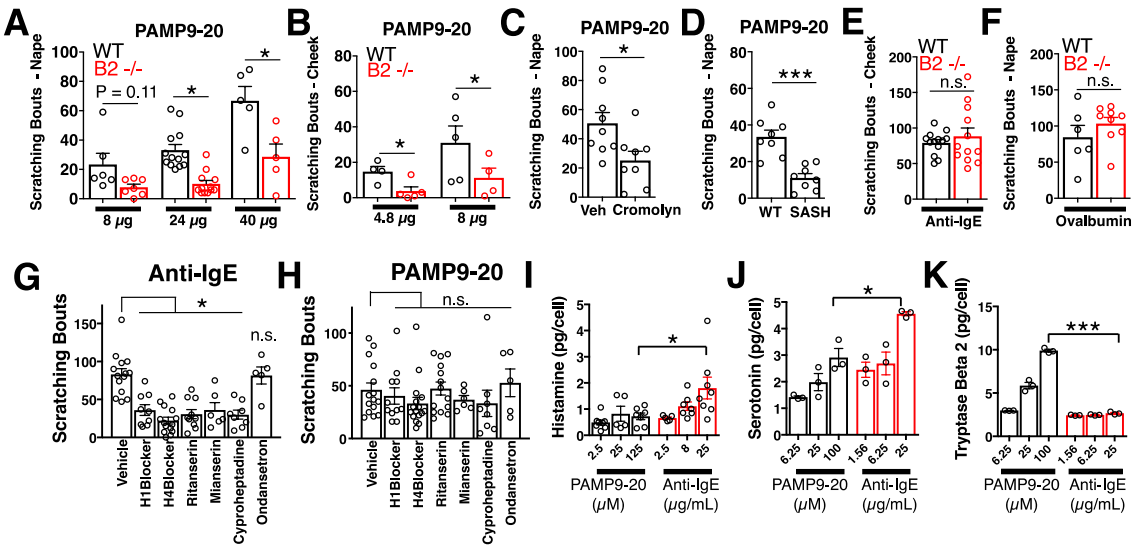

Figure 24. Mrgprb2 agonist PAMP9-20 elicited non-histaminergic itch and differential pruritogen release compared to FcεRI activation. (**A-H**) Scratching bouts from injection of pruritogen at either the nape or the cheek. Mean plus s.e.m. depicted. Each open circle represents an independent mouse data point. (**A-B**) PAMP9-20 injection into either nape (50µL) (**A**) or cheek (10µL) (**B**) of WT and *Mrgprb2*$^{-/-}$ (B2 -/-) animals. (**A**) 8 µg: WT n= 6, B2-/- n= 7; 24 µg: WT n= 13, B2-/- n= 12; 40 µg: WT n=5, B2-/- n=5. (**B**) 4.8 µg: WT n= 4, B2-/- n= 4; 8 µg: WT n=5, B2-/- n= 4. (**C**) Injection of 24 µg PAMP9-20 (50µL of 300µM) at the nape in the presence of either vehicle or cromolyn. Veh n=9, Cromolyn n= 8. (**D**) Injection of 24 µg PAMP9-20 (50µL of 300µM) into the nape of WT and SASH (cKit$^{W\text{-}sh}$) mice. For both, n = 8. (**E**) 1µg anti-IgE injection into WT and B2 -/- mice. WT n= 7, B2 -/- n= 6. (**F**) 50 µg ovalbumin injection into sensitized WT and B2 -/- animals. WT n= 6, B2 -/- n= 9. (**G**) 1µg anti-IgE injection at the cheek with the indicated antagonist. Vehicle, n= 13; H1Blocker, n= 9; H4Blocker, n= 14; Ritanserin, n= 10; Mianserin, n=6; Cyproheptadine, n=8; Ondansetron, n= 5. (**H**) 24 µg PAMP9-20 injection at the nape with the indicated antagonist. Vehicle, n= 15; H1Blocker, n= 11; H4Blocker, n= 16; Ritanserin, n= 14; Mianserin, n=6; Cyproheptadine, n=8; Ondansetron, n= 5. *In vitro* release of histamine (**I**), serotonin (**J**), and tryptase beta 2 (**K**) from mouse peritoneal mast cells upon stimulation by various concentrations of either PAMP9-20 or anti-IgE. For (**J**) PAMP9-20: 2.5 n=8; 25 n=5; 125 n=7. For Anti-IgE: 2.5 n= 5; 8 n= 7; 25 n= 8. Open circles depict independent biological replicates from peritoneal mast cells isolated from > 4 animals. For (**I-K**), mean plus s.e.m. depicted. Open circles depict independent biological replicates from peritoneal mast cells isolated from > 2 animals. All concentrations n=3. (**A-K**) *, $P < 0.05$; ***, $P < 0.001$; n.s. = not significant by two-tailed unpaired Student's *t*-test.

Both histamine (H_1 and H_4) and serotonin (5-HT_2 and 5-HT_7) receptor antagonism have been reported to be effective in controlling various forms of mast cell-associated itch (Dunford et al., 2007; Katagiri et al., 2006; Morita et al., 2015; Shim and Oh, 2008; Yamaguchi et al., 1999). Indeed, cetirizine (H1R antagonist), JNJ7777120 (H4R antagonist), and serotonin receptor antagonists ritanserin, mianserin, and cyproheptadine

substantially reduced anti-IgE-associated itch (**Figure 24G**). In contrast, PAMP9-20-mediated itch was not significantly reduced by any tested antagonist (**Figure 24H**). Of

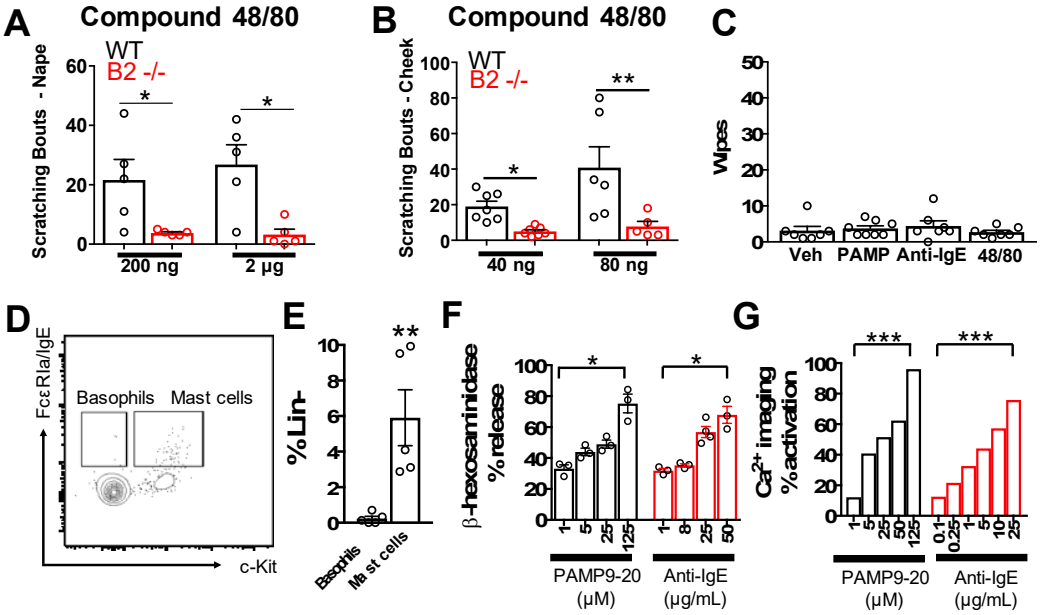

Figure 25. Mrgprb2 agonists elicit itch and not pain. (**A-C**) Mean plus s.e.m. depicted. Each open circle represents an individual mouse. (**A**) Scratching bouts from injection (50µL) of compound 48/80 into the nape of the neck of WT and Mrgprb2-/- mice. For 200 ng: WT n= 5, B2 -/- n= 5; 2 µg: WT n=5, B2 -/- n= 5. (**B**) Scratching bouts associated with injection (10µl) of compound 48/80 into cheek of WT or B2 -/- animals. For 40 ng: WT n= 7, B2 -/- n= 7; 80 ng: WT n=6, B2-/- n= 5. (**C**) Wiping associated with injection (10µl) of the indicated substance into the cheek of WT animals. 300µM PAMP9-20, 10µg/mL compound 48/80, and 100µg/mL Anti-IgE were injected. Veh n= 7, PAMP9-20 n=8, Compound 48/80 n= 7, anti-IgE n=5. (**D**) Representative FACS plot of Live CD45+ Lin- CD11b- cells (basophils) from naïve cheek skin. (**E**) Quantification of the frequency of c-Kit+ Mast cells and c-Kit- Basophils (average ± SD) as a percentage of Lin- cells of n = 2 mice. (**F**) β-hexosaminidase release of mouse peritoneal mast cells, displayed as a percentage of total β-hexosaminidase. For all conditions, n=3. Open circles depict independent replicates. (**G**) Percent activation as detected by Ca^{2+} imaging of mouse peritoneal mast cells. ***, $P < 0.001$ by chi-square test. (**A-G**) Mean plus s.e.m. depicted. Each open circle represents an individual mouse. *, $P < 0.05$; **, $P < 0.01$, n.s. = not significant by two-tailed unpaired Student's *t*-test.

note, the concentrations of ritanserin, mianserin, and cyproheptadine utilized (1mg/kg) would inhibit not only serotonergic but also histaminergic receptors. Ondansetron, a 5-HT_3 antagonist, affected neither anti-IgE nor PAMP9-20 itch (**Figure 24G-H**). These data suggest that Mrgprb2 itch was not mediated by mast cell release of histamine and serotonin, indicating that Mrgprb2 activation may confer functions on skin-resident mast cells different from classical IgE-mediated activation. We stimulated murine peritoneal

mast cells with PAMP9-20 and anti-IgE. At concentrations where mast cells were similarly activated as determined by β-hexosaminidase release assay and Ca^{2+} imaging (**Figure 25F-G**), we detected differential release of well-known pruritogens. Compared to Anti-IgE, PAMP9-20 resulted in lower release of the monoamines, histamine and serotonin, and greater release of tryptase beta 2 (**Figure 24I-K**).

In both rodents and humans, mast cells maintain a close anatomical relationship with sensory nerve fibers (Harvima et al., 2010). Such proximity supports a model whereby peptidergic sensory neurons can activate mast cells, and mast cells, in turn, can excite neurons via degranulation and release of effector molecules (Kleij and Bienenstock, 2005; van Diest et al., 2012). To explore how Mrgprb2 activation of mast cells might stimulate sensory nerves, we performed intravital Ca^{2+} imaging in Pirt-GCaMP6s mice after peripheral injection of Mrgprb2 agonists. Pirt-GCaMP6s mice express GCaMP6s, a genetically encoded fluorescent Ca^{2+} indicator, in > 95% of sensory neurons (Kim et al., 2014) (**Figure 26A-A′**). Following injection of either PAMP9-20 (300μM) or compound 48/80 (10ng/μL) into the footpad of the ipsilateral hindpaw (part of the L4 dermatome), we observed robust activation of a subset of small-diameter sensory neurons in L4 DRG (**Figure 26A-C, 27A**). PAMP9-20 and compound 48/80 activated a similar number of sensory neurons per trial, and both agonists activated significantly fewer neurons in *Mrgprb2*$^{-/-}$ mice (**Figure 26B**). In contrast, anti-IgE and direct activators of neurons, chloroquine (CQ), 5-HT, and β-alanine, excited an equivalent number of sensory neurons in both control and *Mrgprb2*$^{-/-}$ animals (**Figure 26B, D and 27B-C**).

In vitro comparisons of Mrgprb2 agonism with IgE receptor activation have demonstrated that Mrgprb2 agonism triggers more rapid degranulation of smaller

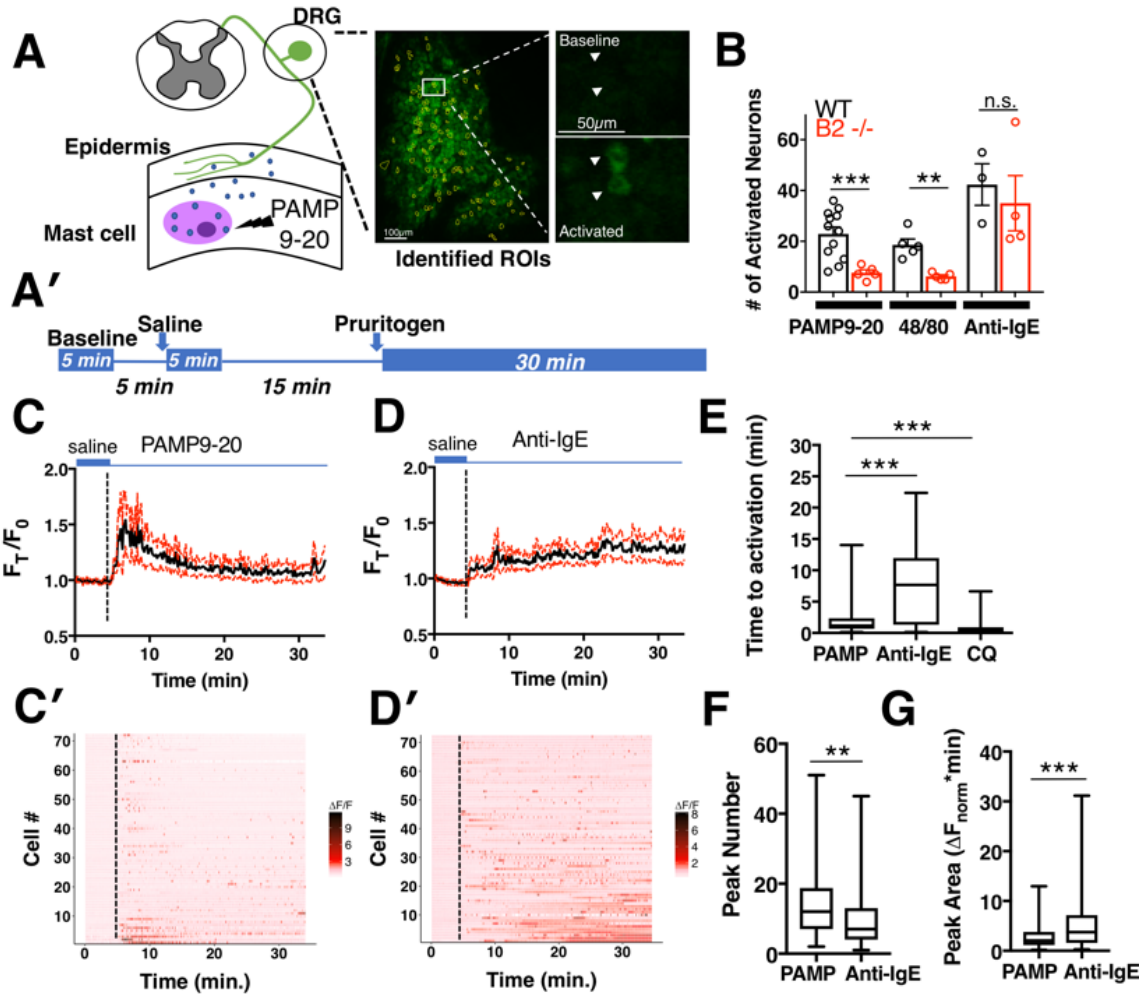

Figure 26. Differential mast cell agonism exhibited varied sensory neuron activation profiles. Graphical depiction (**A**) and experimental flowchart (**A'**) of *in vivo* Ca^{2+} imaging of Pirt-Cre-GCaMP6s sensory neurons. White arrowheads indicate activated neurons. (**B**) Total number of activated neurons for the labeled compound. Mean plus s.e.m. depicted. Open circles represent imaging trials from independent mice. PAMP9-20: WT n= 12, B2 -/- n=5; compound 48/80: WT n= 5, B2 -/- n=5; Anti-IgE: WT n=3, B2 -/- n=4. (**C-D**) Averaged Ca^{2+} imaging traces ± 95% confidence intervals (CI) and heatmaps (**C'-D'**) of individual neurons activated by 300μM PAMP9-20, n= 72 and 100μg/mL anti-IgE, n = 72. (**E-G**) Box (25th and 75th percentiles) and whisker (max and min) plots. (**E**) Time to first detected activation within trial period for neurons activated by the indicated test compounds. PAMP9-20 n= 95; CQ n=79; Anti-IgE n= 79. **(F)** Number of Ca^{2+} signal peaks (>20% increase over baseline) within imaging trial period. PAMP9-20 n= 74; Anti-IgE n= 85. (**G**) Positive peak area (Amplitude over baseline *Duration) within the imaging trial period. PAMP9-20 n= 74; Anti-IgE n= 85. (**A-G**) ******, $P < 0.01$; ***, $P < 0.001$; n.s. = not significant; two-tailed unpaired Student's *t*-test.

granules (Gaudenzio et al., 2016). Intravital Ca^{2+} imaging of mast cell-activated sensory neurons was consistent with this model. In comparison to anti-IgE-associated neurons, Ca^{2+} imaging traces of PAMP9-20-activated neurons displayed earlier excitation,

increased numbers of Ca^{2+} signal peaks, and reduced total peak area (Amplitude*Duration) (**Figure 26E-G**) (See S.T.A.R. Methods for details). Both PAMP9-20 and anti-IgE-associated neuronal excitation was detected later than that associated with chloroquine (CQ), a direct activator of neuronal Mrgpra3 (Liu et al., 2009) (**Figure 26E, 27D-E**).

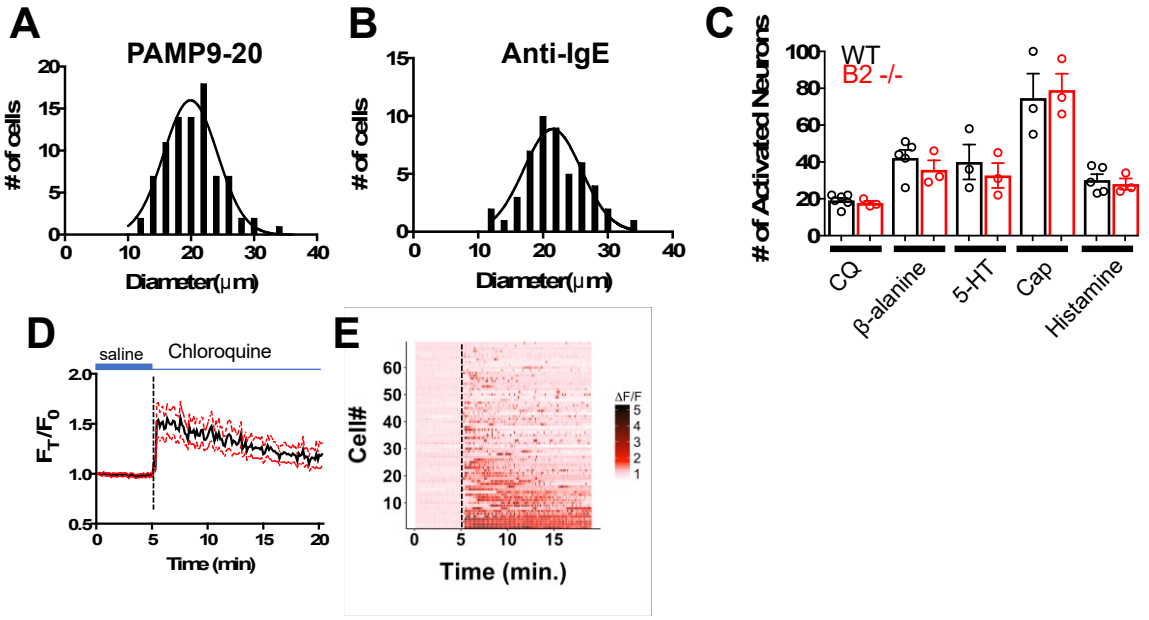

Figure 27. Diameters and total numbers of identified activated neurons associated with mast cell agonists and neuronal activators. (**A**) Histogram of diameters of neurons activated *in vivo* by 300μM PAMP9-20. (**B**) Histogram of diameters of neurons activated *in vivo* by 100μg/mL Anti-IgE. (**C**) The total number of activated neurons identified within each imaging trial period from the labeled test compound. For CQ: WT n= 6, B2 -/- n=3; β-alanine: WT n= 5, B2 -/- n=3; 5-HT: WT n=3, B2 -/- n=3; capsaicin (cap): WT n=3, B2 -/- n=3; histamine: WT n=5, B2 -/- n=3. Mean plus s.e.m. depicted. Open circles represent individual, imaged mouse DRGs. Averaged Ca^{2+} imaging traces (**D**) and heatmaps (**E**) of individual neurons (included in the average) activated by 10mM chloroquine, n= 69. Black dotted lines indicate the start of the test compound imaging period. The solid black line depicts the averaged change in fluorescence of representative, activated sensory neurons, whose individual fluorescent changes are illustrated in the heatmap. The red dotted lines (**D**) are 95% confidence intervals.

Having established that differential activation of mast cells (IgE vs. Mrgprb2) exhibited global differences in neuronal activation signatures, we were interested in examining the specific identity of activated sensory neurons. Based on divergent itch

behavior (**Figure 24**), we hypothesized that differential activation of mast cells would excite separate classes of itch neurons *in vivo*. Single cell RNA-sequencing of mouse sensory neurons has determined three classes of itch neurons typified by expression of three G-protein coupled receptors: *Mrgprd* (NP1), *Mrgpra3* (NP2), or *5ht1f* (NP3) (Usoskin et al., 2015) (**Figure 28A**). In order to identify itch neuron subtypes activated by mast cell agonism, we employed specific agonists for these receptors, β-alanine (Mrgprd), CQ (Mrgpra3), and 5-HT (5ht1f), to functionally identify neurons (**Figure 28A-A′**). Receptor expression is not strictly exclusive to each class of itch neuron. For example, a significant percentage (22%) of Mrgpra3-positive NP2 neurons express Mrgprd and thus would be expected to be activated by both β-alanine and CQ (Usoskin et al., 2015). In the same imaging trial, repeat injections of the same activator should theoretically exhibit 100% overlap in excited neurons. However, in our trials, technical variability limited sensitivity. Of PAMP9-20-activated neurons, approximately 66% (50/76) were activated by a repeat injection of PAMP9-20. Subsequent percent overlap data was thus normalized to this figure. Of all tested compounds, the two Mrgprb2 agonists, compound 48/80 and PAMP9-20, most consistently overlapped (**Figure 28B**). Mrgprb2 agonist-activated neurons exhibited broad overlap with neurons responsive to β-alanine (NP1)-, CQ (NP2)-, and 5-HT (NP3) and significantly less overlap with neurons sensitive to histamine and capsaicin (**Figure 28C-G**). In contrast, anti-IgE-associated neurons overlapped significantly less with neuronal classes identified by β-alanine, CQ, and 5-HT and more with neurons responsive to histamine and capsaicin (**Figure 28C-G**). Further, both cetirizine (H_1R antagonist) and JNJ7777120 (H_4R antagonist) preferentially decreased the number of neurons detected with anti-IgE compared to PAMP9-20-elicited

neurons (**Figure 28H**).

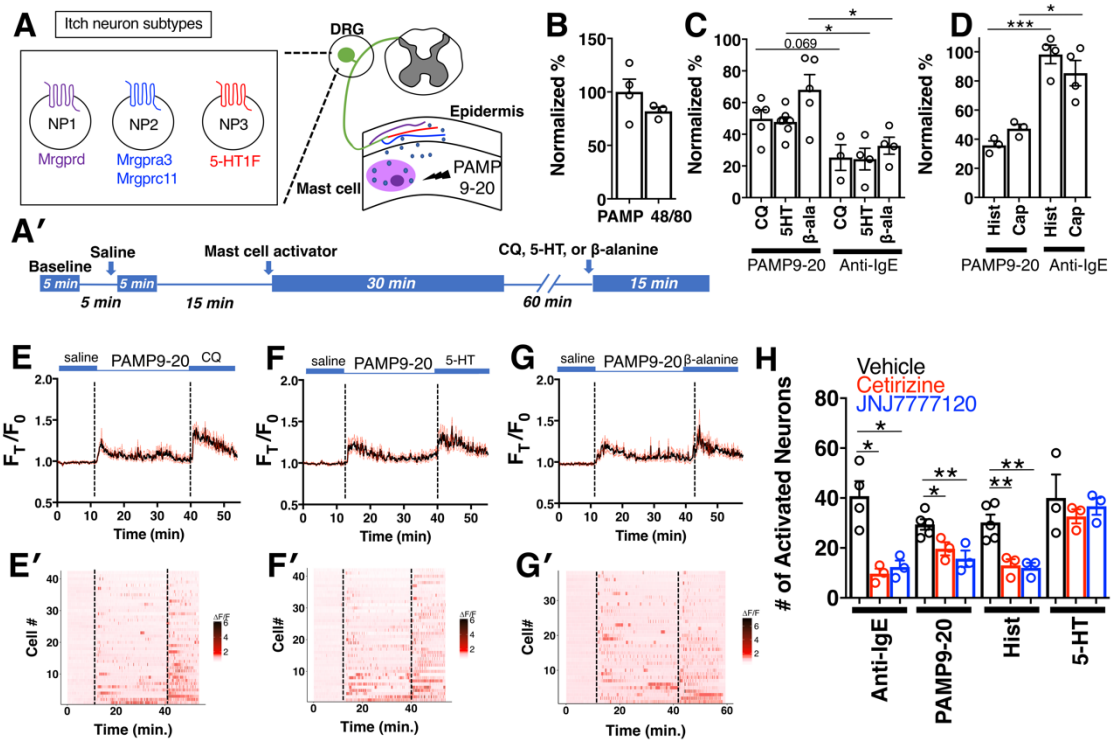

Figure 28. Mrgprb2 agonism excited multiple itch sensory neuron subtypes in an activation pattern distinct from FcεRI. (**A**) Graphical depiction of itch neuron subtypes. (**A'**) Experimental flowchart for *in vivo* Ca^{2+} imaging of mast cell agonists plus neuronal activators. (**B**) Percent overlap of activated sensory neurons from a peripheral injection of 300μM PAMP9-20 and either a repeat injection of 300μM PAMP9-20 n= 4 or 10μg/mL Compound 48/80 n=3. Percent for this and subsequent data normalized to repeated PAMP 9-20 injection. (**C**) Normalized percent overlap between 300μM PAMP9-20 and either 10mM chloroquine (CQ) n= 5, 1mM 5-HT n=6, or 10mM β-alanine n= 5 and between Anti-IgE and either CQ n= 3, 5-HT n=4, or β-alanine n= 4. **(D)** Normalized percent overlap between PAMP9-20 and either 9mM histamine, n= 3, or 3mM capsaicin, n=3, and between Anti-IgE and either histamine, n= 4, or capsaicin, n=4. (**E-G**) Averaged Ca^{2+} imaging traces ±95% CI and heatmaps (**E'-G'**) of individual neurons activated by both PAMP9-20 and either CQ n= 42 (**E-E'**), 5-HT, n= 42 (**F-F'**), or β-alanine, n = 38 (**G-G'**). **(H)** Total number of neurons activated by indicated test compound in the presence of vehicle, cetirizine (H1R antagonist), or JNJ7777120 (H4R antagonist). For Anti-IgE: vehicle (veh) n= 4, cetirizine n=3, JNJ7777120 n= 3; for PAMP9-20: veh n=5, cetirizine n=3, JNJ7777120 n=3; for histamine (Hist): veh n=5, cetirizine n=3, JNJ7777120 n=3; and for 5-HT: veh n=3, cetirizine n=3, JNJ7777120 n=3. (**C-I**) Mean plus s.e.m. depicted. Open circles represent individual, imaged mouse DRGs. *, $P < 0.05$; **, $P < 0.01$; ***, $P < 0.001$; n.s. = not significant; two-tailed unpaired Student's *t*-test.

Given the role of Mrgprb2 in mediating non-histaminergic itch, we sought to investigate the relevance of Mrgprb2 in preclinical models of ACD, a chronic itch

disorder associated with mast cell involvement (Askenase et al., 1983; Dudeck et al., 2011; Gimenez-Rivera et al., 2016; Grimbaldeston et al., 2007). ACD is a type IV hypersensitivity reaction that typically presents as an intensely pruritic, eczematous skin rash that is not amenable to antihistamine treatment (Kostner et al., 2017). In three separate models of ACD, squaric acetyl dibutyl acid (SADBE)- (Fu et al., 2014), oxazolone, and dinitrochlorobenzene (DNCB), treated mice exhibited significantly elevated itch compared to vehicle-treated controls. In all three models, *Mrgprb2*$^{-/-}$ animals scratched substantially less than WT mice (59% reduction in SADBE, 46% reduction in oxazolone, 44% reduction in DNCB) (**Figure 29A-C**). Compared to vehicle-treated skin, DNCB-treatment resulted in an enrichment of immune cells as measured by CD45^{+} cell numbers; however, DNCB-treated *Mrgprb2*$^{-/-}$ skin had significantly lower CD45^{+} cell counts compared to WT skin (**Figure 29D, G**). Both WT and *Mrgprb2*$^{-/-}$ mice had similar ear skin thickness associated with ACD (**Figure 30A**). Further, *Mrgprb2*$^{-/-}$ mice were not protected from itch in the setting of either atopic dermatitis (MC903/calcipotriol) or dry skin (acetone:ether (1:1)-elicited), indicating that Mrgprb2 preferentially regulated ACD-associated itch (Li et al., 2006; Miyamoto et al., 2002) (**Figure 30B-C**).

Mast cells modulate ACD-associated inflammation (Askenase et al., 1983; Dudeck et al., 2011; Gimenez-Rivera et al., 2016; Grimbaldeston et al., 2007). Indeed, compared to healthy control skin, lesional skin from ACD had increased numbers of mast cells as determined by avidin staining (**Figure 29E-F**). Multiple Mrgprb2/X2 agonists have been identified to be upregulated in ACD skin (El-Nour et al., 2006; Scholzen et al., 2001). Here, we found that expression of PAMP1-20, an Mrgprb2/X2 agonist, was

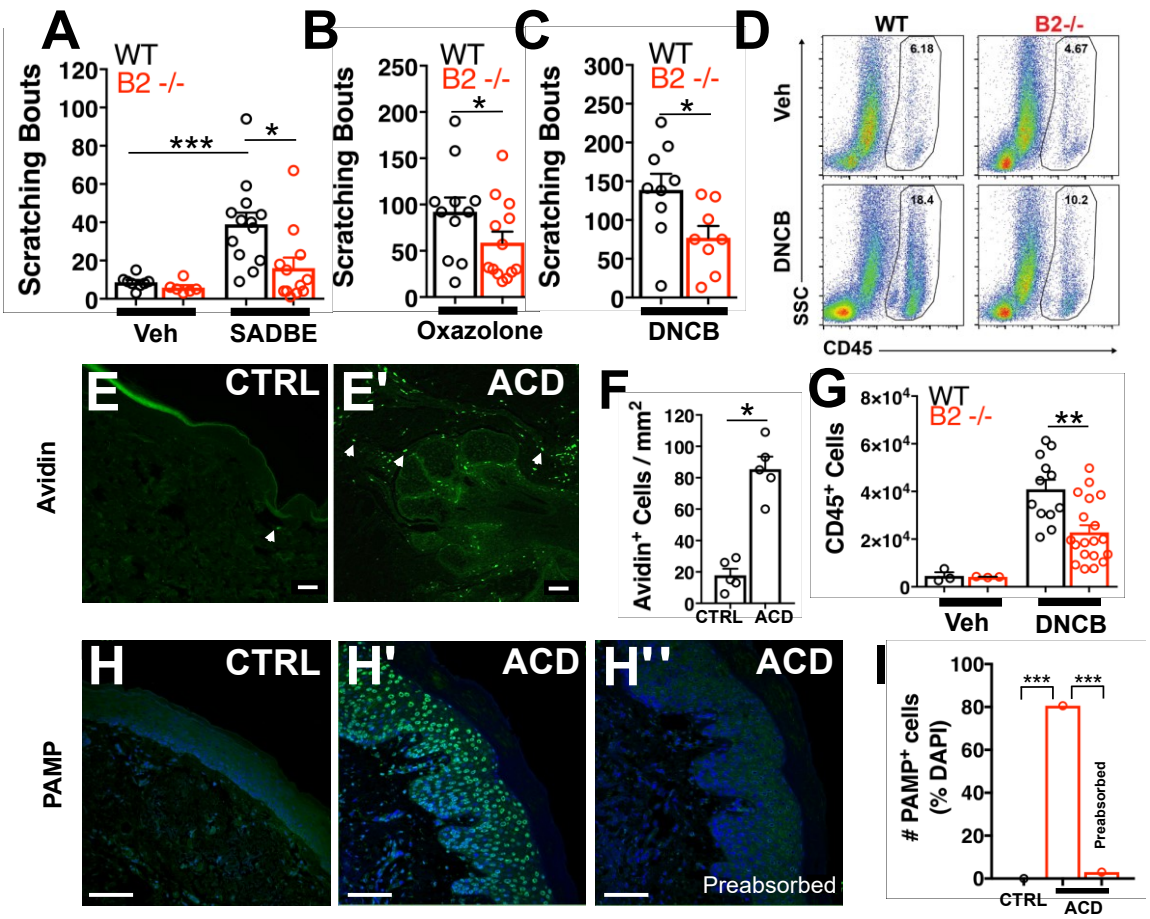

Figure 29. Mast cell Mrgprs mediated a component of murine allergic contact dermatitis (ACD) itch, and PAMP1-20, an MRGPRX2 agonist, is upregulated in human ACD skin. (**A-C**) Scratching bouts in WT and *Mrgprb2*$^{-/-}$ animals with ACD. For all compounds, vehicle was acetone: olive oil (4:1 v/v). (**A**) ACD elicited by Squaric acid dibutyl ester (SADBE). Veh: WT n= 8, B2 -/- n= 6; SADBE: WT n=13, B2 -/- n=12. (**B**) 2-Phenyl-5-oxazolone (oxazolone). WT n= 11, B2 -/- n= 13. (**C**) 1-Chloro-2,4-dinitrobenzene (DNCB). WT n= 9, B2 -/- n= 8. (**D**) Representative flow cytometry plots of DNCB-treated ear skin and vehicle treated ear skin from WT and B2 -/- animals. Numbers indicate the percentage of cells within boxes. (**E-E'**) Representative images of control (**E**) and ACD (**E'**) human skin stained with avidin-FITC. White arrows indicate positive staining. Scale bar is 100 μM. (**F**) Number of avidin stained cells per square millimeter. Each circle represents a separate section. CTRL n= 5; Contact dermatitis n= 5. (**G**) Number of CD45^{+} leukocytes per biopsy from DNCB- and Vehicle-treated WT and B2 -/- mouse ear skin. Open circles represent independent samples from separate mice. For Veh: WT n=3, B2 -/- n=3. For DNCB: WT n=12, B2 -/- n=19. (**H-H"**) Representative images of control (**H**) and ACD human skin (**H'-H"**) stained with either anti-PAMP (1-20) (human) antiserum (**H-H'**) or antiserum preabsorbed with excess PAMP1-20 peptide (**H"**). **H'** and **H"** are from adjacent sections from the same patient. (**I**) Number of PAMP1-20 positive cells as a percentage of DAPI. Control = 0/1616; ACD = 1669/2071; ACD preabsorbed = 63/2097. ***, P < 0.001; by chi-square test. Samples from at least 5 different ACD patients were tested. (**A-G**) Mean plus s. e.m. depicted. *, $P < 0.05$; **, $P < 0.01$; ***, P < 0.001; n.s. = not significant; two-tailed unpaired Student's *t*-test.

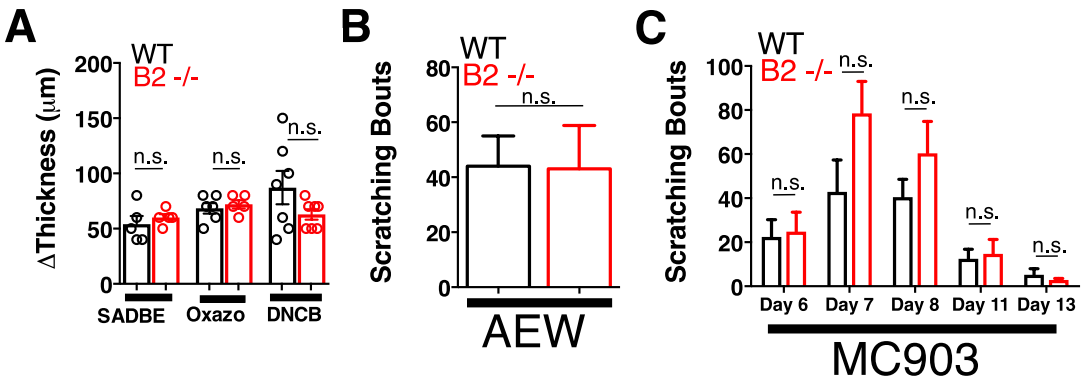

Figure 30. Mrgprb2-/- animals had intact itch in AEW and MC903 chronic itch models. (**A**) Changes in thickness of ear skin from WT and B2 -/- animals treated with either SADBE, Oxazolone, or DNCB contact dermatitis models. Mean ± s.e.m. depicted. n.s, not significant by two-tailed student's t-test. For SADBE: WT n= 5, B2 -/- = 5; for Oxazolone: WT n= 6, B2 -/- = 5; for DNCB: WT n= 7, B2 -/- = 7. (**B**) Scratching bouts from WT and B2 -/- animals subjected to the acetone, ether, water (AEW) model of dry skin. WT n= 4, B2 -/- n= 4. (**C**) Scratching bouts from WT and B2 -/- animals treated with calcipotriol (MC903). For Day 6-8: WT n= 9, B2 -/- n=9; For Day 11: WT n= 7, B2 -/- n= 7; For Day 13: WT n= 5, B2 -/- n= 8. Mean plus s.e.m. depicted. n.s, not significant by two-tailed student's t-test (**B**) or two-way ANOVA (**C**).

similarly upregulated in ACD patient skin while being undetectable in healthy control skin (**Figure 29H-I**). Adrenomedullin, the PAMP1-20 precursor, is produced by keratinocytes (Kapas et al., 2001). In support of this, we observed that anti-PAMP1-20 staining was specific to epidermis (**Figure 29H-I**). A preabsorption control with PAMP1-20 peptide inhibited staining, supporting the specificity of the anti-serum used (**Figure 29H″**). Collectively, these findings support the hypothesis that mast cell-expressed Mrgpr signaling plays a role in the pathogenesis of ACD-associated itch in both mice and humans.

4. Discussion

In this thesis, I set out determine the role that Mrgprs, both sensory neuron- and mast cell-expressed, play in clinically relevant chronic itch conditions. Specifically, I examined the potential function of Mrgprs in mediating itch associated with two conditions: cholestatic pruritus and allergic contact dermatitis. Over the course of the thesis, I presented evidence that Mrgpra1/MRGPRX4 are receptors for bilirubin involved in cholestatic pruritus. I showed additional data that MRGPRX4 is not just a receptor for bilirubin but also activated by bile acids. Finally, I demonstrated that activation of mast cell-expressed Mrgprs resulted in nonhistaminergic itch and that Mrgprb2/ and MRGPRX2 are involved in allergic contact dermatitis itch.

4.1 Mrgpra1/X4 in cholestatic pruritus

Bilirubin has been widely studied as a neonatal neurotoxin and disease biomarker and not as a pruritogen. Our results revealed that bilirubin is a pruritogen that evokes itch by binding and activating MRGPRs on sensory neurons and may be an overlooked source of cholestatic patients' itch. The K_D of bilirubin for Mrgpra1 and MRGPRX4 suggests that bilirubin likely interacts and activates these receptors in individuals with markedly elevated bilirubin and not in healthy people. More narrowly in hepatobiliary diseases such as cholestasis, our data supports a model in which bilirubin is one of several pruritogens that contributes to itch. Genetic deletion of either MRPGRA1 (A1 KO) or bilirubin (BVR KO) strongly attenuates itch. However, mutant mice still exhibit greater itch compared to untreated mice. This suggests that additional pruritogens contribute to itch in hepatobiliary disease, a model which is consistent with the diverse and complex presentations of patients suffering from cholestatic pruritus. These other responsible

pruritogens could include bile acids, endogenous opioids, and LPA. While bilirubin-altering therapies may be effective in reducing itch, not every patient who suffers from hepatobiliary pruritus is jaundiced. Accordingly, in these patients, disease-altering therapies targeting other pruritogens would be applicable.

Although our findings demonstrate that bilirubin is pruritic, not every patient with jaundice experiences itch (the flip side of the previously referenced scenario). For example, patients with genetic hyperbilirubinemias such as Dubin-Johnson syndrome, a disorder involving mutations in the bilirubin transporter ABCC2, or Crigler-Najjar Type 1, a disorder involving mutations in the bilirubin glucuronosyltransferase UGT1A1, rarely complain of pruritus (Levitt and Levitt, 2014; Van Der Veere et al., 1996). Moreover, neonates can have high levels of bilirubin in their skin but not itch. Bilirubin thus appears to exert selective pruritic activity in certain contexts, which we hypothesize may derive from its dynamic biophysical behavior and complex network of interactions.

In isolated genetic hyperbilirubinemias, few – if any – other organic metabolites are elevated. In contrast, in cholestasis, numerous metabolites are elevated in addition to bilirubin (Alemi et al., 2013; Jacobsen and Broderson, 1983; Kalir et al., 1990; Kozaki et al., 1998). These metabolites would be expected to have large effects on bilirubin chemistry and biology. For example, in normal serum, even high levels of bilirubin are effectively buffered by albumin. In contrast, bilirubin's affinity for albumin and other lipoproteins would be disrupted in cholestatic serum by numerous bile agents also upregulated (Ostrow and Celic, 1984; Rege et al., 1988). Accordingly, we hypothesize that bilirubin is more likely to be bound to albumin in isolated hyperbilirubinemias than in cholestasis. Thus, in isolated hyperbilirubinemia, despite elevated serum bilirubin

levels, bilirubin would be less likely to enter the skin where itch fibers and Mrg receptor reside. Notably, a metric with high positive predictive value for cholestatic pruritus is the Mayo risk score, an aggregate score that considers both serum bilirubin and albumin levels (Talwalkar et al., 2003). The Mayo risk score predicts that itch will increase with rising bilirubin and decreasing albumin levels. In this scenario, bilirubin would be less likely to be bound to albumin and thus free to diffuse into skin.

In the specific case of Crigler-Najjar patients who have jaundice yet do not complain of itch, standard bilirubin-altering treatments like phenobarbital and light therapy may be effectively masking underlying pruritic activity. Light therapy induces photoisomerization and/or photolysis of bilirubin, altering its structure and activity, and phenobarbital decreases global neuronal excitability.

In addition to bilirubin, I demonstrated that MRGPRX4, but not Mrgpra1, is also activated by numerous unconjugated and conjugated bile acids. Bile acids activated humanized (+X4) mouse sensory neurons at higher percentages, indicating that these compounds are capable of interacting with neuronally expressed receptor. Humanized mice scratched more in response to both acute injection of bile acids and a chronic model of cholestatic itch. Cholestatic itch in humanized mice rose in conjunction with plasma bile acid concentration. Our results strongly support that MRGPRX4 is a receptor for bile acids. Given the receptor's expression pattern in humans, it is possible that MRGPRX4 mediates a bile acid-component of cholestatic itch.

Despite being structurally similar, bile acids displayed a wide range of affinity for MRGPRX4. Cholic acid, the least potent bile acid, has 3α, 7α, and 12α hydroxyl groups. In contrast, the higher potency bile acids, DCA and UDCA, have only a 3α hydroxyl and

a 12α or 7β hydroxyl group, respectively. Based on this, we hypothesize that bile acid potency for MRGPRX4 is structurally determined by hydroxyl groups at the 7 and 12 position carbons, and their effects on hydrogen bonding, sterics, and water solubility. Cholesterol has no detectable activity towards MRGPRX4 and is most clearly structurally different from bile acids in that cholesterol exhibits more planarity among its four rings due to a double bond between carbons 5 and 6.

UDCA, one of the more potent determined agonists of MRGPRX4, has been shown to reduce itch in a significant number of patients suffering from pruritus associated with intrahepatic cholestasis of pregnancy and primary biliary cholangitis (de Caestecker et al., 1991; Glantz et al., 2008; Matsuzaki et al., 1990). Our data suggests that, UDCA could promote itch via MRGPRX4. There are many possible explanations for this apparent discrepancy. Notably, UDCA may act as an anti-pruritic agent by decreasing hepatocellular injury, inflammation, and fibrosis (de Caestecker et al., 1991; Glantz et al., 2008; Matsuzaki et al., 1990). UDCA treatment also does not appear to increase total serum bile acid levels despite being a bile acid. Rather, while serum UDCA levels increase, UDCA either decreases or leaves total serum bile acids unchanged. The molecular mechanisms by which UDCA improves cholestatic injury could result from a combination of effects, such as improving hepatocellular function, immunosuppressive effects through unknown mechanisms, and improvements in bile acid flow through the digestive system. Improvement of cholestasis in the absence of total bile acid serum level elevation would be expected to improve pruritus and is consistent with our data.

The role of bile acids in eliciting cholestatic itch in patients is complex. Cholestyramine, a bile-acid chelating resin, aids in secretion and is front-line therapy for

cholestatic pruritus. In a double-blind trial, cholestyramine was shown to be effective for treating itch. However, more recently, colesevalam, a bile-acid binding resin many times more effective than cholestyramine, displayed contradictory trial results (Kuiper et al., 2010). This discrepancy in the effectiveness of serum bile acid modulating therapy is buttressed by clinical observations that serum bile acid levels do not correlate with pruritus. Not all patients with pruritus have elevated serum bile acids, and not all patients with elevated serum bile acids exhibit itch. For example, serum bile acid levels are maximally elevated during liver failure, but these patients often report little to no itch.

These data reaffirm our hypothesis that cholestatic itch is multifactorial, with numerous pruritogens present in bile that activate a variety of neuronal receptors. MRGPRX4 is activated by both bilirubin and bile acids, supporting a model whereby both bile acids and bilirubin contribute to cholestatic itch via agonism at the same receptor, MRGPRX4. Even without taking additional pruritogen-receptor interactions into account, serum levels of a single marker would not be expected to perfectly correlate with itch. Therefore, to properly interpret correlations relying on serum metabolite values, multiple components would likely need to be considered in relation to itch. Additional hypotheses for this lack of correlation include possible desensitization and internalization of MRGPRX4 during late-stage liver failure and/or populational polymorphisms in MRGPRX4 sequence that alter receptor affinity. Further research is required to address these possibilities. However, despite these open questions, our data suggests that MRGPRX4 may be a potential therapeutic target for cholestatic itch.

4.2 Mrgprb2/X2 in allergic contact dermatitis and mast cell itch.

It is widely believed that mast cells, via the IgE/FcεRI-histamine axis, contribute to itch in a number of inflammatory skin disorders. However, histamine antagonists have been ineffective in treating many forms of allergic itch, suggesting that alternative mechanisms exist (Kamo et al., 2014; Liu et al., 2016; Usatine and Riojas, 2010). Here, we demonstrated that Mrgprb2 activation of mast cells, compared to classical IgE-mediated activation, promoted the differential release of pruritogens like tryptase beta 2 and evoked non-histaminergic itch. However, due to the complex composition of mast cell granules, Mrgprb2-associated non-histaminergic itch is likely provoked by a number of pruritogens in addition to tryptase. Although largely histamine independent, a minor component of Mrgprb2-associated itch may be histaminergic as antihistamines slightly reduced the number of sensory neurons activated by PAMP9-20. Conversely, IgE-FcεRI associated itch displayed a non-histaminergic component that was resistant to histamine receptor antagonism. These findings suggest that, despite clear divergence, some overlap exists between Mrgprb2- and FcεRI-mediated mast cell itch.

PAMP9-20-excited neurons associated best with $Mrgprd^{+}$ itch neurons while anti-IgE-associated neurons consistently overlapped with histamine-sensitive neurons. In sensory neurons, *H_1R* expression overlaps more with *5ht1f* and *Mrgpra3* expression and less with *Mrgprd* (Usoskin et al., 2015). Thus, the difference in sensory neuron activation between PAMP9-20 and anti-IgE could be explained by differential mast cell degranulation and release of compounds like tryptase beta 2. Tryptases cleave proteinase-activated receptors (PARs) present on itch-sensory neurons (Fu et al., 2014; Liu et al., 2011; Shimada et al., 2006). Further, different forms of PARs like *PAR4* and *PAR2* are

preferentially expressed on Mrgprd^{+} and 5ht1f^{+} neurons, respectively (Usoskin et al., 2015).

Many chronic allergic itch conditions with mast cell involvement are refractory to histamine antagonists, indicating that alternative itch mechanisms exist (Kamo et al., 2014; Liu et al., 2016; Usatine and Riojas, 2010). ACD is one such condition with an enormous occupational health burden (Peiser et al., 2012). In ACD skin, multiple potential Mrgprb2 and MRGPRX2 agonists are upregulated. Indeed, we show that *Mrgprb2*$^{-/-}$ mice were protected from ACD- associated itch and that PAMP1-20 was enriched in lesional ACD patient skin. Despite a significant reduction in pruritus, *Mrgprb2*$^{-/-}$ animals had residual ACD itch which could result from alternative mechanisms like IL-33 activation of neuronal ST2 and T-cell release of IL-31 (Liu et al., 2016; Takamori et al., 2018). Both mast cells and MRGPRX2 agonists are upregulated in atopic dermatitis and psoriasis (Nattkemper et al., 2018). However, *Mrgprb2*$^{-/-}$ animals did not exhibit reduced itch after topical MC903 treatment, a model of atopic dermatitis. However, whether MRGPRX2 is an alternative mast cell-associated target in pruritus of atopic dermatitis in humans remains to be defined. Notwithstanding this, our murine studies suggest that Mrgprb2 played a preferential role in ACD compared to atopic dermatitis or dry skin.

4.3 Future directions

Mrgprs, as receptors for non-histaminergic pruritogens, could play a role in other chronic itch conditions. One prevalent condition in which Mrgpr involvement remains to be tested is uremic itch, itch occurring in the context of renal failure. In uremia, numerous potential Mrgpr agonists are upregulated including adenine and bilirubin byproducts like

urobilinogen. Intriguingly, adenine has been shown to be agonist of Mrgpra9/a11, murine Mrgprs, potentially linking Mrgpr signaling to uremic itch. A key experiment to be performed would be to perform a model of uremic pruritus, such as 5/6 nephrectomy, in WT and Cluster KO littermates and assess for differences in itch.

Thr vast majority of Mrgpr agonists are low potency, micromolar agonists, including those mentioned in this thesis. Thus, a true physiological ligand with nanomolar affinity for most Mrgprs, mouse and human, has yet to be identified. The major exception may be BAM8-22 activation of Mrgprc11/X1 which fits several criteria. One, it is an endogenously produced peptide. Two, it has low nanomolar affinity for receptor. Three, it has *in vivo* effects dependent on receptor activity. However, outside of this interaction, there are no examples of ligand-receptor pairings that fit these criteria. Small-molecule screens for agonist activity against a variety of Mrgprs would be useful in potentially identifying high-affinity interactions as relevant molecular backbones are detected, which could be used to model additional ligands.

Mrgprs, as GPCRs with specific expression, make for attractive drug targets. Assessing whether they could play a role in human pathophysiology would likely be of substantial clinical benefit. This work was performed using mice as models of disease behavior. There are many outstanding questions to address in order to translate these findings to the clinic.

While mice scratch to bilirubin and bile acids, the picture is more complicated in humans. Only one molecule, autotaxin, has ever been demonstrated to correlate with cholestatic itch in humans, and serum levels of bilirubin and bile acids do not correlate with itch. Additionally, there exists numerous clinical examples of non-pruritic jaundice

ranging from acquired diseases like hemolytic anemia to genetic deficiencies in bilirubin processing enzymes like Dubin-Johnson and Crigler-Najjar. Additionally, the itch literature is replete with substances which elicit robust, reproducible itch in mice and very little, if any, in humans such as LTB_4. Of note, even the canonical Mrgpr pruritogen, chloroquine, elicits severe itch in mice and none in humans (Data shared from Robert LaMotte's lab at Yale). An important translation of our study's findings, in regards to bilirubin, would be whether injection of bilirubin into humans elicits itch. We are actively trying to address this question in a collaboration with the LaMotte lab which has IRB-approval to do this study. In July 2018, I volunteered in the study and reported robust itch lasting approximately 30 min. upon injection of both unconjugated (10μL of 2mM) and conjugated bilirubin (10μL of 2mM). Bilirubin elicited itch without pricking, tingling, or stinging sensations. Distinct from pathophysiological, jaundiced itch, the molecule elicited wheal and flare indicating some mast cell involvement. Jaundiced patients do not display wheal and flare, indicating that acute injection of high dose bilirubin can artificially activate mast cells. However, the itch sensation is not believed to be entirely due to this confounding mast cell involvement as psychophysical studies of mast cell activation almost never results in isolated itch, but rather, presents as mixed itch and pain in the form of pricking and stinging. This study is still ongoing as more volunteers are needed to have confidence in the data.

Another important future direction is to understand how MRGPRX4 polymorphisms may affect receptor function. Based on publicly available populational sequencing data, MRGPRX4 is an extremely polymorphic gene with many identified SNPs causing missense mutations. A few of these mutations appearing at high frequency

are associated with drastic changes in receptor response to agonists (Kozlitina et al., 2019). High-frequency appearing polymorphisms of MRGPRX4 should be tested for response to bilirubin, bile acids, and other published agonists like nateglinide in order to more fully understand how these polymorphisms might impact function. Cholestatic patients, with itch and without itch, should be assessed for possible polymorphic differences in MRGPRX4. We showed the skin bilirubin levels correlate with itch in mice. This data should be repeated with human skin samples from cholestatic patients with corresponding psychophysical itch scores. In parallel, small-molecule screens for antagonists and inverse agonists of MRGPRX4 should be conducted in order to identify lead compounds for treating cholestatic itch. Similarly, small-molecule screens for antagonists and inverse agonists of MRGPRX2 should be conducted in order to identify lead compounds for treating allergic contact dermatitis and other mast cell-associated itch conditions.

References

1. Alemi, F., Kwon, E., Poole, D.P., Lieu, T., Lyo, V., Cattaruzza, F., Cevikbas, F., Steinhoff, M., Nassini, R., Materazzi, S.*, et al.* (2013). The TGR5 receptor mediates bile acid-induced itch and analgesia. J Clin Invest *123*, 1513-1530.
2. Andrew, D., and Craig, A.D. (2001). Spinothalamic lamina I neurons selectively sensitive to histamine: a central neural pathway for itch. Nat Neurosci *4*, 72-77.
3. Appleby, V.J., Hutchinson, J.M., and Davies, M.H. (2015). Safety and efficacy of long-term nasobiliary drainage to treat intractable pruritus in cholestatic liver disease. Frontline Gastroenterol *6*, 252-254.
4. Askenase, P.W., Van Loveren, H., Kraeuter-Kops, S., Ron, Y., Meade, R., Theoharides, T.C., Nordlund, J.J., Scovern, H., Gerhson, M.D., and Ptak, W. (1983). Defective elicitation of delayed-type hypersensitivity in W/Wv and SI/SId mast cell-deficient mice. J Immunol *131*, 2687-2694.
5. Avula, L.R., Buckinx, R., Alpaerts, K., Costagliola, A., Adriaensen, D., Van Nassauw, L., and Timmermans, J.P. (2011). The effect of inflammation on the expression and distribution of the MAS-related gene receptors MrgE and MrgF in the murine ileum. Histochem Cell Biol *136*, 569-585.
6. Bader, M., Alenina, N., Andrade-Navarro, M.A., and Santos, R.A. (2014). MAS and its related G protein-coupled receptors, Mrgprs. Pharmacol Rev *66*, 1080-1105.
7. Barry, D.M., Li, H., Liu, X.Y., Shen, K.F., Liu, X.T., Wu, Z.Y., Munanairi, A., Chen, X.J., Yin, J., Sun, Y.G.*, et al.* (2016). Critical evaluation of the expression of gastrin-releasing peptide in dorsal root ganglia and spinal cord. Mol Pain *12*.
8. Bender, E., Buist, A., Jurzak, M., Langlois, X., Baggerman, G., Verhasselt, P., Ercken, M., Guo, H.Q., Wintmolders, C., Van den Wyngaert, I.*, et al.* (2002). Characterization of an orphan G protein-coupled receptor localized in the dorsal root ganglia reveals adenine as a signaling molecule. Proc Natl Acad Sci U S A *99*, 8573-8578.
9. Bergasa, N.V. (1998). Hypothesis: taste disorders in patients with liver disease may be mediated in the brain: potential mechanisms for a central phenomenon. Am J Gastroenterol *93*, 1209-1210.
10. Bergasa, N.V. (2014). Pruritus of Cholestasis. In Itch: Mechanisms and Treatment, E. Carstens, and T. Akiyama, eds. (Boca Raton (FL)).
11. Bergasa, N.V., Schmitt, J.M., Talbot, T.L., Alling, D.W., Swain, M.G., Turner, M.L., Jenkins, J.B., and Jones, E.A. (1998). Open-label trial of oral nalmefene therapy for the pruritus of cholestasis. Hepatology *27*, 679-684.
12. Bergasa, N.V., Talbot, T.L., Alling, D.W., Schmitt, J.M., Walker, E.C., Baker, B.L., Korenman, J.C., Park, Y., Hoofnagle, J.H., and Jones, E.A. (1992). A controlled trial of naloxone infusions for the pruritus of chronic cholestasis. Gastroenterology *102*, 544-549.
13. Beuers, U., Kremer, A.E., Bolier, R., and Elferink, R.P. (2014). Pruritus in cholestasis: facts and fiction. Hepatology *60*, 399-407.
14. Bourane, S., Duan, B., Koch, S.C., Dalet, A., Britz, O., Garcia-Campmany, L., Kim, E., Cheng, L., Ghosh, A., Ma, Q.*, et al.* (2015). Gate control of mechanical itch by a subpopulation of spinal cord interneurons. Science *350*, 550-554.
15. Bulmer, A.C., Verkade, H.J., and Wagner, K.H. (2013). Bilirubin and beyond: a review of lipid status in Gilbert's syndrome and its relevance to cardiovascular disease protection. Prog Lipid Res *52*, 193-205.
16. Caterina, M.J., Leffler, A., Malmberg, A.B., Martin, W.J., Trafton, J., Petersen-Zeitz, K.R., Koltzenburg, M., Basbaum, A.I., and Julius, D. (2000). Impaired nociception and pain sensation in mice lacking the capsaicin receptor. Science *288*, 306-313.

17. Caterina, M.J., Rosen, T.A., Tominaga, M., Brake, A.J., and Julius, D. (1999). A capsaicin-receptor homologue with a high threshold for noxious heat. Nature *398*, 436-441.
18. Cavanaugh, D.J., Lee, H., Lo, L., Shields, S.D., Zylka, M.J., Basbaum, A.I., and Anderson, D.J. (2009). Distinct subsets of unmyelinated primary sensory fibers mediate behavioral responses to noxious thermal and mechanical stimuli. Proc Natl Acad Sci U S A *106*, 9075-9080.
19. Davidson, S., Zhang, X., Khasabov, S.G., Moser, H.R., Honda, C.N., Simone, D.A., and Giesler, G.J., Jr. (2012). Pruriceptive spinothalamic tract neurons: physiological properties and projection targets in the primate. J Neurophysiol *108*, 1711-1723.
20. Davidson, S., Zhang, X., Yoon, C.H., Khasabov, S.G., Simone, D.A., and Giesler, G.J., Jr. (2007). The itch-producing agents histamine and cowhage activate separate populations of primate spinothalamic tract neurons. J Neurosci *27*, 10007-10014.
21. de Andres, B., Rakasz, E., Hagen, M., McCormik, M.L., Mueller, A.L., Elliot, D., Metwali, A., Sandor, M., Britigan, B.E., Weinstock, J.V.*, et al.* (1997). Lack of Fc-epsilon receptors on murine eosinophils: implications for the functional significance of elevated IgE and eosinophils in parasitic infections. Blood *89*, 3826-3836.
22. de Caestecker, J.S., Jazrawi, R.P., Petroni, M.L., and Northfield, T.C. (1991). Ursodeoxycholic acid in chronic liver disease. Gut *32*, 1061-1065.
23. Dong, X., Han, S., Zylka, M.J., Simon, M.I., and Anderson, D.J. (2001). A diverse family of GPCRs expressed in specific subsets of nociceptive sensory neurons. Cell *106*, 619-632.
24. Dudeck, A., Dudeck, J., Scholten, J., Petzold, A., Surianarayanan, S., Kohler, A., Peschke, K., Vohringer, D., Waskow, C., Krieg, T.*, et al.* (2011). Mast cells are key promoters of contact allergy that mediate the adjuvant effects of haptens. Immunity *34*, 973-984.
25. Dunford, P.J., Williams, K.N., Desai, P.J., Karlsson, L., McQueen, D., and Thurmond, R.L. (2007). Histamine H4 receptor antagonists are superior to traditional antihistamines in the attenuation of experimental pruritus. J Allergy Clin Immunol *119*, 176-183.
26. El-Nour, H., Lundeberg, L., Al-Tawil, R., Granlund, A., Lonne-Rahm, S.B., and Nordlind, K. (2006). Upregulation of the axonal growth and the expression of substance P and its NK1 receptor in human allergic contact dermatitis. Immunopharmacol Immunotoxicol *28*, 621-631.
27. Erickson, S., Nahmias, Z., Rosman, I.S., and Kim, B.S. (2018). Immunomodulating Agents as Antipruritics. Dermatol Clin *36*, 325-334.
28. Ernberg, M., Lundeberg, T., and Kopp, S. (2000). Pain and allodynia/hyperalgesia induced by intramuscular injection of serotonin in patients with fibromyalgia and healthy individuals. Pain *85*, 31-39.
29. Flegel, C., Schobel, N., Altmuller, J., Becker, C., Tannapfel, A., Hatt, H., and Gisselmann, G. (2015). RNA-Seq Analysis of Human Trigeminal and Dorsal Root Ganglia with a Focus on Chemoreceptors. PLoS One *10*, e0128951.
30. Fleming, M.S., Ramos, D., Han, S.B., Zhao, J., Son, Y.J., and Luo, W. (2012). The majority of dorsal spinal cord gastrin releasing peptide is synthesized locally whereas neuromedin B is highly expressed in pain- and itch-sensing somatosensory neurons. Mol Pain *8*, 52.
31. Fredriksson, R., Lagerstrom, M.C., Lundin, L.G., and Schioth, H.B. (2003). The G-protein-coupled receptors in the human genome form five main families. Phylogenetic analysis, paralogon groups, and fingerprints. Mol Pharmacol *63*, 1256-1272.
32. Fu, K., Qu, L., Shimada, S.G., Nie, H., and LaMotte, R.H. (2014). Enhanced scratching elicited by a pruritogen and an algogen in a mouse model of contact hypersensitivity. Neurosci Lett *579*, 190-194.

33. Gaudenzio, N., Sibilano, R., Marichal, T., Starkl, P., Reber, L.L., Cenac, N., McNeil, B.D., Dong, X., Hernandez, J.D., Sagi-Eisenberg, R., *et al.* (2016). Different activation signals induce distinct mast cell degranulation strategies. J Clin Invest *126*, 3981-3998.
34. Gimenez-Rivera, V.A., Siebenhaar, F., Zimmermann, C., Siiskonen, H., Metz, M., and Maurer, M. (2016). Mast Cells Limit the Exacerbation of Chronic Allergic Contact Dermatitis in Response to Repeated Allergen Exposure. J Immunol *197*, 4240-4246.
35. Glantz, A., Reilly, S.J., Benthin, L., Lammert, F., Mattsson, L.A., and Marschall, H.U. (2008). Intrahepatic cholestasis of pregnancy: Amelioration of pruritus by UDCA is associated with decreased progesterone disulphates in urine. Hepatology *47*, 544-551.
36. Gmerek, D.E., and Cowan, A. (1983). Bombesin--a central mediator of pruritus? Br J Dermatol *109*, 239.
37. Grimbaldeston, M.A., Nakae, S., Kalesnikoff, J., Tsai, M., and Galli, S.J. (2007). Mast cell-derived interleukin 10 limits skin pathology in contact dermatitis and chronic irradiation with ultraviolet B. Nat Immunol *8*, 1095-1104.
38. Han, L., Ma, C., Liu, Q., Weng, H.J., Cui, Y., Tang, Z., Kim, Y., Nie, H., Qu, L., Patel, K.N., *et al.* (2013). A subpopulation of nociceptors specifically linked to itch. Nat Neurosci *16*, 174-182.
39. Han, S.K., Dong, X., Hwang, J.I., Zylka, M.J., Anderson, D.J., and Simon, M.I. (2002). Orphan G protein-coupled receptors MrgA1 and MrgC11 are distinctively activated by RF-amide-related peptides through the Galpha q/11 pathway. Proc Natl Acad Sci U S A *99*, 14740-14745.
40. Harvima, I.T., Nilsson, G., and Naukkarinen, A. (2010). Role of mast cells and sensory nerves in skin inflammation. G Ital Dermatol Venereol *145*, 195-204.
41. Hegade, V.S., Krawczyk, M., Kremer, A.E., Kuczka, J., Gaouar, F., Kuiper, E.M., van Buuren, H.R., Lammert, F., Corpechot, C., and Jones, D.E. (2016). The safety and efficacy of nasobiliary drainage in the treatment of refractory cholestatic pruritus: a multicentre European study. Aliment Pharmacol Ther *43*, 294-302.
42. Hofmann, A.F., and Huet, P.M. (2006). Nasobiliary drainage for cholestatic pruritus. Hepatology *43*, 1170-1171.
43. Imamachi, N., Park, G.H., Lee, H., Anderson, D.J., Simon, M.I., Basbaum, A.I., and Han, S.K. (2009). TRPV1-expressing primary afferents generate behavioral responses to pruritogens via multiple mechanisms. Proc Natl Acad Sci U S A *106*, 11330-11335.
44. Jordt, S.E., Bautista, D.M., Chuang, H.H., McKemy, D.D., Zygmunt, P.M., Hogestatt, E.D., Meng, I.D., and Julius, D. (2004). Mustard oils and cannabinoids excite sensory nerve fibres through the TRP channel ANKTM1. Nature *427*, 260-265.
45. Kamo, A., Negi, O., Tengara, S., Kamata, Y., Noguchi, A., Ogawa, H., Tominaga, M., and Takamori, K. (2014). Histamine H(4) receptor antagonists ineffective against itch and skin inflammation in atopic dermatitis mouse model. J Invest Dermatol *134*, 546-548.
46. Kapas, S., Tenchini, M.L., and Farthing, P.M. (2001). Regulation of adrenomedullin secretion in cultured human skin and oral keratinocytes. J Invest Dermatol *117*, 353-359.
47. Kashem, S.W., Subramanian, H., Collington, S.J., Magotti, P., Lambris, J.D., and Ali, H. (2011). G protein coupled receptor specificity for C3a and compound 48/80-induced degranulation in human mast cells: roles of Mas-related genes MrgX1 and MrgX2. Eur J Pharmacol *668*, 299-304.
48. Katagiri, K., Arakawa, S., Hatano, Y., and Fujiwara, S. (2006). Fexofenadine, an H1-receptor antagonist, partially but rapidly inhibits the itch of contact dermatitis induced by diphenylcyclopropenone in patients with alopecia areata. J Dermatol *33*, 75-79.
49. Kawamata, Y., Fujii, R., Hosoya, M., Harada, M., Yoshida, H., Miwa, M., Fukusumi, S., Habata, Y., Itoh, T., Shintani, Y., *et al.* (2003). A G protein-coupled receptor responsive to bile acids. J Biol Chem *278*, 9435-9440.

50. Kim, Y.S., Anderson, M., Park, K., Zheng, Q., Agarwal, A., Gong, C., Saijilafu, Young, L., He, S., LaVinka, P.C., *et al.* (2016). Coupled Activation of Primary Sensory Neurons Contributes to Chronic Pain. Neuron *91*, 1085-1096.
51. Kim, Y.S., Chu, Y., Han, L., Li, M., Li, Z., LaVinka, P.C., Sun, S., Tang, Z., Park, K., Caterina, M.J., *et al.* (2014). Central terminal sensitization of TRPV1 by descending serotonergic facilitation modulates chronic pain. Neuron *81*, 873-887.
52. Kleij, H.P., and Bienenstock, J. (2005). Significance of Conversation between Mast Cells and Nerves. Allergy Asthma Clin Immunol *1*, 65-80.
53. Klein, A.H., Iodi Carstens, M., McCluskey, T.S., Blancher, G., Simons, C.T., Slack, J.P., Furrer, S., and Carstens, E. (2011). Novel menthol-derived cooling compounds activate primary and second-order trigeminal sensory neurons and modulate lingual thermosensitivity. Chem Senses *36*, 649-658.
54. Kostner, L., Anzengruber, F., Guillod, C., Recher, M., Schmid-Grendelmeier, P., and Navarini, A.A. (2017). Allergic Contact Dermatitis. Immunol Allergy Clin North Am *37*, 141-152.
55. Kozlitina, J., Risso, D., Lansu, K., Olsen, R.H.J., Sainz, E., Luiselli, D., Barik, A., Frigerio-Domingues, C., Pagani, L., Wooding, S., *et al.* (2019). An African-specific haplotype in MRGPRX4 is associated with menthol cigarette smoking. PLoS Genet *15*, e1007916.
56. Kremer, A.E., Martens, J.J., Kulik, W., Rueff, F., Kuiper, E.M., van Buuren, H.R., van Erpecum, K.J., Kondrackiene, J., Prieto, J., Rust, C., *et al.* (2010). Lysophosphatidic acid is a potential mediator of cholestatic pruritus. Gastroenterology *139*, 1008-1018, 1018 e1001.
57. Kremer, A.E., van Dijk, R., Leckie, P., Schaap, F.G., Kuiper, E.M., Mettang, T., Reiners, K.S., Raap, U., van Buuren, H.R., van Erpecum, K.J., *et al.* (2012). Serum autotaxin is increased in pruritus of cholestasis, but not of other origin, and responds to therapeutic interventions. Hepatology *56*, 1391-1400.
58. Kroeze, W.K., Sheffler, D.J., and Roth, B.L. (2003). G-protein-coupled receptors at a glance. J Cell Sci *116*, 4867-4869.
59. Kuiper, E.M., van Erpecum, K.J., Beuers, U., Hansen, B.E., Thio, H.B., de Man, R.A., Janssen, H.L., and van Buuren, H.R. (2010). The potent bile acid sequestrant colesevelam is not effective in cholestatic pruritus: results of a double-blind, randomized, placebo-controlled trial. Hepatology *52*, 1334-1340.
60. Kuwasako, K., Kitamura, K., Ishiyama, Y., Washimine, H., Kato, J., Kangawa, K., and Eto, T. (1997). Purification and characterization of PAMP-12 (PAMP[9-20]) in porcine adrenal medulla as a major endogenous biologically active peptide. FEBS Lett *414*, 105-110.
61. Lagerstrom, M.C., Rogoz, K., Abrahamsen, B., Persson, E., Reinius, B., Nordenankar, K., Olund, C., Smith, C., Mendez, J.A., Chen, Z.F., *et al.* (2010). VGLUT2-dependent sensory neurons in the TRPV1 population regulate pain and itch. Neuron *68*, 529-542.
62. Lagerstrom, M.C., and Schioth, H.B. (2008). Structural diversity of G protein-coupled receptors and significance for drug discovery. Nat Rev Drug Discov *7*, 339-357.
63. Lansu, K., Karpiak, J., Liu, J., Huang, X.P., McCorvy, J.D., Kroeze, W.K., Che, T., Nagase, H., Carroll, F.I., Jin, J., *et al.* (2017). In silico design of novel probes for the atypical opioid receptor MRGPRX2. Nat Chem Biol *13*, 529-536.
64. Lembo, P.M., Grazzini, E., Groblewski, T., O'Donnell, D., Roy, M.O., Zhang, J., Hoffert, C., Cao, J., Schmidt, R., Pelletier, M., *et al.* (2002). Proenkephalin A gene products activate a new family of sensory neuron--specific GPCRs. Nat Neurosci *5*, 201-209.
65. Li, M., Hener, P., Zhang, Z., Kato, S., Metzger, D., and Chambon, P. (2006). Topical vitamin D3 and low-calcemic analogs induce thymic stromal lymphopoietin in mouse

keratinocytes and trigger an atopic dermatitis. Proc Natl Acad Sci U S A *103*, 11736-11741.
66. Liu, B., Tai, Y., Achanta, S., Kaelberer, M.M., Caceres, A.I., Shao, X., Fang, J., and Jordt, S.E. (2016). IL-33/ST2 signaling excites sensory neurons and mediates itch response in a mouse model of poison ivy contact allergy. Proc Natl Acad Sci U S A *113*, E7572-E7579.
67. Liu, Q., Tang, Z., Surdenikova, L., Kim, S., Patel, K.N., Kim, A., Ru, F., Guan, Y., Weng, H.J., Geng, Y.*, et al.* (2009). Sensory neuron-specific GPCR Mrgprs are itch receptors mediating chloroquine-induced pruritus. Cell *139*, 1353-1365.
68. Liu, Q., Weng, H.J., Patel, K.N., Tang, Z., Bai, H., Steinhoff, M., and Dong, X. (2011). The distinct roles of two GPCRs, MrgprC11 and PAR2, in itch and hyperalgesia. Sci Signal *4*, ra45.
69. Liu, X.Y., Wan, L., Huo, F.Q., Barry, D.M., Li, H., Zhao, Z.Q., and Chen, Z.F. (2014). B-type natriuretic peptide is neither itch-specific nor functions upstream of the GRP-GRPR signaling pathway. Mol Pain *10*, 4.
70. Macpherson, L.J., Dubin, A.E., Evans, M.J., Marr, F., Schultz, P.G., Cravatt, B.F., and Patapoutian, A. (2007). Noxious compounds activate TRPA1 ion channels through covalent modification of cysteines. Nature *445*, 541-545.
71. Matsuzaki, Y., Tanaka, N., Osuga, T., Aikawa, T., Shoda, J., Doi, M., and Nakano, M. (1990). Improvement of biliary enzyme levels and itching as a result of long-term administration of ursodeoxycholic acid in primary biliary cirrhosis. Am J Gastroenterol *85*, 15-23.
72. McNeil, B.D., Pundir, P., Meeker, S., Han, L., Undem, B.J., Kulka, M., and Dong, X. (2015). Identification of a mast-cell-specific receptor crucial for pseudo-allergic drug reactions. Nature *519*, 237-241.
73. Meixiong, J., Vasavda, C., Green, D., Zheng, Q., Qi, L., Kwatra, S.G., Hamilton, J.P., Snyder, S.H., and Dong, X. (2019). Identification of a bilirubin receptor that may mediate a component of cholestatic itch. Elife *8*.
74. Melzack, R., and Wall, P.D. (1965). Pain mechanisms: a new theory. Science *150*, 971-979.
75. Mishra, S.K., and Hoon, M.A. (2013). The cells and circuitry for itch responses in mice. Science *340*, 968-971.
76. Miyamoto, T., Nojima, H., Shinkado, T., Nakahashi, T., and Kuraishi, Y. (2002). Itch-associated response induced by experimental dry skin in mice. Jpn J Pharmacol *88*, 285-292.
77. Morita, T., McClain, S.P., Batia, L.M., Pellegrino, M., Wilson, S.R., Kienzler, M.A., Lyman, K., Olsen, A.S., Wong, J.F., Stucky, C.L.*, et al.* (2015). HTR7 Mediates Serotonergic Acute and Chronic Itch. Neuron *87*, 124-138.
78. Motakis, E., Guhl, S., Ishizu, Y., Itoh, M., Kawaji, H., de Hoon, M., Lassmann, T., Carninci, P., Hayashizaki, Y., Zuberbier, T.*, et al.* (2014). Redefinition of the human mast cell transcriptome by deep-CAGE sequencing. Blood *123*, e58-67.
79. Nattkemper, L.A., Tey, H.L., Valdes-Rodriguez, R., Lee, H., Mollanazar, N.K., Albornoz, C., Sanders, K.M., and Yosipovitch, G. (2018). The genetics of chronic itch: gene expression in the skin of atopic dermatitis and psoriasis patients with severe itch. J Invest Dermatol.
80. Paton, W.D. (1951). Compound 48/80: a potent histamine liberator. Br J Pharmacol Chemother *6*, 499-508.
81. Peiser, M., Tralau, T., Heidler, J., Api, A.M., Arts, J.H., Basketter, D.A., English, J., Diepgen, T.L., Fuhlbrigge, R.C., Gaspari, A.A.*, et al.* (2012). Allergic contact dermatitis: epidemiology, molecular mechanisms, in vitro methods and regulatory aspects. Current

knowledge assembled at an international workshop at BfR, Germany. Cell Mol Life Sci *69*, 763-781.
82. Rau, K.K., McIlwrath, S.L., Wang, H., Lawson, J.J., Jankowski, M.P., Zylka, M.J., Anderson, D.J., and Koerber, H.R. (2009). Mrgprd enhances excitability in specific populations of cutaneous murine polymodal nociceptors. J Neurosci *29*, 8612-8619.
83. Reddy, A.T., Lakshmi, S.P., and Reddy, R.C. (2012). Murine model of allergen induced asthma. J Vis Exp, e3771.
84. Ross, S.E., Mardinly, A.R., McCord, A.E., Zurawski, J., Cohen, S., Jung, C., Hu, L., Mok, S.I., Shah, A., Savner, E.M.*, et al.* (2010). Loss of inhibitory interneurons in the dorsal spinal cord and elevated itch in Bhlhb5 mutant mice. Neuron *65*, 886-898.
85. Sato, H., Macchiarulo, A., Thomas, C., Gioiello, A., Une, M., Hofmann, A.F., Saladin, R., Schoonjans, K., Pellicciari, R., and Auwerx, J. (2008). Novel potent and selective bile acid derivatives as TGR5 agonists: biological screening, structure-activity relationships, and molecular modeling studies. J Med Chem *51*, 1831-1841.
86. Schmelz, M., Schmidt, R., Weidner, C., Hilliges, M., Torebjork, H.E., and Handwerker, H.O. (2003). Chemical response pattern of different classes of C-nociceptors to pruritogens and algogens. J Neurophysiol *89*, 2441-2448.
87. Scholzen, T.E., Steinhoff, M., Bonaccorsi, P., Klein, R., Amadesi, S., Geppetti, P., Lu, B., Gerard, N.P., Olerud, J.E., Luger, T.A.*, et al.* (2001). Neutral endopeptidase terminates substance P-induced inflammation in allergic contact dermatitis. J Immunol *166*, 1285-1291.
88. Shim, W.S., and Oh, U. (2008). Histamine-induced itch and its relationship with pain. Mol Pain *4*, 29.
89. Shimada, S.G., Shimada, K.A., and Collins, J.G. (2006). Scratching behavior in mice induced by the proteinase-activated receptor-2 agonist, SLIGRL-NH2. Eur J Pharmacol *530*, 281-283.
90. Sikand, P., Dong, X., and LaMotte, R.H. (2011). BAM8-22 peptide produces itch and nociceptive sensations in humans independent of histamine release. J Neurosci *31*, 7563-7567.
91. Simone, D.A., Zhang, X., Li, J., Zhang, J.M., Honda, C.N., LaMotte, R.H., and Giesler, G.J., Jr. (2004). Comparison of responses of primate spinothalamic tract neurons to pruritic and algogenic stimuli. J Neurophysiol *91*, 213-222.
92. Solinski, H.J., Gudermann, T., and Breit, A. (2014). Pharmacology and signaling of MAS-related G protein-coupled receptors. Pharmacol Rev *66*, 570-597.
93. Solorzano, C., Villafuerte, D., Meda, K., Cevikbas, F., Braz, J., Sharif-Naeini, R., Juarez-Salinas, D., Llewellyn-Smith, I.J., Guan, Z., and Basbaum, A.I. (2015). Primary afferent and spinal cord expression of gastrin-releasing peptide: message, protein, and antibody concerns. J Neurosci *35*, 648-657.
94. Sommer, C. (2004). Serotonin in pain and analgesia: actions in the periphery. Mol Neurobiol *30*, 117-125.
95. Strassburg, C.P. (2010). Hyperbilirubinemia syndromes (Gilbert-Meulengracht, Crigler-Najjar, Dubin-Johnson, and Rotor syndrome). Best Pract Res Clin Gastroenterol *24*, 555-571.
96. Subramanian, H., Gupta, K., Guo, Q., Price, R., and Ali, H. (2011a). Mas-related gene X2 (MrgX2) is a novel G protein-coupled receptor for the antimicrobial peptide LL-37 in human mast cells: resistance to receptor phosphorylation, desensitization, and internalization. J Biol Chem *286*, 44739-44749.
97. Subramanian, H., Kashem, S.W., Collington, S.J., Qu, H., Lambris, J.D., and Ali, H. (2011b). PMX-53 as a dual CD88 antagonist and an agonist for Mas-related gene 2 (MrgX2) in human mast cells. Mol Pharmacol *79*, 1005-1013.

98. Sun, Y.G., Zhao, Z.Q., Meng, X.L., Yin, J., Liu, X.Y., and Chen, Z.F. (2009). Cellular basis of itch sensation. Science *325*, 1531-1534.
99. Swain, M.G., Rothman, R.B., Xu, H., Vergalla, J., Bergasa, N.V., and Jones, E.A. (1992). Endogenous opioids accumulate in plasma in a rat model of acute cholestasis. Gastroenterology *103*, 630-635.
100. Takamori, A., Nambu, A., Sato, K., Yamaguchi, S., Matsuda, K., Numata, T., Sugawara, T., Yoshizaki, T., Arae, K., Morita, H.*, et al.* (2018). IL-31 is crucial for induction of pruritus, but not inflammation, in contact hypersensitivity. Sci Rep *8*, 6639.
101. Tanaka, Y., Aleksunes, L.M., Cui, Y.J., and Klaassen, C.D. (2009). ANIT-induced intrahepatic cholestasis alters hepatobiliary transporter expression via Nrf2-dependent and independent signaling. Toxicol Sci *108*, 247-257.
102. Tatemoto, K., Nozaki, Y., Tsuda, R., Konno, S., Tomura, K., Furuno, M., Ogasawara, H., Edamura, K., Takagi, H., Iwamura, H.*, et al.* (2006). Immunoglobulin E-independent activation of mast cell is mediated by Mrg receptors. Biochem Biophys Res Commun *349*, 1322-1328.
103. Theoharides, T.C., Alysandratos, K.D., Angelidou, A., Delivanis, D.A., Sismanopoulos, N., Zhang, B., Asadi, S., Vasiadi, M., Weng, Z., Miniati, A.*, et al.* (2012). Mast cells and inflammation. Biochim Biophys Acta *1822*, 21-33.
104. Thornton, J.R., and Losowsky, M.S. (1988). Opioid peptides and primary biliary cirrhosis. BMJ *297*, 1501-1504.
105. Thornton, J.R., and Losowsky, M.S. (1989a). Methionine enkephalin is increased in plasma in acute liver disease and is present in bile and urine. J Hepatol *8*, 53-59.
106. Thornton, J.R., and Losowsky, M.S. (1989b). Plasma leucine enkephalin is increased in liver disease. Gut *30*, 1392-1395.
107. Usatine, R.P., and Riojas, M. (2010). Diagnosis and management of contact dermatitis. Am Fam Physician *82*, 249-255.
108. Usoskin, D., Furlan, A., Islam, S., Abdo, H., Lonnerberg, P., Lou, D., Hjerling-Leffler, J., Haeggstrom, J., Kharchenko, O., Kharchenko, P.V.*, et al.* (2015). Unbiased classification of sensory neuron types by large-scale single-cell RNA sequencing. Nat Neurosci *18*, 145-153.
109. van Diest, S.A., Stanisor, O.I., Boeckxstaens, G.E., de Jonge, W.J., and van den Wijngaard, R.M. (2012). Relevance of mast cell-nerve interactions in intestinal nociception. Biochim Biophys Acta *1822*, 74-84.
110. Vitek, L., Jirsa, M., Brodanova, M., Kalab, M., Marecek, Z., Danzig, V., Novotny, L., and Kotal, P. (2002). Gilbert syndrome and ischemic heart disease: a protective effect of elevated bilirubin levels. Atherosclerosis *160*, 449-456.
111. Vrontou, S., Wong, A.M., Rau, K.K., Koerber, H.R., and Anderson, D.J. (2013). Genetic identification of C fibres that detect massage-like stroking of hairy skin in vivo. Nature *493*, 669-673.
112. Wang, H., and Zylka, M.J. (2009). Mrgprd-expressing polymodal nociceptive neurons innervate most known classes of substantia gelatinosa neurons. J Neurosci *29*, 13202-13209.
113. Wilson, S.R., Gerhold, K.A., Bifolck-Fisher, A., Liu, Q., Patel, K.N., Dong, X., and Bautista, D.M. (2011). TRPA1 is required for histamine-independent, Mas-related G protein-coupled receptor-mediated itch. Nat Neurosci *14*, 595-602.
114. Yamaguchi, T., Nagasawa, T., Satoh, M., and Kuraishi, Y. (1999). Itch-associated response induced by intradermal serotonin through 5-HT2 receptors in mice. Neurosci Res *35*, 77-83.
115. Zhang, L., Taylor, N., Xie, Y., Ford, R., Johnson, J., Paulsen, J.E., and Bates, B. (2005). Cloning and expression of MRG receptors in macaque, mouse, and human. Brain Res Mol Brain Res *133*, 187-197.

116. Zhao, Z.Q., Huo, F.Q., Jeffry, J., Hampton, L., Demehri, S., Kim, S., Liu, X.Y., Barry, D.M., Wan, L., Liu, Z.C.*, et al.* (2013). Chronic itch development in sensory neurons requires BRAF signaling pathways. J Clin Invest *123*, 4769-4780.
117. Zylka, M.J., Dong, X., Southwell, A.L., and Anderson, D.J. (2003). Atypical expansion in mice of the sensory neuron-specific Mrg G protein-coupled receptor family. Proc Natl Acad Sci U S A *100*, 10043-10048.

James Meixiong

Johns Hopkins School of Medicine
MD/PhD Combined Degree Candidate
801 Key Hwy, Unit 342
Baltimore, MD 21230
(706-910-2413, jimeix@gmail.com)

Education
Harvard College '13 *Magna Cum Laude with Highest Honors in field of Molecular and Cellular Biology* **(**GPA: 3.87)
Awards and Professional Honors

2008, The Siemens Competition in Math, Science, and Technology National Finalist (4th Place), the Siemens Foundation, NYC, NY
2009, High School Swimming All-American, National Interscholastic Swimming Coaches Association
2009, Best and Brightest Award Finalist, the Augusta Chronicle, Augusta, GA
2013, Thomas T. Hoopes Prize Recipient, Harvard College, Cambridge, MA
2013, Lawrence J. Henderson Prize for Molecular Biology, Harvard College, Cambridge, MA
2013, Magna cum laude with Highest Honors in Molecular and Cellular Biology, Harvard College, Cambridge, MA
2016, Thomas J. and Mary L. Kelly Award, Johns Hopkins University, Baltimore, MD

Research Funding Awards

- 2010, PRISE Fellow, Program for Research in Science and Engineering (PRISE), Harvard College, Cambridge, MA
- 2011, Harvard College Research Program Fellow, Harvard College, Cambridge, MA

First Author Publications:

1. **Meixiong, J.**, Dong, X. (2017). Mas-Related G-Protein Coupled Receptors and the Biology of Itch Sensation. *Annual Review Genetics*: Nov; 51:103-121.
2. **Meixiong, J.***, Vasavda, C.*, Green, D., Zheng, Q., Qi, L., Kwatra, S.G., Hamilton, J.P., Snyder, S.H., Dong, X. (2019). Identification of a bilirubin receptor that may mediate a component of cholestatic itch. *Elife 8.*
3. **Meixiong, J.**, Vasavda, C., Snyder, S.H., Dong, X. (2019). MRGPRX4 is a G protein-coupled receptor activated by bile acids that may contribute to cholestatic pruritus. *Proceedings of the National Academy of Sciences*: May 9.
4. **Meixiong, J.**, Anderson, M., Limjunyawong, N., Sabbagh, M.F., Hu, E., Mack, M.R., Oetjen, L.K., Wang, F., Kim, B.S., Dong, X. (2019). Activation of Mast-Cell-Expressed Mas-Related G-Protein-Coupled Receptors Drives Non-histaminergic Itch. *Immunity:* April 23.

Additional Publications:

1. Patel, S. P., Vasavda, C., Ho, B., **Meixiong, J.**, Dong, X., Kwatra, S.G. (2019). Cholestatic pruritus: Emerging mechanisms and therapeutics. *Journal of the American Academy of Dermatology.* Apr 19; https://doi.org/10.1016/j.jaad.2019.04.035
2. Salvatierra, J., Diaz-Bustamante, M., **Meixiong, J**., Tierney, E., Dong, X., Bosmans, F. (2018). A disease mutation reveals a role for NaV1.9 in acute itch. *Journal of Clinical Investigation*: Dec; 128(12):5434-5447.
3. Ru, F., Sun, H., Jurcakova, D., Herbstsomer, R.A., **Meixiong, J.**, Dong, X., Undem, B.J. (2017). Mechanisms of pruritogen-induced activation of itch nerves in isolated mouse skin. *J Physiol.* Jun 1;595(11):3651-3666
4. Schaefer, E.A., **Meixiong, J.**, Mark, C., Deik, A., Motola, D.L., Fusco, D., Yang, A., Brisac, C., Salloum, S., Lin, W., Clish, C.B., Peng, L.F., Chung, R.T. (2016).

Apolipoprotein B100 is required for hepatitis C infectivity and Mipomersen inhibits hepatitis C. *World J Gastroenterol*. 22(45):9954-9965.

5. Jilg, N., Lin, W., Hong, J., Schaefer, E.A., Wolski, D., **Meixiong, J.**, Goto, K., Brisac, C., Chusri, P., Fusco, D.N., Chevaliez, S., Luther, J., Kumthip, K., Urban, T.J., Peng, L.F., Lauer, G.M., Chung, R.T. (2014). Kinetic differences in the induction of interferon stimulated genes by interferon-α and interleukin 28B are altered by infection with hepatitis C virus. *Hepatology*: 59(4):1250-61.
6. Luo, S., Zhang, B., Dong, X.P., Tao, Y., Ting, A., Zhou, Z., **Meixiong, J.**, Luo, J., Chiu, F.C.A., Xiong, W.C., Mei, L. (2008). HSP90β Regulates Rapsyn Turnover and Subsequent AChR Cluster Formation and Maintenance. *Neuron:* 60:97-110

Biomedical Research Experience

- 2007, Summer volunteer, Program of Developmental Neurobiology, Institute of Molecular Medicine and Genetics, Medical College of Georgia (MCG)
    - Investigated rapsyn turnover in AChR cluster formation
- 2008, Research Assistant in the laboratory of Dr. Zheng Dong, Department of Cell Biology, Medical College of Georgia
    - Investigated mitochondrial dynamics and its effect on Bcl-2 proteins
- 2010-2011, Research assistant in the laboratory of Dr. Vladimir Denic, Department of Molecular and Cellular Biology, Harvard University
    - Investigated the functions and directions of tail-anchored proteins
- 2011- 2013, Research assistant in the laboratory of Dr. Raymond Chung, Department of Gastroenterology and Hepatology, Massachusetts General Hospital
    - Investigated host-HCV relationships in the context of cholesterol metabolism
- 2015- Present, Graduate student in the laboratory of Dr. Xinzhong Dong, Department of Neuroscience, Johns Hopkins University
    - Investigated the function of Mrgprs in cholestatic itch

Teaching Experience

- 2017, Teaching assistant for Neuroscience of Cognition II, Department of Neuroscience, Johns Hopkins University